

Chapter 2

Transparent Ceramic Materials

2.1 Introduction

As stressed in previous chapter, to be transparent ceramics, materials should have an isotropic lattice structure, i.e., cubic structure. Actually, there have been various transparent ceramics with such a lattice structure, including simple oxides [1–9], sesquioxides [10–19], complex oxides [20–26], and aluminum oxynitride [27–30]. However, various transparent ceramics that have noncubic lattice structures, such as tetrahedral ferroelectric PLZT [31–33], orthorhombic mullite [34, 35], and hexagonal Al_2O_3 [36–51], emerged in recent years. To make these transparent ceramics, various sintering techniques, including vacuum sintering, high pressure (HP) and hot isostatic pressure (HIP), spark plasma sintering (SPS), and microwave sintering, have been used for different materials. In order to improve the sintering behaviors of the precursor powders, various synthesis methods, especially wet-chemical routes, such as chemical co-precipitation, sol–gel and gel combustion, have been employed to produce powders with ultrafine particle/grain sizes. In some cases, special packing technologies, like tape casting, slip casting, or gel casting, have been used to form green bodies of the transparent ceramics. For example, tape casting is able to produce thin sheets with large sizes, while slip or gel casting enables to form rod-like or specially shaped items. This chapter is aimed to cover the ceramic materials that could be made to be transparent, which have been reported in the open literature.

2.2 Simple Oxides

2.2.1 Alumina (Al_2O_3)

The only thermodynamically stable crystallographic modification of alumina (Al_2O_3) is $\alpha\text{-Al}_2\text{O}_3$, or known as corundum. Corundum has a hexagonal crystal

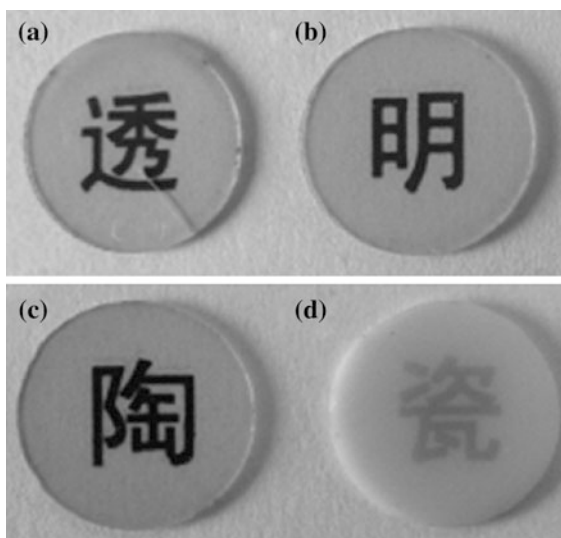
lattice with cell parameters $a = 4.754 \text{ \AA}$ and $c = 12.99 \text{ \AA}$. The O^{2-} ions are arranged in close hexagonal arrangement, with the cation Al^{3+} occupying two-thirds of the octahedral interstitial positions [52]. It has a density of 3.95 g cm^{-3} , with melting point of $2072 \text{ }^\circ\text{C}$ and boiling point of $2977 \text{ }^\circ\text{C}$.

Alumina exhibits many interesting properties, such as high strength, high hardness, and excellent corrosive resistance. This makes transparent Al_2O_3 ceramics a promising candidate for applications as electromagnetic windows, transparent armor, and envelopes of HP metal halide lamps [53]. Sintered Al_2O_3 ceramics with submicron grain size are the hardest materials among all transparent armors, even including sapphire. Therefore, transparent polycrystalline alumina is believed to be a promising alternative for sapphire. Photographs of representative Al_2O_3 transparent ceramics, which were processed by using SPS, are shown in Fig. 2.1 [53].

Traditional transparent Al_2O_3 ceramics were prepared by sintering in hydrogen at temperatures of generally above $1700 \text{ }^\circ\text{C}$ [54, 55]. The high sintering temperature caused extensive grain growth, which in turn seriously affected mechanical strength and hardness of the materials. Also, the large grain sizes of up to $410 \text{ }\mu\text{m}$ led to significant light scattering caused by the birefringence of the coarse Al_2O_3 grains [50]. Therefore, its in-line transmission was typically below 10 %. The low strength and in-line transmission posed an almost insurmountable obstacle for their applications in fields where high transparency and good mechanical properties are required.

Optical and mechanical properties of transparent Al_2O_3 ceramics are highly dependent on their grain size and residual porosity. Various strategies have been employed to control the grain sizes and minimize the residual porosity. For this purpose, fine-grained transparent Al_2O_3 ceramics have recently attracted much

Fig. 2.1 Photographs of representative alumina (Al_2O_3) ceramics that were spark plasma sintered at **a** $1250 \text{ }^\circ\text{C}$, **b** $1300 \text{ }^\circ\text{C}$, and **c–d** $1350 \text{ }^\circ\text{C}$, using the pretreated (**a–c**) and the untreated Al_2O_3 powder (**d**). Reproduced with permission from [53]. Copyright © 2010, John Wiley & Sons



attention [45–51]. The fine-grained ceramics demonstrated a significant improvement in mechanical strength and optical transparency. It has been reported that typical fine-grained transparent Al_2O_3 ceramics had strength of up to 600–800 MPa and high in-line transmission of up to 60 % [47, 49]. Various strategies and technologies have been used to fabricate fine-grained transparent Al_2O_3 ceramics.

A multiple-step pressureless sintering has been used to obtain high quality transparent Al_2O_3 ceramics [56]. Nanosized Al_2O_3 ceramics with an average grain size of 70 nm and a relative density of 95 % were obtained by using a two-step sintering. In this case, α - Al_2O_3 powders, with a mean particle size of about 10 nm and a weak agglomeration, were synthesized by using an α - Al_2O_3 seeded polyacrylamide gel method. The densification and the suppression of the grain growth are realized by exploiting the difference in kinetics between grain boundary diffusion and grain boundary migration. The densification was promoted by the slower grain boundary diffusion without promoting grain growth in second-step sintering. Unfortunately, the nanosized Al_2O_3 ceramics were not optically transparent.

By float packing and sintering in air, transparent alumina with submicrometer grains were obtained [57]. Commercial α -alumina powder with high purity, submicrometer particle size, and narrow particle-size distribution was used as starting material. The powder was dispersed and stabilized in a water-based suspension. Controlled consolidation and drying by float packing led to homogeneous green compacts, which could be densified without additives by sintering in air at 1275 °C to transparency, while the mean grain size remained to be 0.4 μm . The in-line transmittance at wavelengths of 300–450 nm was comparable to commercial polycrystalline alumina tubes for lighting technologies, whose grain sizes are larger by a factor of 40.

A method of combining injection molding and pressureless sintering in hydrogen was reported to manufacture transparent alumina ceramics [58]. Transparent alumina components with small size and high precision were fabricated in such a stable, efficient, and low-cost route. Excellent rheological properties of the feedstocks for injection molding were obtained through a method of powder pretreatment with stearic acid induced by ball milling. The average grain size of the sintered body was 30–50 nm, with no significant pores and abnormal grain growth observed. The real in-line transmission was higher and more stable than those via other forming technologies and pressureless sintering reported in the literatures.

A similar powder injection molding (PIM) was employed to produce translucent alumina brackets [59]. For PIM, alumina precursor powders were mixed with a binder consisting of a mixture of paraffin wax and polyethylene. After injection molding, debinding was performed using the wicking method. Samples were sintered in a vacuum at 1700 °C to achieve high density. Sintering aids, including MgO , La_2O_3 , and Y_2O_3 , were used to promote the densification and decrease the porosity of the final ceramics. An improvement in translucency by promoting grain growth during the pressureless sintering was observed. Vickers hardness, bending strength, density, and transmittance of the fabricated items were found to be comparable with those of the commercially available dental brackets.

Solid loading is a critical factor to the fabrication of ceramic compacts with high densities by using ceramic injection molding. Different from the traditional approaches in which stearic acid (SA) was introduced just in the powder blending process, a new strategy has been developed to prepare feedstock with a much higher solid loading, which was up to 64 vol% by using a prior ball milling treatment of the ceramic powders with a small amount of SA [60]. In this way, SA could be coated homogeneously on the powder surfaces, due to the chemical reaction induced by the ball milling treatment. Highly translucent Al_2O_3 ceramics were fabricated from the precursors.

Doping has been found to be an effective technique in fabricating transparent ceramics. MgO doping, combined with pre-sintering heat treatment, was used to accomplish a high translucency in polycrystalline Al_2O_3 ceramics sintered at 1700 °C in vacuum [61]. The concentrations of MgO were 140, 500, and 2500 ppm. A pre-sintering heat treatment was 800 °C for 50 h in air. It was found that the pre-sintering heat treatment improved the sample transmittance in the visible range (400–700 nm) significantly. This enhanced transmittance was explained in terms of the removal of residual pores and the homogenization of the microstructure, due to the lowering of the boundary mobility, as a result of the MgO addition and the suppression of local densification through the pre-coarsening step.

Wet-chemical approaches have been used to fabricate transparent alumina ceramics, which had higher homogeneous dopant distribution [62]. In this approach, alumina powder was first mixed with metal nitrates and dispersed by PEG-2000 as dispersant, and then the pH value was controlled by introducing the $\text{NH}_3 \cdot \text{H}_2\text{O}$ into the suspension to favor the precipitation of Mg^{2+} and Y^{3+} onto the Al_2O_3 matrix. It is found that the dopants were smaller in size and more homogeneously dispersed through the chemical precipitation in the translucent alumina sample as compared with those derived from conventional ball milling. The samples prepared by doping through chemical precipitation had much higher transparency.

Translucent alumina ceramics were also obtained through incorporating $\text{MgO}/\text{Y}_2\text{O}_3/\text{La}_2\text{O}_3$ additives using infiltration and gelling technique, combined with sintering in H_2 atmosphere [63]. The improved microstructural homogeneity, finer grain size, and enhanced transmission properties of infiltration processed samples over those processed by conventional ball milling method were corroborated by experimental results. Triple doping via infiltration appears to be significantly beneficial for achieving enhanced transmission. The sample with a thickness of 0.75 mm exhibited a high transmittance of 36.3 % at wavelength of 800 nm.

Advanced powder compaction technologies have been widely adopted in fabrication of transparent alumina ceramics. For example, a slip casting method was reported to create transparent alumina ceramics, with the addition of oligosaccharide alcohol to the alumina slurry [64]. Transmittance of the Al_2O_3 ceramics produced by slip casting using the slurry with both NH_4 -PMA and oligosaccharide alcohol was higher than that of the ceramics produced by using slip casting from the slurry with NH_4 -PMA alone. The increased optical property of the ceramics was

attributed to the low viscosity of the slurry, due to the addition of oligosaccharide alcohol, at a high solid content.

Sintering techniques are equally important in reducing sintering temperature and enhancing transparency of transparent ceramics. For instance, it was reported that by HIP, the sintering temperature of Al_2O_3 could be reduced to 1200–1300 °C, at which the porosity could be easily decreased to less than 0.05 % and the grain size was suppressed to be less than 1 μm [47, 50]. Similarly, an effective method was developed to fabricate Al_2O_3 ceramics with almost 100 % relative density by using HIP, which was combined with colloidal dispersion casting and a natural pre-sintering step [65]. The Al_2O_3 ceramics prepared in this way had 60 % of relative transparency for a 1 mm thick sample, which was enough to observe well-resolved pictures at several kilometers through such windows. The transparent ceramics had an average grain size of about 600 nm. The properties of transparent Al_2O_3 ceramics are also related to the characteristics of the starting Al_2O_3 powders [64].

SPS has become a popular new technique to sinter alumina ceramics. A self-doping approach, combined with SPS, was reported to prepare transparent alumina ceramics with controlled grain growth [66]. Highly transparent Al_2O_3 ceramics were obtained by using SPS from both pure and aluminum ethoxide-doped powders. It was found that the porosity was reduced in the self-doped samples, when the doping content is below 1 %. In this case, the improvement in in-line transmittance of the ceramics could be explained by considering the grain and pore size distributions.

A new trend in transparent ceramics is the presence of nanocomposite transparent ceramics. For example, transparent alumina/ceria nanocomposites have been developed by using SPS [67]. It was found that the ceria nanoparticles strongly enhanced the transparency of the SPS sintered compacts, which was attributed to at least two factors. On the one hand, the ceria nanoparticles served as powder lubricant, increasing the initial density of the powder in the SPS die by about 15 %. On the other hand, the ceria nanoparticles, have a very low solid solubility in the alumina grains, so that they were located at grain boundaries, thus hindering alumina grain growth through pinning effect. Therefore, densification could be accomplished at 1430 °C and 80 MPa for 2 min. However, this effect was found to be effective only at vacuum conditions.

Effects of the nature of the dopants, thermal pretreatment, and sintering temperature on SPS of transparent alumina have been systematically investigated [68]. A slurry of $\alpha\text{-Al}_2\text{O}_3$ was doped with Mg, Zr, and La nitrates or chlorides, with concentrations of 150–500 weight ppm and then freeze-dried to produce nanosized doped powders (~ 150 nm). The powders were sintered by SPS to yield transparent polycrystalline alumina ceramics. Transparency of the nanosized Al_2O_3 ceramics was shown to depend mainly on the way the powder was prepared, as well as the nature of the dopants. RIT values at 640 nm of the samples doped with ZrO_2 , MgO , and La_2O_3 were 40.1, 44.1, and 48.1 %, as compared to 30.5 % for pure alumina.

A two-step pressing method was reported to be able to significantly improve the optical properties of alumina ceramics with SPS at high heating rates [69]. In this case, commercial alumina powder could be consolidated at 1150 °C at a heating

rate of $100\text{ }^{\circ}\text{C min}^{-1}$. The effects of the pressure application mode were examined, in terms of microstructure, porosity, and optical transparency. Two ways of application of pressure were compared. In the first case, a constant pressure of 80 MPa was applied for the entire duration of the sintering process, which was called constant pressure. In the second case, an initial pressure of 35 MPa was applied, which was subsequently increased to a higher level, in 3 min after the beginning of dwelling time, i.e., two-step pressure. The application of two-step pressure allowed for homogeneously densified translucent alumina ceramics at a high heating rate.

The influences of SPS sintering pressure and temperature, as well as Mg, Y, and La single or co-doping with concentrations of 75–450 ppm, on the RIT and grain size of Al_2O_3 ceramics, were systematically studied [70]. Using optimized sintering parameters, RITs of >50 % could be obtained in the visible wavelength (640 nm) for 0.8 mm thick samples for almost all the different methods. The optimized doping was the triple dopant, showing a RIT of 57 % at a total dopant level of 450 ppm, which was the highest value among those processed by using SPS in the open literature. It means that a combination of doping and SPS could produce transparent Al_2O_3 ceramics with improved performances.

Microwave sintering is another new sintering technique that has been applied to transparent Al_2O_3 ceramics [71]. With no holding at the sintering temperature, microwave-sintered samples could reach 95 % density at $1350\text{ }^{\circ}\text{C}$, which was much lower than the $1600\text{ }^{\circ}\text{C}$ for conventionally heated samples. The microwave-sintered sample was almost fully densified after sintering at $1400\text{ }^{\circ}\text{C}$, while the density of the sample sintered through the conventional sintering was only about 50 %. It was also found that grain growth behavior of alumina ceramics was not affected by the way of sintering. Therefore, the enhancement in densification of Al_2O_3 by the microwave sintering was not attributed to the fast heating rate. However, the microwave densification had an apparent activation energy of $85 \pm 10\text{ kJ mol}^{-1}$, which was much lower than the value of $520 \pm 14\text{ kJ mol}^{-1}$ for the conventional sintering, implying that the densification mechanisms of the two sintering techniques are different.

Mechanical strength of transparent Al_2O_3 ceramics is closely related to their grain size and size distribution [47, 51, 72–74]. Fine-grained transparent Al_2O_3 ceramics, with high optical and mechanical properties, can be developed by using various methods and strategies, as discussed above. Mechanical strength is crucial for certain applications, such as IR windows and armors.

Besides the applications for lighting and domes, transparent nanostructured $\gamma\text{-Al}_2\text{O}_3$ ceramics have various other applications, such as a humidity sensor of $\gamma\text{-Al}_2\text{O}_3$ [75]. Nanostructured $\gamma\text{-Al}_2\text{O}_3$ ceramics were prepared from Al-Sec-Butoxide ($\text{C}_{12}\text{H}_{27}\text{AlO}_3$) by using a sol–gel process. The sensors had a long term stability of up to two years.

2.2.2 Zirconia (ZrO_2)

Zirconia (ZrO_2), with a density of 5.68 g cm^{-3} , melting point of 2715°C , and boiling point of 4300°C , has been widely used because of its exceptional mechanical and functional properties, such as high toughness, high oxygen diffusivity, and low thermal conductivity. Based on these properties, transparent ZrO_2 ceramics, especially yttria-stabilized zirconia or YSZ, have been extensively and widely investigated. The introduction of yttria can stabilize the cubic or tetragonal structure of zirconia with the presence oxygen vacancies, as shown in phase diagram in Fig. 2.2 [76]. This improves ionic conductivity and makes stabilized ZrO_2 appropriate for use as an electrolyte in solid oxide fuel cells.

Recently, polycrystalline transparent cubic yttria-stabilized zirconia (ZrO_2 -8 mol% Y_2O_3 , c-YSZ) ceramics have attracted increasing attention because of their unique combination of mechanical and optical properties [77–87]. Cubic zirconia has a refractive index of 2.2, which has never been attained in optical glasses and is higher than other oxides. Therefore, high transparencies, together with large refractive indices and high dielectric constants, make YSZ ceramics to be a new group of transparent ceramics [78, 88, 89]. Figure 2.3 shows photographs of representative YZS transparent

Fig. 2.2 Portional binary phase diagram of ZrO_2 - Y_2O_3

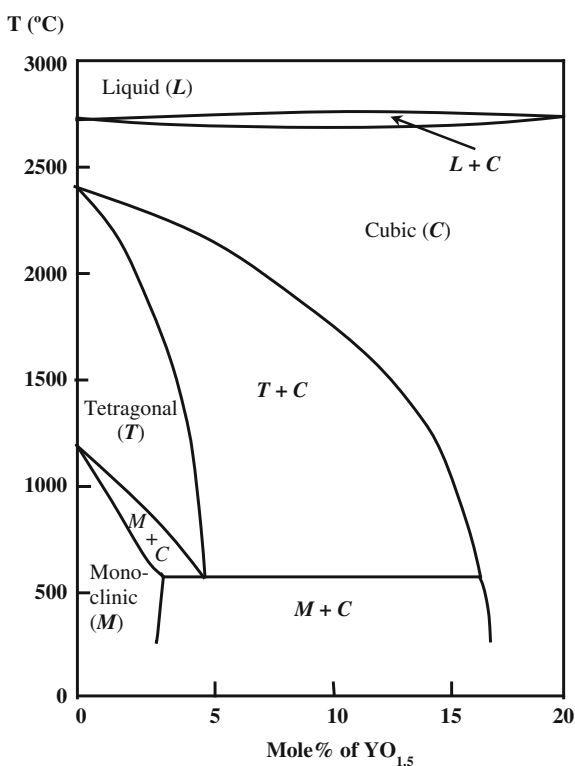




Fig. 2.3 Photographs of representative YZS transparent ceramics, which were made from commercial powder with hot isostatic pressing sintering method. Reproduced with permission from [88]. Copyright © 2008, John Wiley & Sons

ceramics, which were made from commercial powder by hot isostatic pressing sintering method [88].

Translucent cubic zirconia (15 mol% $\text{Y}_2\text{O}_3\text{--ZrO}_2$) was prepared by using a HP hot pressing technique [80]. In this report, submicron particles of monoclinic ZrO_2 , with and without stabilizing oxides of CaO or Y_2O_3 , were subjected to pressures ranging from 0.5 to 30 kbars and sintered at temperatures ranging from 1300 to 1750 °C, at heating rates of 1000 °C h^{-1} and cooling rates of 500 °C h^{-1} , so as to translucent monoclinic and cubic stabilized ZrO_2 . Samples with near theoretical density, including monoclinic $\text{ZrO}_2 = 5.61 \text{ g cm}^{-3}$, 15 mol% CaO-stabilized cubic $\text{ZrO}_2 = 5.54 \text{ g cm}^{-3}$, and 15 mol% Y_2O_3 -stabilized cubic $\text{ZrO}_2 = 5.61 \text{ g cm}^{-3}$, could be achieved by using HP hot pressing. The samples had an average in-line light transmittance of 12 %. An increase in grain size from 1 to 5 μ was observed from the center of the samples to their outer edge, due to the pressure gradients.

Translucent cubic zirconia (6 mol% $\text{Y}_2\text{O}_3\text{--ZrO}_2$) was fabricated by using the conventional sintering technique [81]. The precursor powder of high surface activity with a grain size of less than 1 μm was synthesized through simultaneous decomposition of yttrium and zirconium alkoxides. The mixed oxide powder was consolidated by calcining at 1000 °C for 30 min. High density fully stabilized 6 mol% $\text{Y}_2\text{O}_3\text{--ZrO}_2$ ceramics were obtained by sintering at 1450 °C. Translucent tetragonal zirconia (3 mol% $\text{Er}_2\text{O}_3\text{--ZrO}_2$) by the conventional sintering technique, using powders synthesized through alkoxides hydrolysis method [82]. These studies indicated that sintering process and sinterability of the starting powders are critical parameters for translucency.

Transparent polycrystalline c-YSZ could be prepared by using hot isostatic pressing (HIP) [79, 85]. It was found that TiO_2 was a good additive for developing transparent c-YSZ by using HIP, as demonstrated by the in-line transmittance curves of the ZrO_2 (10 % Y_2O_3) ceramics doped with TiO_2 [79]. The transparent ceramics were made from cubic stabilized ZrO_2 (c- ZrO_2) powder by sintering at vacuum of $1 \times 10^{-3} \text{ Pa}$ at 1650 °C for 3 h, followed by HIP treatment at 1750 °C for 1 h at a pressure of 196 MPa. Post-thermal annealing at 1000 °C was conducted to decolorize the as-sintered samples. The role of TiO_2 was regarded as a grain growth promoter and a pore scavenger. The optical properties of these zirconia

ceramics were comparable to those of their single crystal counterparts. In addition, transmission performances of the ceramics were sensitive to the microstructure of the pre-sintered compacts. Microstructural features, such as fine grains and small intergranular pores, were critical to achieve high transparency. Therefore, high sintering temperatures of HIP led to samples with large grains, which is not desirable in terms of mechanical properties [79, 85].

SPS has been shown to be better than HIP in fabricating transparent c-YSZ ceramics. For example, SPS has been used to process a nanosized cubic yttria-stabilized zirconia (ZrO_2 -8 mol% Y_2O_3) powder synthesized by using a glycine-nitrate process combined with high-energy ball milling [76]. The powder could be consolidated by using SPS at 1200–1350 °C for 5 min, while transparent ceramics could be fabricated at 1300 °C. Another example was the use of HP SPS to fabricate translucent cubic zirconia ceramics at 1000–1200 °C [89]. The total forward transmittance and in-line transmittance of the SPS samples were mainly affected by the color centers, with a limited contribution from residual pores, whereas the changes in reflectance were only related to the porosity. Because the number of color centers and the density of the residual pores increased with increasing sintering temperature, the total forward and in-line transmittances of the as-sintered zirconia ceramics were decreased.

A cost-effective technology has been reported for the development of larger quantities of transparent cubic ZrO_2 ceramics [90]. The key strategy was the application of a multistep sintering process. Yttrium-stabilized ZrO_2 powder was treated by dry pressing, together with subsequent cold isostatic pressing. The obtained ZrO_2 ceramics were reported to be comparable to perovskite ceramics, in terms of optical performance. The in-line transmittance was related to thickness of the samples. The real in-line transmissions of the unscattered transmitted light at a wavelength of 640 nm were 57 % for 4 mm thickness, 59 % for 3 mm thickness, and 65 % for 2 mm thickness, respectively. Due to the high refractive index of ZrO_2 , the reflection losses are 12 % on both surfaces. Therefore, depending on the sample thickness, the transmission of the 4 mm plate was 0.75 of the theoretical maximum, while that of the 2 mm plate was 0.85. Hardness HV10 measured at a testing load of 10 kg was up to 13 GPa, approaching the upper limit of ZrO_2 ceramics. Average grain size of the ZrO_2 ceramics was about 5 μm .

It was found that cubic ZrO_2 ceramic has relatively low mechanical strength, which is <600 MPa. In contrast, tetragonal ZrO_2 ceramics have a strength of >900 MPa. Also, nearly dense YSZ ceramics with a grain size of <100 nm can exhibit a fracture toughness of about 8 $\text{MPa m}^{1/2}$, which is higher than a typical cubic material with a toughness of 2.8 $\text{MPa m}^{1/2}$. Therefore, tetragonal ZrO_2 ceramics deserve to be further developed, especially mechanical strength is an important requirement [86, 91].

The influences of grain size and birefringence on transparency of partially Y_2O_3 -stabilized tetragonal ZrO_2 (YSZ) ceramics have been systematically studied [92]. It was confirmed that optical birefringence was the main factor that limited the transparency of tetragonal pore-free ZrO_2 ceramics. The conditions to obtain transparent tetragonal ZrO_2 ceramics (partially stabilized by yttria) have been

predicted by comparing the experimental data for sintering of nanopowder with scattering calculations. The simulations were validated well by experimental data for tetragonal ZrO_2 (3 mol% Y_2O_3) ceramics made from a powder with an initial particle size of ~ 10 nm. The sintering was carried out in air and with HIP. A maximum in-line transmission of about 77 % was observed at IR wavelengths of 3–5 μm in the samples.

It was found that tetragonal ZrO_2 ceramics with grain sizes of 50–55 nm could be obtained by using SPS, which suppressed effectively the grain growth of the nanosized powders [86]. These works further confirmed that dense tetragonal ZrO_2 ceramics are less transparent than their cubic counterparts.

Munir et al. prepared transparent tetragonal (3 mol% yttria) and cubic (8 mol% yttria) YSZ ceramics derived from nanosized powders using a pulsed electric current sintering process [78]. Both the tetragonal and cubic ceramics had an average grain size of about 50 nm. Consolidation pressure was found to show a positive effect on the transparency of both samples. Transmittances of the samples with 1 mm thickness in the near-infrared region were >60 % for the cubic 8 % YSZ and >50 % for the tetragonal 3 % YSZ ceramics, representing between 70 and 80 % of the theoretical values of the two materials. The samples had a yellowish-brown color, which was attributed to the presence of color centers. Annealing in oxygen improved the transmittance initially, but prolonged annealing resulted in translucent samples.

By using powders with very fine particles, nanocrystalline 3YSZ ceramics with grain sizes of 22–45 nm have been developed by using HIP [93]. Amorphous to nanocrystalline ZrO_2 -3 wt% Y_2O_3 powders were synthesized by using a chemical precipitation method from mixed nitrate salt solutions. The powders were cold pressed and pre-sintered in air for 2–6 h at temperatures of 1100–1300 °C. HIP was carried out at 1150–1350 °C for 2–3 h at 150 MPa in argon. Fully dense pellets with grain size of 22–45 nm were formed by application of low pre-sintering temperatures. However, these samples had a significant amount of monoclinic phase.

2.2.3 Sesquioxides

2.2.3.1 Yttria (Y_2O_3)

Y_2O_3 , as a promising optical material, has excellent physical and chemical properties, such as high melting point (2430 °C), broad range of transparency (0.2–8 μm), and high corrosion resistance, with density of 5.01 g cm^{-3} and boiling point of 4300 °C. Typical physical properties of Y_2O_3 include thermal conductivity of 13.6 $\text{W m}^{-1} \text{K}^{-1}$ at 300 K, refractive index of ~ 1.935 , density of 5.04 g cm^{-3} , and effective atomic number of 36.7 [94]. Y_2O_3 has a cubic crystal structure with group of Ia3, as shown in Figs. 2.4 and 2.5.

Due to its high effective atomic number and high density, i.e., 35 and 4.56 g cm^{-3} , respectively, Y_2O_3 could be a more effective scintillator than Yttrium

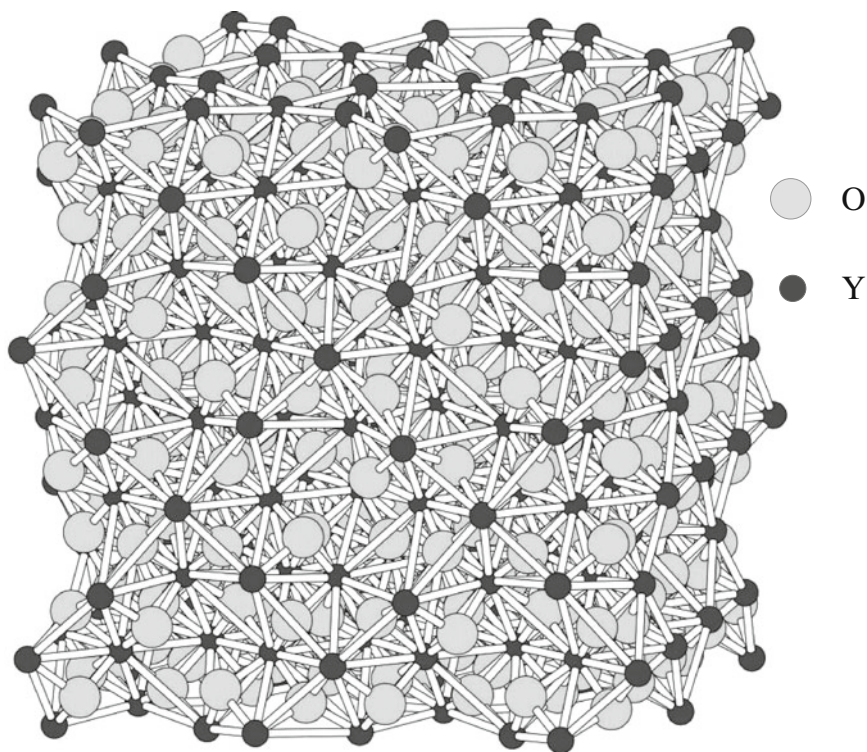
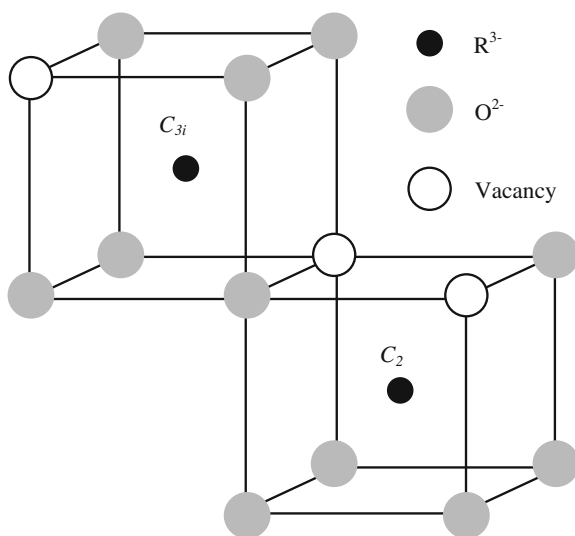


Fig. 2.4 Crystal structure of Y_2O_3 , which was created by using Electron Microscopy Software (EMS) (version 3.3111U2008)

Fig. 2.5 Crystal structure of R_2O_3 structure with the two crystallographic cationic sites C_2 and C_{3i}



aluminum garnet (YAG) [95]. Y_2O_3 possesses a higher thermal conductivity and a lower thermal expansion coefficient than the widely used YAG, which is critical for thermal management, because more heat will be generated, as laser powers continue to increase. Other potential applications of Y_2O_3 transparent ceramics include infrared domes, nozzles, refractories, components of semiconductor devices, and efficient NIR-visible upconverter [96–98]. Due to its refractory characteristics, Y_2O_3 has been mainly developed in transparent ceramics rather than single crystals. The first transparent yttria ceramic was reported about 50 years ago [99].

There have been quite a number of reports on Y_2O_3 transparent ceramics by using pressureless sintering in vacuum or in H_2 atmosphere [100–107]. One example is the preparation of transparent ZrO_2 -doped Y_2O_3 ceramics through a combined processing of vacuum sintering to fabricate from commercial power using aqueous slip casting technique [103]. Figure 2.6 shows photographs of the ZrO_2 -doped Y_2O_3 ceramics with different contents of ZrO_2 , after sintering at 1860 °C for 8 h. The samples with ZrO_2 of above 2 mol% were all highly transparent. The starting Y_2O_3 power had an average particle size of 2 μm , which was reduced to about 0.34 μm after ball milling in ethanol for 12 h. The powder with reduced particle size was beneficial for densification. It was shown that 5 mol% ZrO_2 was the optimum concentration in terms of in-line transmittance of the final ceramics. The optical properties of the ceramics were attributed to the enhanced densification and suppressed grain growth behaviors due to the presence of ZrO_2 .

Advanced sintering techniques, including HP [108, 109], HIP [110, 111], and SPS [112–116], have all been employed to obtain transparent Y_2O_3 ceramics. For example, transparent Y_2O_3 ceramics were fabricated by using HP at 1800 °C for 20 h [109]. Another example is the application of a uniaxial hot pressing to develop Y_2O_3 ceramics, at a maximum pressure of 40 MPa and a maximum temperature of 1580 °C [108]. Optical transparency could be optimized through a stepwise application of pressure. The use of SPS could reduce the processing temperature of Y_2O_3 ceramics [116]. It was reported that the samples sintered at 1300 °C and annealed at 1050 °C had a transmittance of 81.7 % at wavelength of 2000 nm. Due to the low temperature, SPS is able to control the grain growth of yttria ceramics [114]. The Y_2O_3 specimen sintered at 1050 °C for 1 h exhibited an in-line transmittance of 6–46 % in a wavelength range of 400–800 nm. Heating rate and sintering temperature could be optimized to improve the optical properties of SPS-processed Y_2O_3 ceramics [117].

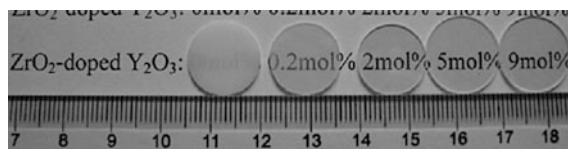


Fig. 2.6 Photographs of representative Y_2O_3 ceramics doped with different levels of ZrO_2 , processed through the combination of slip casting and vacuum sintering. Reproduced with permission from [103]. Copyright © 2010, Elsevier

Various strategies, such as use of nanosized precursor powder, introduction of sintering aids, and adoption of multiple-step sintering process, have been employed to obtain Y_2O_3 ceramics with relatively high density, small grain size, and high transparency. Wet-chemical methods, such as chemical precipitation and co-precipitation, have been widely used to synthesize pure and doped Y_2O_3 nanopowders, in order to achieve high sinterability [101, 118, 119].

An yttria nanopowder with an average particle size of 60 nm was synthesized by using a chemical precipitation process [118]. Hydroxide precursor of Y_2O_3 with an approximate composition of $Y_2(OH)_5NO_3 \cdot H_2O$ was obtained by using ammonia water as precipitant and yttrium nitrate as the starting salt. By employing appropriate striking method and optimum synthetic conditions, yttrium hydroxide with a card-house or spherical structure was formed. Normal striking-derived powders had higher sinterability than the reverse striking-derived powders. The addition of a small amount of ammonia sulfate in the yttrium nitrate solution could decrease the agglomeration and particle size of the yttria powder. Nanocrystalline yttria powders were obtained by calcining the precursor at 1100 °C for 4 h. Transparent yttria ceramics were fabricated from the nano Y_2O_3 powder by vacuum sintering at 1700 °C for 4 h, with optimized in-line transmittance of 52 % at wavelength of 1000 nm.

Various sintering aids, such as ThO_2 [105], La_2O_3 [106], HfO_2 [120], LiF [121], and ZrO_2 [122], as well as their combinations [123], have been used to fabricate transparent Y_2O_3 ceramics. The use of sintering aids led to Y_2O_3 ceramics with small grain sizes due to the reduced sintering temperatures. Doping effect could be enhanced, when combining with compaction and sintering techniques, such as slip casting, vacuum sintering [103], and sintering in oxygen atmosphere [124]. With the addition of zirconia and other additives to control the grain growth, pores could be eliminated at a temperature of <1650 °C, deriving Y_2O_3 ceramics with an average grain size of 1 μm [124].

Optical properties of Y_2O_3 ceramics, doped with rare-earth ions, are of special interest for some applications, such as solid-state lasers and scintillators [95]. Luminescence properties, such as upconversions, are also of special significance. For instance, RE/Yb co-doped Y_2O_3 transparent ceramics (RE = Er, Ho, Pr and Tm), exhibited very efficient NIR-visible upconverters [96].

Through the combination of two-step sintering and vacuum sintering, transparent lanthanum-doped yttrium oxide ceramics have been fabricated [100]. The samples were first sintered at an intermediate temperature T_1 (1450 °C) in air. Then, the temperature was decreased quickly to a lower point T_2 (900–1100 °C) in air and held for more than 20 h in order to facilitate densification with limited grain growth. Nanocrystalline yttria ceramics with a high relative density were then obtained, which could be further densified at higher temperature T_3 (1700 °C) in vacuum. The final transparent yttria ceramics doped with 10 % lanthanum, with an average grain size of about 25 μm , had a transmittance of 77 % at 580 nm. Microstructural analysis results indicated that the mean particle size of the samples after the second step was just slightly larger than that of those after the first step processing, but the relative density was over 90 %. However, because the significant shrinkage was

mainly observed in this step, pores were isolated by grains. Therefore, grain boundary diffusion was thought to be the main matter transport mechanism.

A similar two-step sintering combined with HIP was reported to fabricate Y_2O_3 ceramics with submicron grain sizes [125]. Microhardness and fracture toughness of the transparent yttria ceramics with an average grain size of $0.3\ \mu\text{m}$ made by using the modified two-step sintering were higher than those of the ones fabricated by using conventional sintering, by 25 and 70 %, respectively. The conventional processing led to ceramics with an average grain size of $\sim 300\ \mu\text{m}$. The submicron transparent yttria ceramics exhibited a transparency of single crystals in the near-infrared spectral region.

2.2.3.2 Scandia (Sc_2O_3)

Sc_2O_3 (scandia) belongs to the cubic space group $IA\bar{3}$ [126]. Its unit cell contains 16 f.u., with 32 cations that form 24 sites of C_2 symmetry and 8 sites of C_{3i} symmetry. The C_2 site is an eightfold cubic structure with two oxygen vacancies on a face diagonal, while the C_{3i} site corresponds to a cube with two vacancies on a body diagonal. The RE^{3+} dopants are assumed to occupy randomly both sites, but the induced electric dipole transitions are allowed only for C_2 centers. The cationic density ($3.338 \times 10^{22}\ \text{cm}^{-3}$) is rather high compared to other oxides. Sc_2O_3 has the smallest lattice parameter of 0.986 nm, high melting point, high bulk refractive index of $n_H = 2.0$ at $\lambda = 300\ \text{nm}$, high band gap of 5.7 eV (corresponding to an ultraviolet cutoff of 215 nm), high thermal conductivity of $17\ \text{W m}^{-1}\ \text{K}^{-1}$, and high chemical stability in alkali metal steam.

The combination of these excellent optical and thermal properties makes Sc_2O_3 attractive for applications as damage-resistant and high reflection materials in light-emitting diodes and high power pulsed ultraviolet lasers. It is also very useful as infrared transmitting devices, host materials for high power and ultrashort pulse solid-state lasers, and heat-resistant optical windows [127–133]. Due to its high melting point ($2430\ ^\circ\text{C}$), it is difficult to fabricate Sc_2O_3 single crystal. Therefore, transparent polycrystalline Sc_2O_3 ceramics are expected to be more and more important.

Vacuum sintering is the most widely used method to prepare transparent Sc_2O_3 ceramics, with nanosized precursor powders to provide additional benefit to ensure high quality of the final products [127, 128, 131–135]. Various chemical routes have been used to synthesize nanosized Sc_2O_3 powders. For example, a homogeneous precipitation method was used to synthesize nanocrystalline Sc_2O_3 powder [135]. A highly reactive Sc_2O_3 powder was made through pyrolyzing a basic sulfate precursor, $(\text{Sc}(\text{OH})_{2.6}(\text{SO}_4)_{0.2} \cdot \text{H}_2\text{O})$, at $1100\ ^\circ\text{C}$, which was precipitated from scandium sulfate solution with $(\text{CH}_2)_6\text{N}_4$ as the precipitant [127]. Similar reactive Sc_2O_3 powders were obtained through thermal pyrolysis of a scandium sulfate salt, $\text{Sc}_2(\text{SO}_4)_3 \cdot 7.8\text{H}_2\text{O}$ [131]. The Sc_2O_3 ceramics obtained by using vacuum sintering have relatively large grain sizes, due to the significant grain growth during the final stage of sintering [127, 128, 131–135].

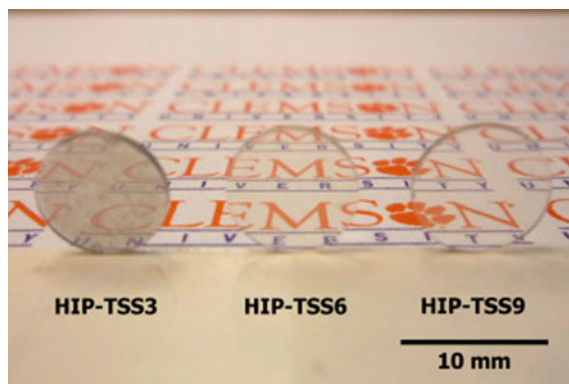


Fig. 2.7 Photographs of representative Er-doped Sc_2O_3 ceramics hot isostatic pressing two-step sintered (HIP-TSS). Reproduced with permission from [136]. Copyright © 2010, John Wiley & Sons

Pressure-assisted sintering techniques have been used to develop transparent Sc_2O_3 ceramics with smaller grain sizes. For example, HIP was used to fabricate erbium-doped transparent Sc_2O_3 ceramics with an average grain size of $0.3\ \mu\text{m}$, from solution-derived nanoparticles, using a two-step sintering process [136]. The two-step sintered ceramics showed a remarkable decrease in grain size with relative density of over 98 % before HIP. After HIP, the Sc_2O_3 ceramics became highly transparent with negligible grain growth. The samples exhibited an optical transmittance of about 80 %. Photographs of representative Sc_2O_3 ceramics are shown in Fig. 2.7.

Spectroscopic properties of Sc_2O_3 ceramics doped with various ions are attractive for different applications. For instance, spectral characteristics of Ho^{3+} : Sc_2O_3 transparent ceramics have been analyzed in detail [126]. Spectroscopic parameters, including JO intensity parameters, oscillator strengths, radiative transitions probabilities radiative lifetimes and branching ratios, were obtained. Intensity parameters of Tm^{3+} doped transparent Sc_2O_3 ceramics as laser materials have also been reported. They are potential candidates for applications in diode-pumped solid-state laser, emitting at about $2\ \mu\text{m}$ [17]. Crystal field analysis of Er^{3+} in Sc_2O_3 transparent ceramics has been made, which was compared with rare-earth ions in Y_2O_3 [137].

2.2.3.3 Lutetia (Lu_2O_3)

Lu_2O_3 (lutetia) has a cubic crystal structure, with a representative structure shown in Fig. 2.8. It is an attractive host material for various activators because of its wide band gap and favorable properties, such as phase stability, low thermal expansion, and chemical stability. In particular, Lu_2O_3 is the one with the highest doping concentration of Yb^{3+} , while maintaining high heat conductivity, due to the

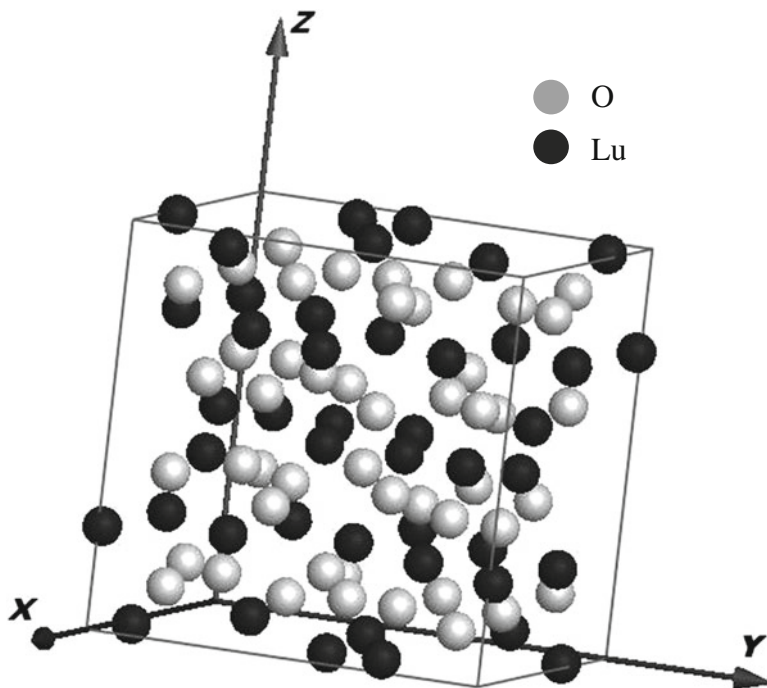


Fig. 2.8 Crystal structure of Lu_2O_3 , which was created by using Electron Microscopy Software (EMS) (version 3.3111U2008)

comparable mass and ionic radius between Lu^{3+} and Yb^{3+} [138]. The superiority of Lu_2O_3 to Y_2O_3 is its high density of $\sim 9.42 \text{ g cm}^{-3}$, as well as the high Z number of Lu (71), which makes Lu_2O_3 to have an exceptionally high stopping power for ionizing radiation. Lu_2O_3 ceramics doped with Nd or Yb are promising high power ceramic laser materials. Europium-doped Lu_2O_3 ceramic scintillator can find applications in digital X-ray imaging technology, due to its high density resulting in high stopping power, efficient X-ray to visible light conversion of up to 90,000 photons MeV^{-1} [16], and visible emission at $\sim 600 \text{ nm}$ coupling well with the silicon CCD spectral response [16, 139]. The use of an optically transparent scintillator screen requires high transparent Lu_2O_3 : Eu to avoid excess background noise, loss of resolution, and scatter-induced ghosting.

A co-precipitation method was used to synthesize Lu_2O_3 ultrafine powder, which could be used to fabricate transparent ceramics [12]. Eu-doped Lu_2O_3 powder was prepared by using ammonium hydroxide ($\text{NH}_3 \cdot \text{H}_2\text{O}$) and ammonium hydrogen carbonate (NH_4HCO_3) as mixed precipitant, from solutions of nitrate salts. The precipitates were calcined at 1000°C for 2 h, which was the optimized condition to



Fig. 2.9 Representative photographs of mirror-polished 5 % Eu³⁺-doped Lu₂O₃ ceramics sintered at 1850 °C for 6 h, with thickness of 1 mm. Reproduced with permission from [12]. Copyright © 2006, John Wiley & Sons

obtain precursor powder with high dispersity and desired sinterability. Highly transparent polycrystalline Eu-doped Lu₂O₃ ceramics with a relative density of ~99.9 % were developed by using pressureless sintering in flowing H₂ at 1850 °C for 6 h without any additives. The final ceramics with grain sizes of 50–60 μm exhibited optical transmittance in the visible light region of 600–800 nm with a thickness of 1 mm reached 80.3 %. Figure 2.9 shows photographs of representative Eu-doped Lu₂O₃ ceramics.

HIP has been combined with vacuum sintering to fabricate Eu:Lu₂O₃ ceramics with high performances [15]. Nanosized precursor powder, synthesized by using a co-precipitation method, was first uniaxially pressed and sintered under high vacuum at temperatures of 1575–1850 °C to reach relative densities of 94–99 %. The sintered compacts were then subjected to reach full density by using HIP, which resulted in highly transparent ceramics without the need of further air annealing. The Eu:Lu₂O₃ ceramics showed about four times higher light yield than commercially used scintillating glass, indicating that transparent ceramics could be used for high-energy radiography devices with improved performances. Vacuum sintering above 1650 °C led to rapid grain growth prior to densification, so that the pores were immobile. Sintering between 1600 and 1650 °C resulted in closed porosity. Because the grains were fine, the pores were mobile during the subsequent HIP step. As a result, fully dense Eu:Lu₂O₃ transparent ceramics could be prepared without the requirement of subsequent air annealing.

Transparent Lu₂O₃ ceramics have also been produced by using SPS from commercial powders [138, 140]. Sintering conditions, such as sintering temperature, pressure, and holding time, all have effects on the density and optical properties of the final ceramics. It was found that transparency of the Lu₂O₃ ceramics could be further improved by using a two-step pressure profile, combined with a low heating rate [138]. The effects of preload pressures from 10 to 100 MPa and heating rates from 0.03 to 1.67 K s⁻¹ on microstructures and optical properties of the materials were investigated. The samples obtained at a preload pressure of 30 MPa at a heating rate of 0.17 K s⁻¹ had transmittances of 60 % at 550 nm and 79 % at 2000 nm, showing a significant improvement in optical properties.

2.2.4 Magnesia (MgO)

MgO has a cubic crystal structure, as shown in Fig. 2.10. MgO ceramics have excellent thermal and mechanical properties with a high melting point of 2850 °C and low density of 3.58 g cm⁻³. It has an isotropic cubic crystal structure, which meets one of the requirements to be transparent. Polycrystalline infrared-transparent MgO is a potential substitute for sapphire IR windows and protectors for sensors. Due to the high sintering temperature required for full densification of MgO, fabrication of transparent MgO ceramics is still a challenge. Almost all techniques discussed above have been used to prepare transparent MgO ceramics [3].

LiF is a popular sintering aid for the fabrication of transparent MgO ceramics. One example is the development of transparent MgO ceramics from commercial powder [4]. The commercial MgO powder had very high purity, high surface area, fine crystallites, and low aggregation. LiF suspended in 2-propanol was added to the nano-MgO powder at content levels of 2 and 4 wt%. After compaction, the pellets were burnout binder and then were loaded in a graphite die for hot pressing carried out in Ar at 45 MPa, at heating rates of 3 or 10 °C min⁻¹. Figure 2.11 shows photographs of representative samples of the transparent MgO ceramics.

The addition of LiF as sintering aid could reduce the sintering temperature of MgO transparent ceramics [141, 142]. It has been acknowledged that densification

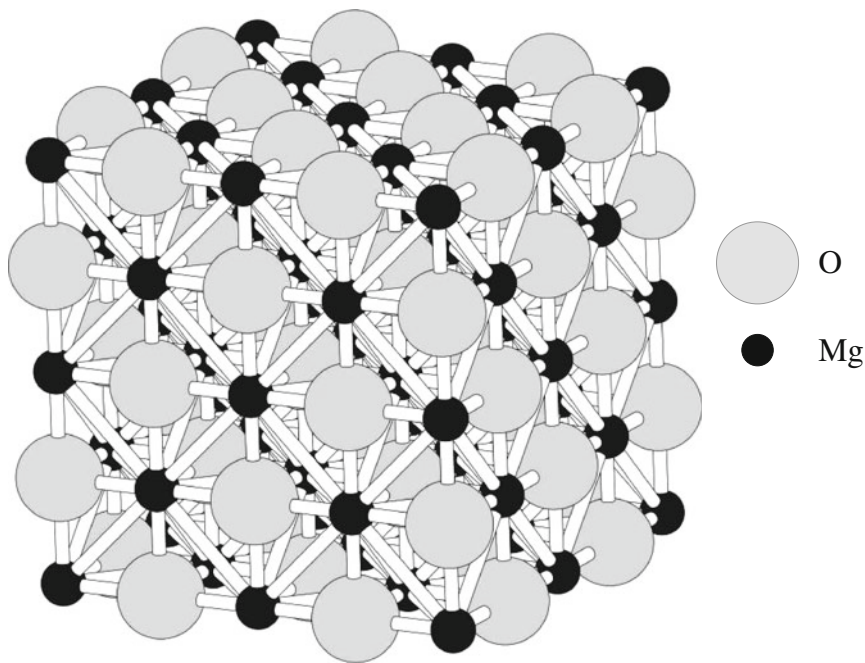


Fig. 2.10 Crystal structure of MgO, which was created by using Electron Microscopy Software (EMS) (version 3.3111U2008)

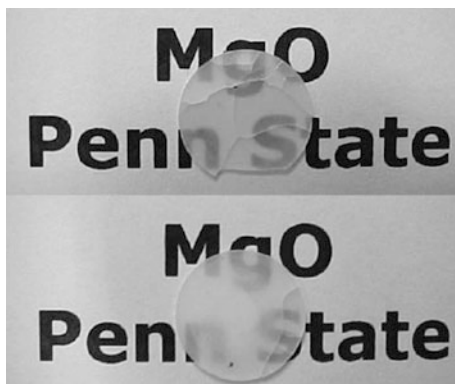


Fig. 2.11 Photographs of representative as-annealed MgO ceramics fabricated through hot pressing of the nano-MgO powder containing 4 % LiF at 1100 °C for 1 h in Ar, with sizes of 12.7 mm in diameter and 0.5 mm in thickness. Reproduced with permission from [4]. Copyright © 2004, Elsevier

of MgO with LiF was enhanced due to the formation of a liquid phase, which acted initially as a lubricant for the rearrangement of the MgO particles and later as a material transport medium to support pressure-enhanced liquid phase sintering [143].

Although sintering aids can be used to reduce the sintering temperature of MgO, they could have negative effects on the intrinsic properties of MgO. It was demonstrated that transparent MgO ceramics could be at 1600 °C by a HIP technique, without using sintering aids [144]. Before HIP, MgO compacts were obtained by using pressureless sintering. A nonagglomerated MgO powder with an average primary particle size of 57 nm was used as precursor. The relative density and average grain size of MgO compact pressureless sintered at 1600 °C for 5 h were 96.7 % and 10.7 μm , respectively.

Transparent MgO ceramics have also been fabricated by using SPS [1]. As-received commercial powder was put into graphite die with an inner diameter of 12 mm, and prepressed to 150 MPa before heating. The pressure was then reduced to 10 MPa during the heating procedure. The pressure was increased to 100 MPa within 20 s upon reaching the final sintering temperature. The sintering was conducted at that temperature for 5 min hold. Lower sintering temperatures were used, when a high pressure of 150 MPa was applied for 3 and 5 min during the sintering. With SPS, fully dense optically transparent MgO ceramics from nanocrystalline powders could be produced at 800 °C and 150 MPa for 5 min.

A simple pressureless sintering was applied to MgO transparent ceramics [3]. The powder used in this study was synthesized by using a chemical precipitation method. Magnesium nitrate hexahydrate ($\text{Mg}(\text{NO}_3)_2 \cdot 6\text{H}_2\text{O}$, 98 % purity), ammonium hydrogen carbonate (NH_4HCO_3), and ammonium hydroxide (NH_4OH , 28.0 %) were used the precipitation. The precipitate was aged for 24 h, before centrifugation, washing, and drying. The dried powder was then calcined at various temperatures for 2 h. The powder calcined at 700 °C for 2 h was used to obtain

MgO ceramics. The MgO green bodies were sintered at 1400 °C for 2 h in ambient atmosphere. The as-sintered MgO ceramics had a relative density of 98.1 % with an average grain size of 6 μm and an average hardness of 6.8 GPa [3].

2.3 Complex Oxides

2.3.1 Garnet

Yttrium aluminum garnet ($\text{Y}_3\text{Al}_5\text{O}_{12}$ or YAG) is a crystalline material of the garnet group. It is also one of the three phases of yttria–aluminum compounds, while the other two are yttrium aluminum monoclinic (YAM) and yttrium aluminum perovskite (YAP), as illustrated in the binary phase diagram of Y_2O_3 and Al_2O_3 in Fig. 2.12. YAG has a cubic crystal structure and belongs to the isometric crystal system [145]. Crystal structure of YAG with the three cationic sites, i.e., dodecahedral, octahedral, and tetrahedral, is schematically shown in Fig. 2.13, while a more comprehensive crystal structure is illustrated in Fig. 2.14.

Due to the centrosymmetric cubic crystalline structure, its optical properties are isotropic. Owing to its high thermal stability, stable chemical properties, and unique homogenous optical properties, transparent YAG ceramics are not only an important high-temperature structural material, but also an excellent host material for

Fig. 2.12 Phase diagram of Y_2O_3 and Al_2O_3 with the formation of YAG phase

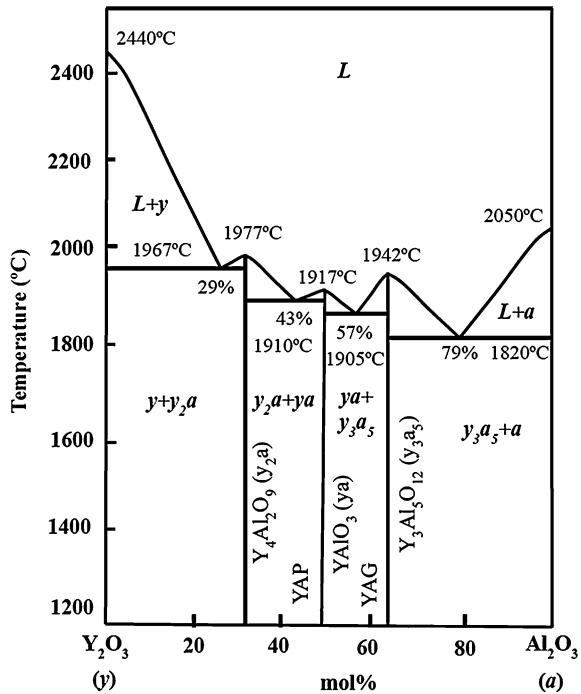
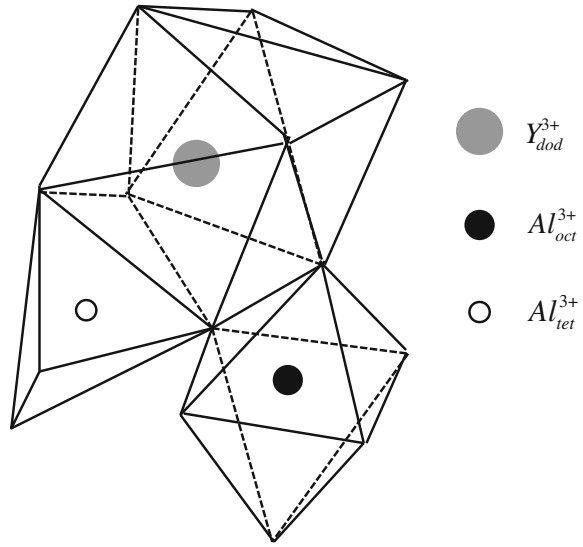


Fig. 2.13 Crystal structure of YAG with the three cationic sites: dodecahedral, octahedral, and tetrahedral



fluorescence application and high power solid-state lasers [146]. Nd- and Er-doped YAG ceramics are typical laser materials. Ce-doped YAG (Ce:YAG) is used as phosphor in cathode ray tubes and white light-emitting diodes and as scintillator. Since the first report on transparent polycrystalline Nd:YAG ceramics for laser media by Ikesue et al. [147] in 1995, extensive attentions have been paid to the development and fabrication of YAG ceramics [148].

Solid-state reaction (SSR) has been widely used to fabricate transparent polycrystalline YAG ceramics. The most cost-effective SSR is the use of commercial oxide powders. For example, mixture of commercial α -Al₂O₃ and Y₂O₃ powders, together with tetraethoxysilane (TEOS) and MgO as sintering aids, was used as precursors to prepare transparent YAG ceramics through SSR [149]. The mixture was made by using ball milling. The milled mixture was dried and compacted. Pressed samples were sintered from 1500 to 1750 °C in vacuum. Figure 2.15 shows XRD patterns of the green body (YAG composition, Y:Al = 3:5) after vacuum sintering at different temperatures for 10 h. As stated earlier, the Al₂O₃–Y₂O₃ system experienced three phases during the reaction or reactive sintering, i.e., monoclinic phase (YAM, Y₄Al₂O₉), perovskite phase (YAP, YAlO₃), and cubic phase (YAG, Y₃Al₅O₁₂). Phase compositions and formation temperature ranges for each composition are described as follows:



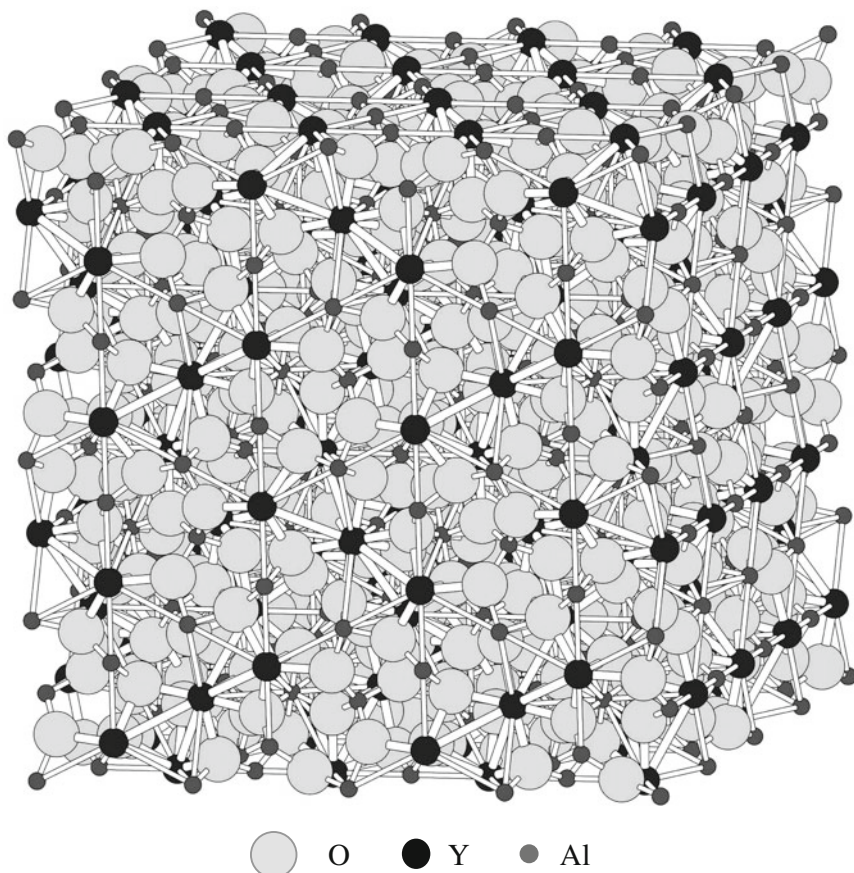


Fig. 2.14 A schematic of crystal structure of YAG, which was created by using Electron Microscopy Software (EMS) (version 3.3111U2008)



Undoped YAG transparent ceramics are usually prepared by using vacuum sintering, HP, and SPS. A YAG precursor powder was synthesized through a co-precipitation method using ammonium hydrogen carbonate as precipitant, which could be used to develop transparent YAG ceramics by using vacuum sintering at 1700°C for 1 h [150]. With the mixture of Y_2O_3 and Al_2O_3 commercial powders, YAG transparent ceramics could be obtained by using HP at 1750°C for 4 h at a pressure of about 300 atm [151]. SPS was applied to fabricate YAG transparent ceramics at 1400°C for 3 min starting from nanocrystalline YAG powders [23]. In this case, fully dense and transparent polycrystalline cubic YAG ceramics with micrometer grain sizes were obtained. Nanosized YAG transparent ceramics have also been developed by using HP sintering process [152]. The nanostructured YAG

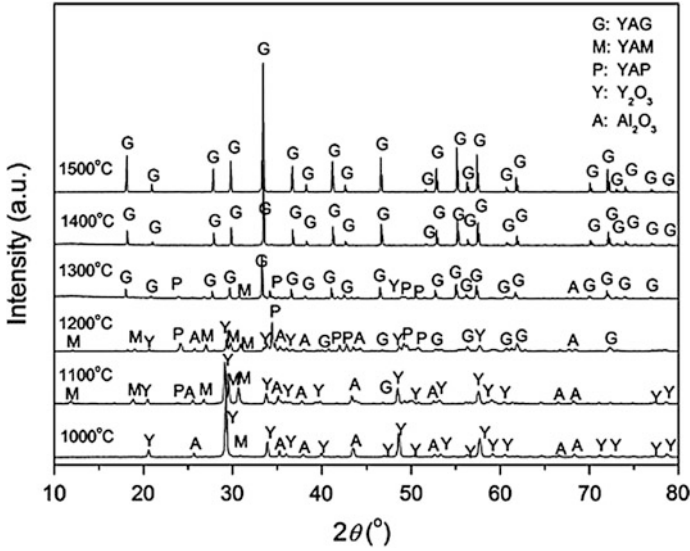


Fig. 2.15 XRD patterns of the samples for the preparation of YAG sintered at temperatures of 1000–1500 °C for 10 h. Reproduced with permission from [149]. Copyright © 2014, Elsevier

compacts were prepared at high pressure and modest temperature, or HPMT, 2.0–5.0 GPa and 300–500 °C. Prior to sintering, pellets were also heat treated in vacuum. After the samples were treated at 2.0–5.0 GPa and 300–500 °C for 30 min, the pressure was reduced to ambient pressure, and then the samples were quenched to room temperature at a cooling rate of ~ 15 °C min⁻¹. The temperature was found to be sufficiently low to prohibit the grain growth of the YAG ceramics, which is beneficial for improvement in mechanical properties.

For practical laser applications, YAG ceramics should be doped with different elements. For example, highly transparent polycrystalline Er³⁺:Y₃Al₅O₁₂ (Er:YAG) ceramics with concentrations of Er³⁺ ion from 1 to 90 % were prepared by the SSR and the vacuum sintering technique [153]. In-line transmittances of mirror-polished Er:YAG ceramics were all up to 84 % at 1100 nm wavelength, which were attributed to high density of the samples.

A two-step sintering process was developed to synthesize Nd:YAG ceramics [154]. In this two-step sintering process, the furnace temperature was first arisen to a higher temperature T_1 (1800 °C), at a heating rate of 10 °C min⁻¹, and then the temperature was rapidly decreased to a certain sintering temperature T_2 (1550–1750 °C) for 1–8 h in a vacuum graphite tube furnace at 1.0×10^{-3} Pa during the holding process. The transparent ceramics prepared by using this method exhibited pore-free and homogeneous microstructure, with transparency of up to 84.98 % at the visible and near-infrared band and 87 % in the mid-infrared wavelength range. The absorption cross section of a 0.3 % Nd:YAG sample at 808 nm was 5.47×10^{-20} cm², while the emission cross section at 1064 nm was 4.66×10^{-19} cm².

To achieve full density and highest transparency, YAG ceramics have also been prepared by using sintering aids [155–159]. MgO is one of the most effective sintering aids to produce Nd:YAG ceramics [160]. The addition of small amount of MgO could reduce the degree of agglomeration and particle size of the Nd:YAG precursor powders. The MgO doped Nd:YAG powders possessed better dispersion characteristics as compared with the undoped powders. The sample with 0.01 wt% MgO were of spherical particles of 100 nm in diameter. The well-dispersed precursor powders resulted in ceramics with homogenous microstructure. Optimized ceramic samples exhibited transmission of 82.6 % at the wavelength of 1064 nm, which was comparable to that of Nd:YAG single crystals. La_2O_3 is another effective sintering aid for Nd:YAG ceramics [156]. The addition of 0.8 wt% La_2O_3 was at optimized concentration, which led to Nd:YAG transparent ceramics having the highest transmittance in the wavelength region from 400 to 1100 nm.

Co-doping with MgO + SiO_2 has been found to be a promising technique to improve the sinterability of YAGs [161, 162]. By optimizing the concentrations of the dopants, transparent YAG ceramics with desired optical properties can be readily achieved. For example, the Nd:YAG ceramic samples with 0.4 wt% TEOS as the precursor of SiO_2 combined with 0.08 wt% MgO possessed the highest transparency at 1064 nm [162]. It was also found that the function of SiO_2 was to eliminate pores and remove secondary phases, while MgO contributed to homogeneous microstructure of the ceramics, which has been confirmed by scanning electron microscopy (SEM) analysis results [157].

It is well known that the sinterability of a ceramic precursor powder is highly dependent on various characteristics, such as particle size, size distribution, morphology, and degree of agglomeration. This is also applicable to YAG transparent ceramics [163, 164]. The effect of powder properties on the densification and performance of YAG transparent ceramics has been systematically studied [165]. It was observed that the YAG ceramics derived from nanosized powder exhibited higher optical transparency, due to their smaller grain size and less residual pores. The properties of precursor powders could be also modified by adjusting pH values when using co-precipitation method [164]. pH values could affect the performance of the final Nd:YAG ceramics by influencing the morphology as well as the (Nd + Y):Al mole ratio of the powders. Optimized pH values were found in the range of 7.9–8.2.

If the (Nd + Y):Al molar ratio was much lower than 0.6, superfluous Al_2O_3 was present, while it was much higher than 0.6, superfluous Y_2O_3 was present which led to intermediate phases (YAP and YAM). The powders prepared within the range of pH value of 7.9–8.2 had (Nd + Y):Al molar ratio very close to 0.6 (0.598 and 0.603). In this case, no secondary phases were observed and fully dense Nd:YAG ceramics with homogeneous microstructures were obtained. The conclusion was further confirmed by the cross-sectional SEM analysis. The fracture styles of samples with (Nd + Y):Al molar ratios of 0.576 and 0.648 are both intracrystalline, because secondary phases and pores in them enhanced strength of the grain boundaries. In contrast, the samples from the powders with ratios of 0.598 and

0.603 possessed pore-free microstructure and clean grain boundaries, thus having intergranular fracture behavior.

Other technologies used to further improve the quality of precursor powders of transparent YAG ceramics include spray drying [166, 167] and freeze-drying [168, 169]. High purity Al_2O_3 , Y_2O_3 , and Nd_2O_3 powder mixture was processed using spray drying technology. Polyvinyl butyral (PVB) was used for granulation of the powders and inhibition of the compositions segregation. The effect of the addition of PVB (0, 1, 2, and 3 wt%) on the morphologies and compositions of the spray-dried powders was evaluated. The powder with 2 wt% PVB after calcination at 1000 °C for 2 h led to Nd:YAG transparent ceramics. Figure 2.16 shows photographs of representative samples of the Nd:YAG transparent ceramics [167].

It has been demonstrated that freeze-drying could play an important role in the synthesis of high quality Nd:YAG nanosized powders [169]. Submicronic neodymium-doped YAG ($\text{Y}_3\text{Al}_5\text{O}_{12}$) powder was synthesized from freeze-dried precursors. The powder calcined at 1200 °C, with small crystallite size and the lowest amount of organic residues, showed the highest sinterability. With these powder, although color centers were detected by transmission, transparent ceramics were obtained after a vacuum sintering at 1700 °C for 3 h and completed with a HIP treatment at 1700 °C, 160 MPa of Ar for 90 min.

Optical properties of rare-earth doped YAG ceramics are important requirements for practical applications, which has been a subject of numerous studies in the literature [170–176]. For example, thermal annealing had a strong effect on optical properties of Cr-doped YAG ceramics [170]. After annealing at high temperatures, the absorption intensity was increased and the two peak wavelengths shifted from 430 to 600 nm to approximately 465 and 612 nm, respectively, which could be attributed to valence changing from Cr^{3+} to Cr^{4+} . The presence of Cr^{4+} ion was confirmed by emission measurement.

The application of transparent Ce:YAG ceramic phosphors for white LED has been reported widely. For instance, the Ce:YAG ceramics had a broad emission band peaked at 530 nm due to the 5d-4f transition of Ce^{3+} [172]. The transmittances of the samples were 70–87 % at 800 nm. The absorption coefficient and emission intensity of Ce^{3+} were increased with increasing sample thickness. Under 465 nm LED excitation, the color coordinates of the Ce:YAG ceramics shifted from blue

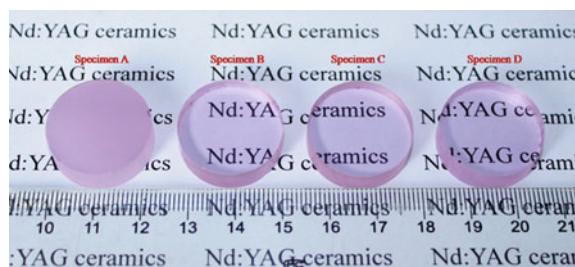


Fig. 2.16 Photographs of representative samples of the Nd:YAG transparent ceramics. Reproduced with permission from [167]. Copyright © 2012, Elsevier

region to yellow region with increasing sample thickness, passing nearby the theoretical white point in the chromaticity diagram. The highest value of luminous efficacy of the ceramic white LED was 73.5 lm W^{-1} . The LED's current dependence of luminous efficacy and luminous intensity for a 0.632 mm thick sample under 465 nm LED excitation has been studied. The luminous efficacy was decreased from 74 to 44 lm W^{-1} , while the luminous intensity was increased from 100 to 1550 mCd with increasing current.

When studying optical properties of transparent $\text{Eu}^{3+}:\text{Y}_3\text{Al}_5(1-x)\text{Sc}_{5x}\text{O}_{12}$ ceramics, a reduced peak splitting of Eu^{3+} for $^5\text{D}_0\text{--}^7\text{F}_1$ and $^5\text{D}_0\text{--}^7\text{F}_2$ was observed when 10 at.% Al_{31} was substituted by Sc_{31} [173]. The enhanced symmetry of the Eu sites in YAG lattice, which resulted from the expanded YASG lattice due to the Sc_{31} doping, was the main reason for the reduced peak splitting.

Other garnets, such as $\text{Lu}_3\text{Al}_5\text{O}_{12}$ (LuAG) and $\text{Tm}_3\text{Al}_5\text{O}_{12}$ (TmAG), have emerged as new members of transparent ceramics of garnet family [177–186]. Yb:LuAG laser ceramics with different Yb^{3+} doping concentrations were fabricated by using a solid-state reactive sintering method [182]. SEM results demonstrate that the samples had a dense and pore-free microstructure. According to the spectroscopic studies, the ceramics exhibited a large emission cross section of $2.7 \times 10^{-20} \text{ cm}^2$ at 1030 nm emission peak. CW laser operation of the samples generated 7.2 W output power with 65 % slope efficiency.

2.3.2 Spinel (MgAl_2O_4)

The crystal structure of magnesium aluminate “spinel” (MgAl_2O_4) is based on an FCC close-packed oxygen sublattice, in which a fraction of the octahedral and tetrahedral sites is filled. It is characterized by magnesium ions tetrahedrally coordinated with oxygen and aluminum octahedrally coordinated with oxygen. A unit cell contains 32 oxygen ions, 16 octahedral cations, and 8 tetrahedral cations, as shown schematically in Fig. 2.17. The polycrystalline structure of the magnesia spinel is optically isotropic. Magnesia spinel undergoes no polymorphic transformations and hence is devoid of any thermally induced phase changes.

Spinel is transparent to electromagnetic radiation from the ultraviolet through the mid-infrared (0.2–5.5 μm) [187–189]. Spinel has a distinct transmission advantage over sapphire and AlON in the range of 4.5–5.5 μm , a region of particular importance for seeker and electro-optic imaging systems. The combination of unique optical and mechanical properties makes spinel one of the most outstanding optically transparent ceramics. Figure 2.18 shows photographs of two spinel ceramics without and with sintering aid of LiF, which were processed by using SPS [190].

Given its high strength and excellent transmittance properties up to the mid-IR wavelength, spinel is a very attractive material to manufacture high performance optical components, such as lenses, IR windows, and domes. Very good UV-VIS and medium wavelength IR transparency coupled with high hardness and high resistance

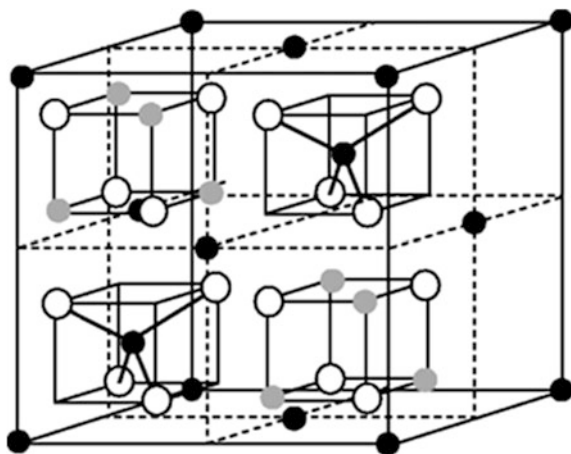


Fig. 2.17 Crystal structure of MgAl_2O_4 spinel, *filled black circles*—Mg site, *filled gray circles*—Al site, and *open circles*—O site

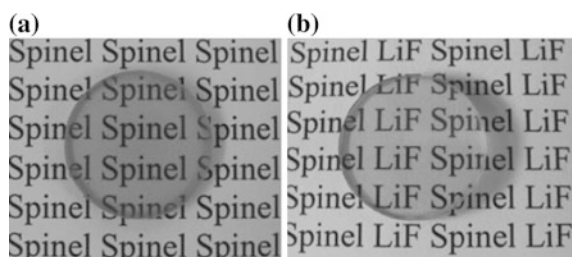


Fig. 2.18 SPS processed spinel ceramics: **a** undoped sample fabricated at sintering temperature of 1300°C , at heating rate of 2°C min^{-1} for 30 min, applied pressure of 63 MPa, and thickness of 2 mm, **b** 1.0 wt% LiF-doped sample fabricated at sintering temperature of 1400°C , with heating rate of $15^\circ\text{C min}^{-1}$, for 120 min, and thickness of 2 mm

to erosion make spinel an excellent material for protective windows for aircraft, ship, and submarine IR sensors, as well as missile domes. Spinel is also very promising for applications as windows or windshields for military vehicles such as large and bulletproof windows, due to its mechanical and ballistic properties [191].

Since it was shown to be transparent in early 1960s, spinel has received considerable worldwide attention [192, 193]. Transparent spinel is difficult to fabricate directly from high purity precursor powders by using the conventional pressureless sintering techniques [192–194]. Therefore, it is necessary to use HP, HIP, or SPS [193, 195–202]. By the way, fine precursor powders, together with sintering aids, such as B_2O_3 [203], CaO [192], and LiF [204], have been shown to be very helpful in developing transparent spinel ceramics.

It was reported that by using a combination process of pre-sintering and HIP, fine-grained highly transparent spinel ceramics could be obtained from powders

with a wide range of properties [205]. Clear transparent components with a thickness of up to 20 mm and lateral dimensions up to 240 mm were manufactured equally successfully from both the spinel powders with lower specific surface areas and the nanosized powders. Recently, a similar process was developed to fabricate spinel ceramics with large-scale production [206].

A similar two-step process, i.e., HP followed by HIP, has been used to prepare optically transparent polycrystalline spinel ceramics [193, 195]. The effect of HP temperature on optical properties of the final ceramics HIP sintered at 1900 °C for 1 h under a pressure of 189 MPa was studied. Three HP temperatures, 1400, 1450, and 1500 °C in vacuum of 10^{-2} Pa for 1 h at 50 MPa, were examined. The sample HP pre-sintered at 1400 °C had the maximum transmittance of over 60 and 70 % in the UV-visible and near-IR wavelength regions, respectively. The light transmittance was well correlated with the microcracked grain boundary surface area per unit volume of the samples.

Very recently, SPS has been proved to be an alternative technique for the fabrication of fine-grained transparent spinel. Several studies have been conducted for enhancing the transparency by using additives [199], controlling heating rates [197, 202], or applying two-step pressure profile during sintering [196]. Although the transparency of the spinel fabricated by SPS is lower than that by HIP at present, an improvement for higher transmission can be made in SPS by controlling the sintering parameters such as pressure, temperature, heating rate, atmosphere, and powder preparation.

A commercial magnesium aluminate powder could be made into transparent ceramics by using SPS, at the low heating rate of $10\text{ }^{\circ}\text{C min}^{-1}$, with LiF as sintering aid, [199]. The presence of 1 wt% LiF dopant affected dramatically the spinel morphology, which caused the formation of large well-defined grains and thus eliminated residual boundary phases. Therefore, relatively high levels of light transmission could be achieved in this way.

In a separate study, the densification of a fine-grained high purity spinel was realized for only 20 min at a low temperature of 1300 °C without any sintering aids. For heating rates $<10\text{ }^{\circ}\text{C}\cdot\text{min}^{-1}$, the spinel exhibits an in-line transmission of 47 % for a visible wavelength of 550 nm and a fracture strength of >500 MPa. The high in-line transmission can be explained by lower residual porosity ($<0.5\%$) [197].

Preheating the precursor powder is a useful strategy to enhance the transparency of spine ceramics processed by using SPS [201]. The commercial MgAl_2O_4 spinel powder had a purity of $>99.97\%$ and an average particle size of $0.36\text{ }\mu\text{m}$. The as-received powder was heated at 800–1100 °C for 3 h in air and before subject to SPS processing. Preheating at 1100 °C had almost no influence on final density of the ceramics, while the particle growth during the preheating led only slight increase in grain size, because of the large particle size of the starting powder. Preheating at lower temperatures of $\leq 1000\text{ }^{\circ}\text{C}$ had less effect on the microstructure, and preheating at higher temperatures of $\geq 1200\text{ }^{\circ}\text{C}$ made it impossible to obtain transparent spinel with large grain sizes. Therefore, 1100 °C was the optimized preheating temperature.

Both the pressure sintering and SPS have the problem of contamination [197, 199]. It has been shown that graphite contamination has a negative effect on the optical properties of transparent spinel obtained by SPS [207]. They found that residual porosities and second-phase graphite particles had a strong negative influence on in-line transmittance of the ceramics. The carbon contamination was proposed to be arisen from a CO-containing residual atmosphere during the SPS experiments, because of the graphite configuration of the equipment. During SPS, a rotary pump was used to generate vacuum in which the residual gases gave rise to an atmosphere containing CO_2 . Such an atmosphere infiltrated the porous body at the beginning of sintering and CO_2 was possibly reduced to CO at high pressure within the shrinking pores, which was finally carbonized into particles. The presence of such carbon particles made the in-line transmittance to be less than theoretical value of single crystalline MgAl_2O_4 . Therefore, special carefulness should be taken when using pressure-aided techniques to fabricate transparent ceramics and more systematic studies should be carried out on this important issue.

Because the performance of spinel windows is also very sensitive to the quality of the precursor materials (both purity and morphology), there have been researches that can be found in the open literature. To produce better spinel precursor powders, various methods have been developed. For example, a new method has been used to synthesize spinel powders from boehmite, in which Mg^{2+} ion was metal exchanged onto the surface of boehmite particles [208]. In this method, particle size, size distribution, purity, and stoichiometry of the Mg-doped boehmite powders could be well controlled. Such powders exhibited good sinterability and resulted in spinel ceramics with desired optical properties.

Fine precursor powder has been synthesized by using flame spray pyrolysis to prepare, in order to prepare high quality spinel transparent ceramics [209]. The powder possessed excellent sinterability, allowing the attainment of very high densification levels after the pre-sintering stage at 1400°C . HIPing is necessary to attain high transparency for thickness of >2 mm. The minimal HIPing conditions (for a reasonable transparency are for specimens sintered at 1400°C for 80 h). A low-temperature HIP processing, 1500°C , 3 h and 200 MPa, led to 2 mm thick samples with a real in-line transmission of 63 % at 635 nm. The samples had an average grain size of 2.2 μm and a hardness of 13.2 GPa.

An alternative method, by using $\text{Mg}(\text{OH})_2$, $\gamma\text{-Al}_2\text{O}_3$ and AlOOH , toward the direct production of transparent MgAl_2O_4 ceramics, was reported [210]. The samples derived from the mixture of $\text{Mg}(\text{OH})_2$ and $\gamma\text{-Al}_2\text{O}_3$ under optimized processing conditions showed in-line transmittances of 84.2 ± 1.0 % at 550 nm, with thicknesses of 3.5–4 mm. Typical mechanical properties observed in the ceramics included Knoop hardness of ~ 12 GPa, elastic modulus of ~ 280 GPa and biaxial flexural strength of 85–136 MPa. There was a slight difference between $\gamma\text{-Al}_2\text{O}_3$ and AlOOH as the precursor components.

A simple reactive method named self-heat-sustained (SHS) technique employing metallic aluminum as one of the reactants to produce very high phase-purity magnesium aluminate powder under rather mild experimental conditions was also developed more recently [211]. Powders with small particle size and narrow

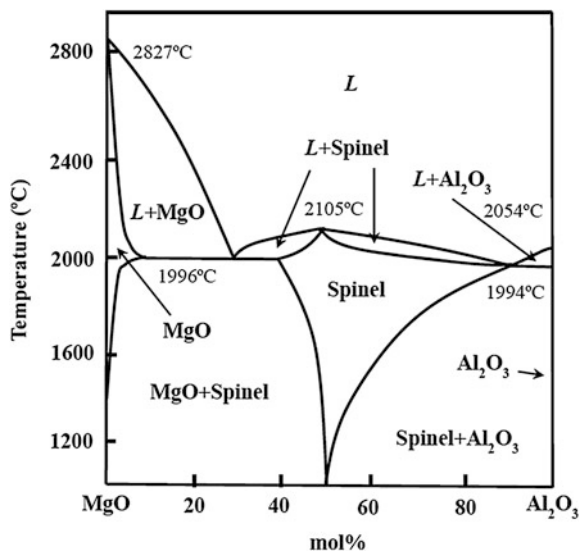
particle size distribution were obtained, which could be used to fabricate spinel ceramics with high optical performances.

Another strategy for developing transparent spinel ceramics is the use of sintering aids. It was found that the addition of a small amount of boron oxide (0.05–0.5 mass%) was very effective in promoting the sintering behavior of a fine MgAl_2O_4 powder processed by using HIP [203]. Experimental results indicated that the presence of B_2O_3 not only reduced the sintering temperature of the precursor powder, but also suppressed the grain growth of the ceramics which was important to ensure high transparency. The optimal concentration of B_2O_3 was 0.15 wt%, with which the samples could achieve a high optical transmittance of 80 % at 1 mm thickness.

Besides B_2O_3 , LiF has also been widely used as a sintering aid for spinel ceramics [212–216]. By using 1 wt% LiF, MgAl_2O_4 transparent ceramics could be obtained by using HP process at a temperature as low as 1550 °C for 2 h [213]. The samples had an excellent visible transmittance of ~ 85 %. The effect of LiF on sintering kinetics of MgAl_2O_4 was also investigated [215]. Powders with 0, 0.5, and 1.0 wt% LiF were densified by using a vacuum HP under a range of uniaxial pressures. According to the sintering mechanisms derived from the experimental studies, the vacuum HP processing schedule could be further optimized.

According to MgO – Al_2O_3 phase diagram, spinel is the only compound, as shown in Fig. 2.19. However, the spine phase can act as a parent structure type of solid solutions whose compositional range increases with increasing temperature. The compositions can be expressed by the formulation of $\text{MgO} \cdot n\text{Al}_2\text{O}_3$, with $n = 1.0$ corresponding to the stoichiometry of MgAl_2O_4 . At appropriate temperatures, n can range from 0.8 (MgO-rich) to 3.5 (Al_2O_3 -rich). Conceptually, as all solid solution compositions share 1.0-spinel's cubic crystal structure, they should

Fig. 2.19 Binary phase diagram of MgO and Al_2O_3 with the formation of spinel MgAl_2O_4 and solid solutions at high temperatures



all have the potential to be prepared as transparent, single-phase ceramics; however, exsolution of excess alumina frequently undermines the formation of single-phase $\text{MgO} \cdot n\text{Al}_2\text{O}_3$ solid solution polycrystalline ceramics. It has been reported that $\text{MgO} \cdot n\text{Al}_2\text{O}_3$ polycrystalline ceramics with Al-rich compositions ($n > 1$) possess varied levels of light transmission at infrared wavelengths, although generally the transmission in the visible spectrum is low. As a consequence, there has been increasing interest in $\text{MgO} \cdot n\text{Al}_2\text{O}_3$ ceramics with $n > 1$ [193, 217, 218].

Transparent spinel ceramics with a composition of $\text{MgO} \cdot 1.2\text{Al}_2\text{O}_3$ have been developed by using HP and HIP [218]. The processing consisted of HP at 1600 °C for 5 h under vacuum and 20 MPa uniaxial load for pre-sintering and HIP at 1850 °C for 5 h under 200 MPa in argon. The samples obtained exhibited an average in-line transmission of $84.8 \pm 2.7\%$ at 550 nm and $>82\%$ throughout the visible spectrum. Final grain sizes of the ceramics ranged between 300 and 1000 μm , with flexural strength of 176.8 ± 46.2 MPa, hardness of 12.3 ± 0.2 GPa, and elastic modulus of 292.9 ± 7.5 GPa.

A detailed study on the relationship between composition and mechanical properties of spinel transparent ceramics has been reported [195]. In this study, HP and HIP were also used, but with commercial MgO and Al_2O_3 powders as the precursor. Three compositions of $\text{MgO} \cdot n\text{Al}_2\text{O}_3$ were investigated, with $n = 1:0$, 1.5, and 2.0. The spinel ceramic with MgO to Al_2O_3 molar ratio of 1:1 demonstrated the highest scattering coefficient due to its highest amount of grain boundary microcracking. Al_2O_3 rich compositions possessed a specular transmission of 40–60 % in the same wavelength range. The spinel ceramic with $n = 2.0$ exhibited the highest fracture toughness with a mean value of $\sim 2.02 \text{ MPa m}^{1/2}$. Based on their optical and mechanical properties, the Al_2O_3 -rich non-stoichiometric polycrystalline spinel ceramics would be potential candidate for engineering applications requiring high optical transparency and fracture toughness.

Other studies on spinel transparent ceramics include the effect of grain boundary microcracking on optical performance [193], nanoporosity effect, and elimination of precursor powders [219]. Light transmittance losses occurred when the sintered MgAl_2O_4 ceramics had microcracked grain boundaries which facilitated light scattering [193]. It was recognized that the nanoscale pores of <100 nm could be readily eliminated by using pressure-assisted reactive sintering of MgO– Al_2O_3 mixtures, starting with coarser powders with median particle sizes of 100–200 nm instead of sintering pre-calcined raw spinel powders <100 nm [219].

Due to the special requirement in mechanical properties for some specific applications, such as armor [220], a new direction of research on spinel transparent ceramics appeared recently, which is nanocomposite transparent ceramics. This concept was well demonstrated in a recent publication [221]. In this case, the nanocomposites were MgAl_2O_4 spinel matrix dispersed with Si_3N_4 nanoparticles. The as-processed nanocomposites were found to have a high transparency of $>70\%$ in the critical infrared wavelength range of 3–4.5 μm and an acceptable transparency in the visible region. The optical properties of the nanocomposites remained almost unchanged upon heat treatment at 1000 °C for 4 h in air, which, however, resulted in a 29 % increase in the average strength, accompanied by almost

doubling of the Weibull modulus, and an 85 % increment in the indentation toughness. The improvements in mechanical properties after the heat treatment in these nanocomposites were attributed to surface-oxidation-induced surface compression and flaw healing.

TEM observation indicated that no residual porosity could be found in this as-processed spinel/ Si_3N_4 nanocomposite. The spinel grain size is 300 nm and the size of is about 100 nm. The nanosized Si_3N_4 particles were located both at grain boundaries and within the spinel grains. The as-processed spinel/ Si_3N_4 nanocomposite ceramics with a thickness of 2 mm showed good transparency in the visible range, allowing to view distant objects through it. Therefore, this type of transparent ceramics could be used for possible armor applications [221].

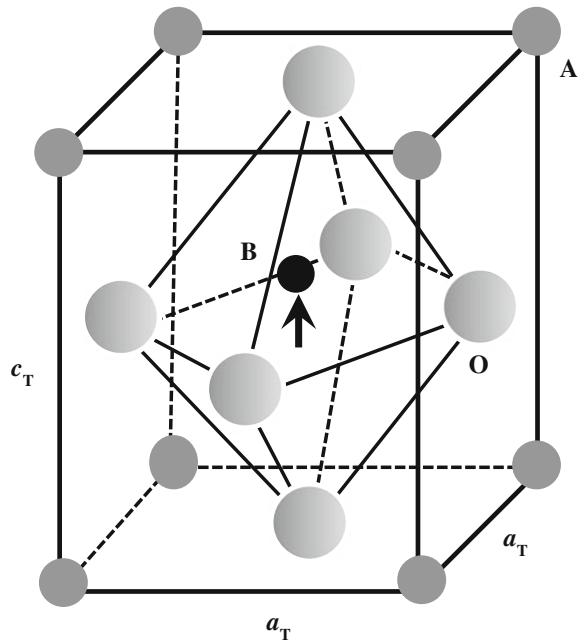
More recently, a nanocrystalline spinel ceramics with 50 % increase in hardness was reported [222]. It is well known that mechanical strengthening by grain refinement is a method, i.e., the strength and hardness of a material can be increased by decreasing its grain size, as described by the empirical Hall–Petch relationship, which provided a guidance to produce stronger materials. Base on this principle, an integrated approach was developed by using nanosized spinel powder, combined with HP and low-temperature sintering to fabricate fully dense and high purity nanocrystalline ceramics with nanometersized grains. The Hall–Petch relationship was confirmed by the hardness of the transparent spinel ceramics with grain sizes down to 28 nm. As a result, the nanosized spinel ceramics exhibited a 50 % increase in hardness without a decline in fracture resistance. More importantly, the nanocrystalline spinel ceramics had near theoretical optical transparency. However, this technique has a difficulty in making large-sized items.

2.4 Electro-optic Ferroelectric Ceramics

Opto-ceramics is a family of special transparent oxide materials. Their crystallography structure is perovskite type with formulation of ABO_3 , with unit cell shown schematically in Fig. 2.20, which is tetragonal with $c_T > a_T = b_T$. Due to its small size, the center ion (B) could be displaced either upward or downward to form spontaneous polarization, which is also the reason why the polarization can be switched by the application of external electric fields. This behavior is known as ferroelectricity.

The typical representatives of this family include $\text{Pb}_{1-x}\text{La}_x(\text{Zr}_y\text{Ti}_{1-y})_{1-x/4}\text{O}_3$ (PLZT), $\text{Pb}(\text{Mg}_{1/3}\text{Nb}_{2/3})\text{O}_3$ - PbTiO_3 (PMN-PT), and $\text{Pb}(\text{Zn}_{1/3}\text{Nb}_{2/3})\text{O}_3$ - PbTiO_3 (PZN-PT). The PLZT formula assumes that La substitutes for Pb^{2+} in the A-site and the B-site vacancies are created for electrical balance. To achieve highest transparency and electro-optic coefficient, some elements, such as Ba and/or La, are usually introduced into the solid solutions of PMN-PT and PZN-PT. Material synthesis and properties of transparent electro-optic ceramics, including PLZT and PMN-PT, have well been summarized and documented [223].

Fig. 2.20 Unit cell of perovskite ABO_3 , in which the center ion (B) is displaced upward to form a spontaneous polarization. The center ion can also be displaced downward



2.4.1 PLZT Ceramics

PLZT ceramics possess much higher electro-optic coefficient than LiNbO_3 single crystals. PLZT ceramics also have higher transparency than other ferroelectric materials. Specifically, $\text{Pb}_{(1-x)}\text{La}_x(\text{Zr}_y\text{Ti}_{1-y})_{1-x/4}\text{O}_3$, i.e., PLZT9/65/35, exhibits outstanding electro-optic coefficients with little hysteresis and no remnant polarization. Therefore, PLZT9/65/35 ceramics are potential candidates for applications in digital light modulators and large aperture light shutters [31, 33].

Transparent PLZT ferroelectric ceramics were reported by Haertling in 1971 [32]. The quality of transparent PLZT ceramics is mainly determined by the properties of the precursors. High quality powders should have small particle size, narrow size distribution, and no hard agglomeration. Several wet chemistry-based methods, such as chemical co-precipitation, sol-gel processing, and hydrothermal processing, as well as dry method of high-energy ball milling, have been developed to prepare PLZT powders. Moreover, special sintering techniques, such as HP/HIP and atmosphere-controlled sintering, are also very useful in fabricating high quality transparent PLZT ceramics [32].

The sintering atmosphere is demonstrated to be important in determining the final microstructure of the PLZT ceramic because of the volatility of lead oxide (PbO). A controlled oxygen partial pressure sintering method was established to obtain transparent $(\text{Pb}, \text{La})(\text{Zr}, \text{Ti})\text{O}_3$ ceramics [224]. PLZT(7/60/40) ceramics with large piezoelectric coefficients were prepared by using a two-step sintering process

with controlled oxygen partial pressure. At the first step, the samples were sintered under a low oxygen pressure (vacuum) at low temperature of 1150 °C, while they were then processed under higher oxygen pressure of 0.22 MPa at higher temperature (1250 °C), at the second step. Fully densified transparent PLZT ceramics with an average grain size of 3 μm could be readily fabricated in this way. The samples possessed k_p and d_{33} of as high as 0.71 and 850×10^{-12} C/N, respectively. The piezoceramics were transparent, with an optical transmittance of 15 % ($\lambda = 610$ nm), for a sample thickness of 1 mm.

Pressure sintering techniques have also been used to fabricate transparent lanthanum-doped lead zirconate titanate (PLZT) ceramics in air and in oxygen-gas atmosphere [31]. The microstructure of the sintered body was not uniform; it was completely dense near the surface, but it was porous at the center. The thickness of the dense layer increased with sintering time and oxygen-gas pressure in the sintering atmosphere. Vaporization of PbO from the specimen surface and resultant formation of lattice vacancies were attributed to this microstructural evolution. Diffusion of the gas trapped in the pores was also important in determining the thickness of the dense layer. When the PLZT specimen was sintered in air at 1200 °C for 8 h, the thickness of the dense layer was 0.25 mm. Therefore, if the specimen thickness was 0.5 mm, the whole specimen was dense and transparent. When the specimen was sintered in an oxygen-gas atmosphere under the same conditions, the specimen thickness increased markedly.

When a specimen with the same composition was sintered in argon, the thickness of the dense layer decreased. Furthermore, it is apparent that the outer region was not completely pore-free as was the case of the specimen sintered in air. On the other hand, when the specimen was sintered in a 33 % oxygen-gas atmosphere, the dense layer became thicker than the case of sintering in air. As the oxygen partial pressure of the sintering atmosphere was further increased, the dense layer continued to grow until the whole specimen became dense in a pure oxygen atmosphere.

A three-stage-atmosphere-sintering technique was used to obtain PLZT transparent ceramics [225]. This technique consists of three stages: (i) sintering in an oxygen atmosphere, (ii) elimination of pores in a carbon dioxide atmosphere, and (iii) elimination of oxygen vacancies in an oxygen atmosphere. The experimental results reveal that use of a carbon dioxide atmosphere effectively decreases residual pores and improves optical transmittance. From commercially available raw powders, an optical transmittance of 51 % at wavelength of 550 nm can be achieved for 0.7 mm thick polished PLZT9/65/35 ceramics using a carbon dioxide atmosphere, whereas the value is only 34 % without a carbon dioxide atmosphere. The advantage of this technique is that PLZT ceramics having high optical quality can be obtained using conventional sintering tools.

A simple and feasible repeated annealing process was available to obtain transparent PLZT(9/65/35) ceramics [226]. The experiment was started from nanosized powder of PLZT, which was synthesized directly from commercially available constituent oxides by using a high-energy ball milling at near room temperature. Transparent PLZT ceramics were obtained by annealing the samples

pre-sintered at 1125 °C for 6 h, which was repeated for 4 times without using hot pressing or oxygen flow. The annealing temperature was 1200 °C. The optical properties together with the electrical characteristics of the PLZT ceramics produced in this way were comparable with the literature results. The most significant aspect of this study is the low-cost large-scale fabrication of the PLZT nanosized powders, which is not available by most of the wet-chemical synthesis routes.

SPS has been confirmed to be a viable technique to synthesize PLZT transparent ceramics. An example is the preparation of PLZT(8/65/35) ceramics [227]. The PLZT powder was synthesized by using a wet–dry combination method. Due to the contamination of carbon from the graphite mold, the samples after the SPS sintering should be annealed in air or oxygen. Optical properties of the samples were affected by the SPS temperature, as well as the post-annealing temperature. It was found that 700 °C was the optimal sintering temperature when transmittance was considered.

2.4.2 Other Ferroelectric Ceramics

$\text{Pb}(\text{Mg}_{1/3}\text{Nb}_{2/3})\text{O}_3$ (PMN) with perovskite structure is known as one of the best representative relaxor ferroelectrics [228]. However, the Curie point (T_C) of PMN is below room temperature and the synthesis of single PMN is always a challenge. Another perovskite structure ferroelectric PbTiO_3 (PT) has a high T_C of about 490 °C and very phase stability. Incorporation of PT with PMN has been widely used to form new solid solution PMN-PT, which has T_C of above room temperature and is easy to be synthesized [229–234]. More importantly, PMN-PT has an isotropic minimum energy stable structure and a higher electro-optic coefficient than PLZT (about 10–30 times). To the same index change (or phase shift), the applied voltage onto PMN-PT could be much lower than that required when using PLZT. Moreover, the electric hysteresis of PMN-PT can be readily minimized [229]. In addition, PMN-PT is the most promising nonlinear optical materials because of its extremely high electro-optic (EO) coefficient and strong photorefractive effect [235]. Its EO effect is about 2–5 times higher than that of PLZT and nearly 100 times than that of LiNbO_3 at room temperature. The remarkably good transparency over a wide wavelength range of 500–7000 nm makes PMN-PT suitable for almost all the visible to mid-IR optical applications.

Detailed investigation on the optical characteristics, including the electro-optic phase modulation, electric hysteresis property, and thermo-optic coefficient, of transparent PMN-PT electro-optic ceramics have been conducted [229]. A polarization independent PMNT electro-optic switch by using π -shifted fiber Sagnac interferometer structure was constructed and analyzed experimentally. Some switch performances, including thermal characteristic and different switching frequency response, were also realized.

Preparation and characterization of transparent ceramics of La-doped PMN-0.25PT by a two-stage sintering method from conventional raw materials were reported in Ref. [236]. Optical characteristics of Er^{3+} -doped PMN-PT transparent

ceramics have been investigated [237], with doping concentrations of 0.5, 1.0, 2.0, and 5.0 mol%. Figure 2.21 shows photographs of the PMN-PT ceramics.

The presence of Er^{3+} over 0.5–2.0 mol% could enhance the optical transmittance of the samples and modify the optical absorption near the band gap energy of the materials. Transmittance of the undoped PMN-0.25PT in the visible region was estimated to be 43.0 %. The transparent ceramics doped with Er^{3+} levels of 0.5, 1.0, and 2.0 mol% were 50, 53, and 57 %, respectively. However, the transmittance was decreased to 28.0 % in the sample with Er^{3+} of 5.0 mol%, which was considered to be closely related to the formation of a trace of pyrochlore phase. By the way, the absorption edge shifted to higher energy as the doping concentrations were <2.0 mol% and a redshift was observed in the samples with higher doping concentration (5.0 mol%). The observations were explained by considering the combined effects of ion polarization and localized defect energy level.

$\text{Pb}(\text{Zn}_{1/3}\text{Nb}_{2/3})\text{O}_3$ (PZN) single crystal exhibits outstanding dielectric and electrostrictive properties and also shows a very large electro-optic coefficient [238–241]. However, single-phase PZN ceramics cannot be prepared due to the thermodynamics inhibition. Therefore, it becomes a natural idea to combine PMN and PLZT, aiming at creating new compounds with advantages of both materials, such as excellent piezoelectric and dielectric properties, high optical transmittance in a wide range of wavelength, and strong electro-optical effect. Transparent PZN-PLZT ferroelectric ceramics have been prepared by using HP sintering in oxygen atmosphere [242]. Uniform cylindrical samples with diameter as large as 50 mm could be readily obtained. The product showed a pure perovskite phase, thin grain boundaries, and homogeneous dense microstructures. The ceramics exhibited very good transparency from near ultraviolet to infrared regions.

Besides ferroelectric transparent ceramics, there have also been reports on antiferroelectric ceramics. For example, lead zirconate stannate titanate ($\text{Pb}_{0.97}\text{La}_{0.02}(\text{Zr}_{0.77}\text{Sn}_{0.14}\text{Ti}_{0.09})\text{O}_3$, PLZSnT) ceramics by using SPS at 900–950 °C [243]. The samples had nearly full density and fine grain size of about 300 nm. Compared with samples made by using conventional sintering (CS), the SPS sintered samples showed higher permittivity and lower dielectric loss tangent, as well as special strain hysteresis loops similar to those of ferroelectric relaxors.



Fig. 2.21 Photographs of the Er^{3+} -doped PMN-0.25PT transparent ceramics with a thickness of 1.5 mm. The numbers in the photographs are the Er^{3+} doping levels in mol%. Reproduced with permission from [237]. Copyright © 2012, Elsevier

Lead-free ferroelectric and some microwave dielectric ceramics have been made to be transparent [244–248]. Bismuth-modified potassium sodium niobate, $\text{K}_{0.48}\text{Na}_{0.52}\text{Nb}_{1-x}\text{Bi}_x\text{O}_3$ ($x = 0.05$ – 0.15), transparent ceramics were fabricated by a hot pressing method [244]. Both hot pressing conditions, including pressure, temperature, and duration, and Bi content had strong influences on densification, optical transparency, electro-optical coefficient, and electrical properties of the ceramics. Under the hot pressing conditions of 1060°C for 5 h at 5.5 MPa, the optimized Bi content was 7.5 at.%. These ceramics display good optical transmission in the visible and especially in the infrared region. In visible region, the highest transmission of a polished 0.5-mm thick plate was about 60 % at a wavelength of 800 nm, while in infrared region, the transmission value could be 80 % at 4000 nm. The effective linear electro-optic coefficient of the ceramics was 42 pV m^{-1} . The dielectric permittivity and loss tangent of the KNNB ($x = 0.075$) ceramics were 716 and 0.031 at room temperature. Representative photographs of the ceramics are shown in Fig. 2.22.

Another group of lead-free transparent electro-optic ceramics, $(\text{K}_{0.5}\text{Na}_{0.5})_{1-x}\text{Li}_x\text{Nb}_{1-x}\text{Bi}_x\text{O}_3$, has also been fabricated by using the similar process [245]. The co-modification with Li and Bi was able to transfer the ceramics into a nearly cubic structure with minimal optical anisotropy. At the same time, a diffuse phase transformation was induced, making the ceramics to be more relaxor-like and contain more polar nanoregions. These would reduce the light scattering by the grains, at the grain boundaries and at the domain walls, thus leading to ceramics with high optical transparency. For the ceramic modified with 5 mol% Li⁺ and Bi⁵⁺, the optical transmittance reached as high as 60 % in the near-IR region. The ceramics also exhibited a strong linear EO response, offering a large effective linear EO coefficient of 120–200 ppm V^{-1} . Figure 2.23 shows photographs of representative samples of the transparent ceramics.

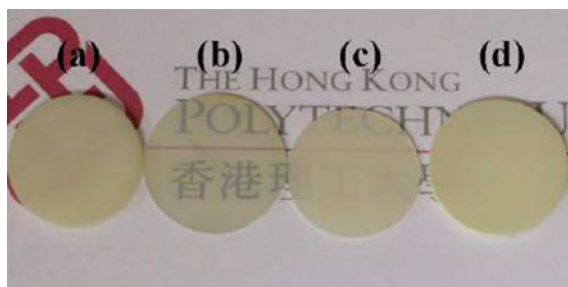


Fig. 2.22 Photographs of the $\text{K}_{0.48}\text{Na}_{0.52}\text{Nb}_{1-x}\text{Bi}_x\text{O}_3$ ceramics with different compositions: **a** $x = 0.05$, **b** $x = 0.075$, **c** $x = 0.10$, and **d** $x = 0.15$, which were hot pressed at 1060°C for 5 h at a pressure of 6.1 MPa. Reproduced with permission from [244]. Copyright © 2011, Elsevier

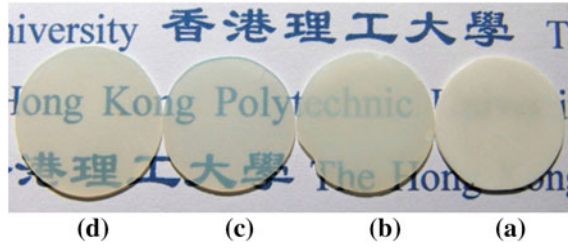


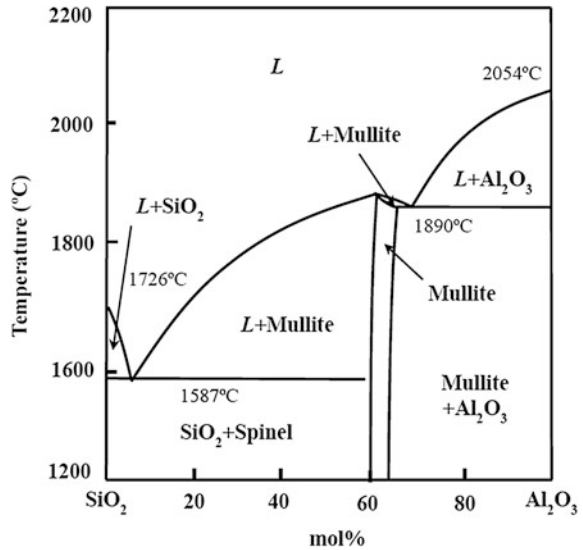
Fig. 2.23 Photographs of the KNNLB- x transparent ceramics: **a** $x = 0.02$, **b** $x = 0.03$, **c** $x = 0.05$, and **d** $x = 0.07$. Reproduced with permission from [245]. Copyright © 2013, Elsevier

2.5 Mullite

Mullite, a crystalline aluminum silicate phase, with a stoichiometric composition of $3\text{Al}_2\text{O}_3 \cdot 2\text{SiO}_2$, is a very interesting mineral constituting silicate ceramics. With an orthorhombic crystal structure, its lattice parameters are $a = 7.5785(6) \text{ \AA}$, $b = 7.6817(7) \text{ \AA}$ and $c = 2.8864(3) \text{ \AA}$. Depending on the real composition, mullite ceramics have densities in the range of $3.11\text{--}3.26 \text{ g cm}^{-3}$, with a melting point of 1840°C . Figure 2.24 shows a binary phase diagram of SiO_2 and Al_2O_3 .

It is one of the most widely used ceramic materials because of its unique properties, like high-temperature strength, thermal shock resistance, and low dielectric constant [249]. It is also a good refractory material, due to its high melting

Fig. 2.24 Binary phase diagram of SiO_2 and Al_2O_3 with the formation of mullite



point [250], low thermal expansion coefficient, low thermal conductivity, high strength, and good creep resistance. Due to its low dielectric constant, $\epsilon = 6.7$, which is lower than 9.8 of Al_2O_3 , it can be used as a promising candidate for substrates in electronic packaging [251]. Because mullite has a coefficient of thermal expansion (CTE) that is the closest to that of silicon (Si), it has been acknowledged to be the most promising candidate as the substrates of Si thin film solar cell [252–255]. Moreover, mullite can be employed as window materials, especially at high temperatures, because it has a good transmission at high temperatures in the middle infrared band. Low dielectric constant and optical transmittance of fine-grained polycrystalline mullite could be a good host material of solid-state laser activators [34].

Pore-free translucent mullite was reported in 1972 by using HP sintering at 1500–1650 °C and 30–50 MPa, and vacuum HP, with high purity submicron-mixed oxide precursor powders derived from metal alkoxides [256]. Infrared-transparent mullite ceramics with 72 wt% Al_2O_3 were obtained by using HP sintering at 1630 °C and with 76 wt% Al_2O_3 by using HIP pressing at 1650 °C [257]. Visible spectrum translucent and infrared-transparent mullite ceramics were prepared by using pressureless sintering at 1750 °C [258]. Transparent mullite ceramics could also be developed through a combination of HIP pressing and pressureless sintering using commercial fused mullite precursor [259]. Both processing methods led to mullite ceramics with fine-grained microstructures (mean grain size of 5–10 μm) with equiaxed grains and a narrow grain size distribution. The pressureless sintered mullite had a porosity of 5.5 % and a transmittance of 20 % in the VIS and NIR ranges, while the HIP sintered mullite showed a porosity of 1 % and a transmittance of 40 % in the VIS range and up to 80 % in NIR range. This optically translucent mullite ceramics are suitable for optical windows in the VIS and NIR ranges [259].

Mullite ceramics, transparent in both mid-infrared and visible light regions, have been reported by using SPS from monophasic precursors [35]. In this method, the effects of calcination temperature, properties of precursor powders and sintering parameters on microstructure, and optical performances of the mullite ceramics were systematically investigated. The samples with a relative density of above 97.5 % exhibited an infrared transmittance of 75–82 % in wavelength of 2.5–4.3 μm . It was found that, as the precursor powders were calcined at temperatures of below 1100 °C, the residual OH, H_2O , and organic compound could not be completely eliminated, which in turn had negative effects on optical properties of the final ceramics. However, if the calcination temperature was too high, the precursors could not fully densified, due to the absence of viscous flow of amorphous phase. At a given calcination temperature, optical transmittance of the mullite ceramics was decreased with increasing sintering temperature above 1450 °C owing to the elongated grain growth. In addition, microwave sintering provided a rapid heating, accelerated mullitization, enhanced densification, and limited grain growth for developing transparent mullite ceramics with diphasic gels [34].

2.6 Other Oxide Ceramics

2.6.1 Newly Emerged Oxide Ceramics

Various transparent ceramics of complex oxides with pyrochlore structure, including $\text{Lu}_2\text{Ti}_2\text{O}_7$ [260–262], $\text{Lu}_2\text{Zr}_2\text{O}_7$ [263, 264], Lu_3NbO_7 [265, 266], $\text{LaGdZr}_2\text{O}_7$ [267], have been fabricated by using SPS. Nonmagnesium spinel transparent ceramics, e.g., zinc spinel or ZnAl_2O_4 , have been reported [268–270]. Lanthanum silicate oxyapatite, with a formula of $\text{La}_{9.33}\text{Si}_6\text{O}_{26}$, ion-conducting materials presenting a strong aversion against densification, has been prepared in the form of dense transparent ceramics, by combining the beneficial use of freeze-drying and SPS methods [271]. Another example is $\text{Sr}_2\text{Y}_8(\text{SiO}_4)_6\text{O}_2$ oxyapatite translucent ceramics, which were derived from pure powder by using SPS combined with ball milling [272]. The microstructures and transmittances in the completely and incompletely densified ceramics were investigated. The ceramic sintered at 1500 °C is translucent with 0.7 % porosity and its total forward light transmittance can reach about 52 % in the infrared region. The transmittance was interpreted based on the microstructures of the ceramic samples and the Mie scattering theory. It was accepted previously that these ceramics cannot be processed to be transparent by using the conventional sintering techniques.

A simple combustion method was used to synthesize $\text{LaGdZr}_2\text{O}_7$ powder, which was then used to produce $\text{LaGdZr}_2\text{O}_7$ transparent ceramics by using vacuum sintering at 1850 °C for 6 h [267]. The final transparent ceramics, with a density of 6.46 g cm^{-3} , had an in-line transmittance of 70.7 % at 1000 nm and a refractive index of 2.08 at 632.8 nm. Figure 2.25 shows photographs of representative samples of the transparent ceramics.

The starting materials were $\text{Zr}(\text{NO}_3)_4 \cdot 3\text{H}_2\text{O}$, $\text{La}(\text{NO}_3)_3 \cdot 6\text{H}_2\text{O}$, and glycine. Gadolinium nitrate solution was prepared by dissolving Gd_2O_3 (99.99 %) in excess nitric acid solution. Stoichiometric amounts of the reactants were mixed thoroughly to form clear solutions. After that, ammonia solution was added into the solutions, so that their pH value was about 4. The solutions were then heated to facilitate gelation and finally trigger the combustion. The as-synthesized precursors were calcined at 800 °C for 2 h to obtain oxide powders. The powders were ball-milled with zirconia balls as grinding media 20 h. After drying, the powders were cold



Fig. 2.25 Photographs of the $\text{LaGdZr}_2\text{O}_7$ ceramics vacuum sintered at 1850 °C for 6 h and annealed at 1500 °C for 5 h in air, with a thickness of 1 mm. Reproduced with permission from [267]. Copyright © 2013, Elsevier

isostatically pressed into pellets ($\varnothing 20 \text{ mm} \times 2.5 \text{ mm}$) at 200 MPa for 2 min. The green pellets were sintered at 1850 °C for 6 h in vacuum of 10^{-3} to 10^{-4} Pa and then annealed at 1500 °C for 5 h in air.

2.6.2 Transparent Ceramics Derived from Glasses

More recently, a new method to fabricate transparent ceramics was demonstrated, in which glasses with certain compositions were prepared first and then converted to transparent ceramics by using simple annealing at very low temperatures in air. Such transparent ceramics include BaAl_4O_7 [273], $\text{Sr}_3\text{Al}_2\text{O}_6$ [274], and $\text{Sr}_{1+x/2}\text{Al}_{2+x}\text{Si}_{2-x}\text{O}_8$ ($0 \leq x \leq 0.4$) [275], which will be discussed in the following part.

The first example is barium aluminate, BaAl_4O_7 , which had two orthorhombic polymorphs with micrometer grain size and both were optically transparent in the visible region [273]. Starting precursor materials of BaCO_3 (>99.8 % purity) and Al_2O_3 (>99.997 % purity) were weighed, mixed in a 1:2 molar ratio, and pressed into pellets. Glasses with that composition were first prepared by using an aerodynamic levitator with a conical nozzle equipped with two CO_2 lasers. A single glass bead was obtained by melting the mixed precursor pellet of ~0.1 g at 2100 °C, followed by rapid quenching. The glassy beads were then crystallized into transparent ceramics by annealing in air. Crystallization temperatures were selected according to the differential scanning calorimetry (DSC) measurements. Figure 2.26 shows photographs of the glass and the two ceramic samples, together with the two crystal structures and thermal analysis result of the glass sample.

The method was also applied to the conversion of $\text{Sr}_3\text{Al}_2\text{O}_6$ and $\text{Sr}_3\text{Ga}_2\text{O}_6$ glasses [274]. The $\text{Sr}_3\text{Al}_2\text{O}_6$ and $\text{Sr}_3\text{Ga}_2\text{O}_6$ glasses were first synthesized from high purity SrCO_3 (99.99 %), Al_2O_3 (99.98 %), and Ga_2O_3 (99.99 %) using the method as discussed above. For doped samples, Eu_2O_3 , Er_2O_3 , Ho_2O_3 , and CeO_2 oxides were used. The starting materials were made into pellets and then melted to form glasses. Full glasses were finally annealed at 840 °C for 5 h in air to be converted into transparent ceramics.

Figure 2.27 shows a photograph of the $\text{Sr}_3\text{Al}_2\text{O}_6$ polycrystalline ceramics obtained by full crystallization from the glasses, together with transmission curve. It was highly transparent in the visible region, covering a wide range from the visible to infrared ranges, i.e., 300 nm–6 μm . The absorption below 300 nm was due to the optical band gap absorption of the strontium aluminate, whereas the absorption observed around 3 μm corresponds to moisture in the sample, i.e., O–H bonds. The difference between the measured transparency and the theoretical maximum value of 87.4 ± 0.5 % for an average refractive index of 1.70 ± 0.02 was very small in the visible range and was negligible in the IR range, which implied that there were only limited number of scattering centers within the polycrystalline ceramics. Furthermore, luminescence of the $\text{Sr}_3\text{Al}_2\text{O}_6\text{:Eu}^{3+}$ and $\text{Sr}_3\text{Al}_2\text{O}_6\text{:Er}^{3+}$ ceramics, with strong emissions in the visible and infrared ranges, was observed. The $\text{Sr}_3\text{Al}_2\text{O}_6\text{:Ce}^{3+}$ ceramics exhibited scintillation properties under X-ray excitation.

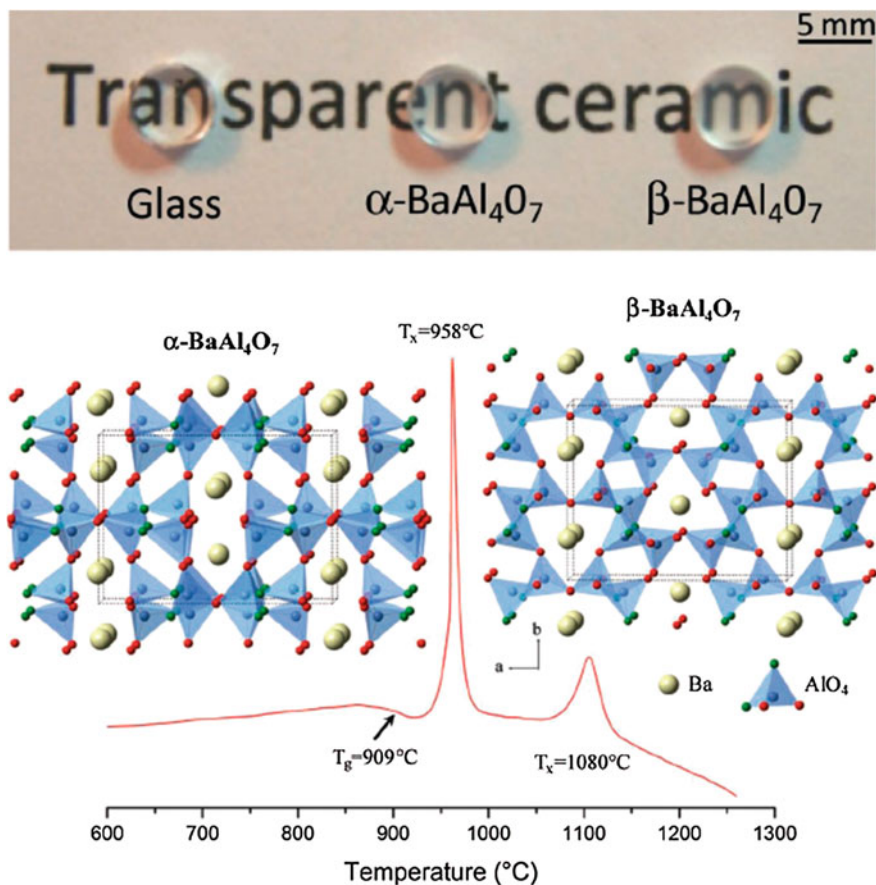


Fig. 2.26 Top panel: dense ~ 1.5 mm thick disks of the BaAl₄O₇ parent glass sample, α -polymorph and β -polymorph transparent ceramics. *Middle panel* Crystal structures of the α - and β -BaAl₄O₇ polymorphs. The corner-sharing AlO₄ tetrahedra form channels occupied by barium. The two polymorph frameworks are not structurally related, but both of them exhibit structural anisotropy. The tricluster oxygen ions appear in *green*. *Bottom panel* Differential scanning calorimetry measurement of the BaAl₄O₇ glass showing the glass transition at $909 \pm 1^\circ\text{C}$ and a strong exothermic peak corresponding to crystallization of the α phase at $958 \pm 1^\circ\text{C}$ followed by a broader second exothermic peak corresponding to the α - to β -BaAl₄O₇ transition at $1080 \pm 1^\circ\text{C}$. Reproduced with permission from [273]. Copyright © 2012, John Wiley & Son

The latest development was to use normal glass technique to large size and flat samples [275]. The five Sr_{1+x/2}Al_{2+x}Si_{2-x}O₈ ($x = 0, 0.1, 0.2, 0.3$, and 0.4) polycrystalline ceramics were first prepared as glass materials from high purity SrCO₃ (99.9 %), Al₂O₃ (99.98 %), and SiO₂ (99.8 %) precursors. Stoichiometric ratios for each composition were thoroughly mixed. The mixed powders were then placed in rhodium/platinum crucibles and calcined at 1700°C for 10 min in a preheated

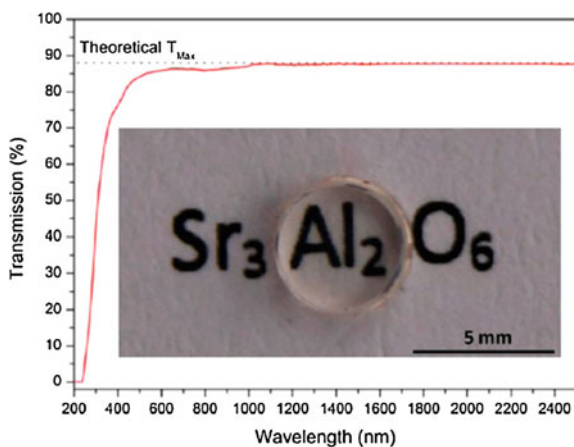


Fig. 2.27 Transmission spectra of the $\text{Sr}_3\text{Al}_2\text{O}_6$ transparent polycrystalline ceramic (obtained from a 1.5 mm thick sample). The *dotted black line* corresponds to the theoretical maximum transmission calculated as 87.4 % for an average refractive index of 1.70. A photograph of the $\text{Sr}_3\text{Al}_2\text{O}_6$ material is also shown. Reproduced with permission from [274]. Copyright © 2013, American Chemical Society

electric furnace first, and then heated to 1750 °C for 10 min and back to 1700 °C for 30 min. The samples were then cooled in air. The glasses were annealed at 1020 °C for 3 h in air to form transparent ceramics. Representative samples and optical properties of the transparent ceramics are shown in Fig. 2.28.

2.6.3 Multiphase Transparent Ceramics

An open question is whether binary or multicomponent systems that are from different transparent ceramics are still transparent. Recent studies provided with positive answers to the question [276, 277]. $\text{MgAl}_2\text{O}_4/\text{Ce}:\text{YAG}$ transparent ceramics have been fabricated by using hot pressing sintering and hot isostatic pressing sintering techniques, with high purity yttrium aluminum garnet (YAG:Ce) powder and MgAl_2O_4 powder [276]. The MgAl_2O_4 powder was synthesized by using a metal alkoxide method with magnesium, aluminum, and isopropanol as precursors. The transparent ceramics contained both magnesium-aluminum spinel (MgAl_2O_4) and YAG, in which the YAG phase was dispersed uniformly in the matrix of MgAl_2O_4 . The grain size of YAG was about 8 μm . The ceramics of 2 mm in thickness had an in-line transmittance of >40 % at 530 nm. The main absorption peak centered at 460 nm, indicates that the $\text{MgAl}_2\text{O}_4/\text{Ce}:\text{YAG}$ transparent ceramics could be promising fluorescent materials and have potential for application in white LED.

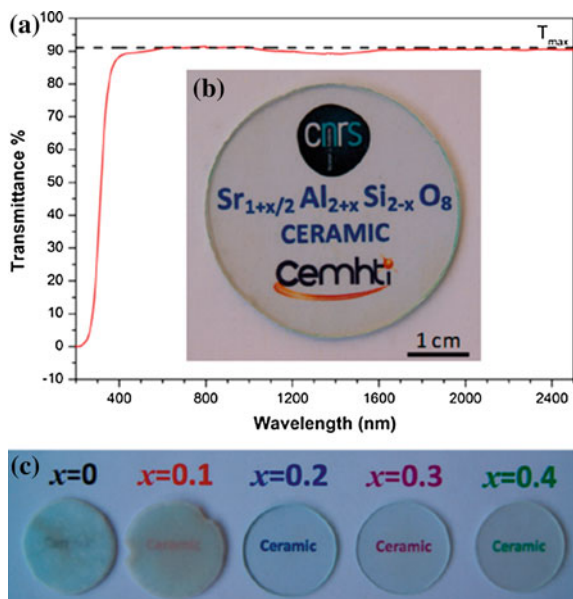


Fig. 2.28 Transparency of the $\text{Sr}_{1+x/2}\text{Al}_{2+x}\text{Si}_{2-x}\text{O}_8$ ($0 \leq x \leq 0.4$) polycrystalline ceramics. **a** Transmission spectrum measured on the sample with $x = 0.2$ ($\text{Sr}_{1.1}\text{Al}_{2.2}\text{Si}_{1.8}\text{O}_8$) at a thickness of 1.5 mm. The $n = 1.59$ refractive index implies a 90.1 % maximum theoretical transparency (dashed line). **b** Photograph of the same material illustrating the almost perfect 90 % transparency. **c** Photograph of the $\text{Sr}_{1+x/2}\text{Al}_{2+x}\text{Si}_{2-x}\text{O}_8$ ($x = 0, 0.1, 0.2, 0.3$, and 0.4) polycrystalline ceramics showing transparency evolution along the reported solid solution. Reproduced with permission from [275]. Copyright © 2015, American Chemical Society

2.7 Nonoxide Ceramics

2.7.1 AION

Aluminum oxynitride (AION) has a defect cubic spinel crystal structure with chemical formula of $\text{Al}_{(64+x)/3}\text{O}_{32-x}\text{N}_x$ ($2 \leq x \leq 5$). The addition of a small amount of nitrogen converts the rhombohedral crystal structure of alumina into the cubic spinel structure of AION. Nitrogen stabilizes the cubic spinel crystal structure over a wide range of compositions. AION is optically transparent ($\geq 80\%$) over the region from near-ultra violet to visible and near-infrared wavelength of the electromagnetic spectrum. It is 4 times harder than fused silica glass, 85 % as hard as sapphire, and nearly 15 % harder than MgAl_2O_4 spinel. Furthermore, the cubic structure of AION exhibits isotropic optical properties. Combined with its good optical and mechanical properties, AION can be used in defence and commercial applications, such as military aircraft and missile domes, transparent armors, IR windows, hyper-hemispherical domes, laser windows, military aircraft lenses,

semiconductor processing applications, and scanner windows. The history of development of AlON transparent ceramics has been well documented in the open literature [278].

Over the years, several processing routes have been used to produce fully dense transparent polycrystalline AlON ceramics. Initial work was reported by McCauley et al. [279] in 1979, using reactive sintering of Al_2O_3 -AlN mixtures. Then the reactive sintering technique was widely used by other researchers [280].

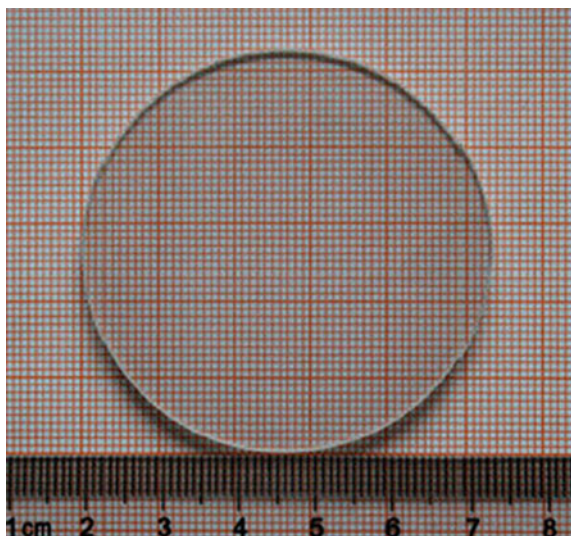
The conventional method for the fabrication of transparent AlON ceramics involves several steps, including synthesis of precursor AlON powder, forming green body with the powder, and then sintering in a nitrogen atmosphere at high temperatures ($>1850^\circ\text{C}$) for extended period (20–100 h). AlON precursor powders can be synthesized by several methods, such as reaction of Al_2O_3 and AlN, carbothermal reduction (CR) of Al_2O_3 , SSR, plasma arc synthesis, and self-propagating high-temperature synthesis (SHS) [281]. Among these methods, CR and SSR have been the most widely used ones, because CR is very cost effective while SSR is extremely simple. However, CR method has too many influencing factors, making it difficult to synthesize pure AlON powders without residual AlN or Al_2O_3 [282]. SSR method requires high purity and fine AlN powders to ensure high sinterability. In this respect, a combinational method of CR and SSR synthesis of γ -AlON powders was developed [283]. Ultrafine, phase pure, and low-cost γ -AlON powders were easily synthesized by using organic sucrose instead of carbon black as a reducing agent.

Highly transparent AlON ceramics have been made with powders synthesized by using direct nitridation method [284, 285]. As an example, the work of [285] is presented here. Commercial available submicron Al_2O_3 (99.99 % purity) and Al (99.95 % purity) were used as starting materials, while MgO, Y_2O_3 , and La_2O_3 (99.99 % purity) were used as sintering additives. The reactants were dispersed in alcohol and then vacuum dried at 80°C for 3 h. The homogeneous mixture was heated in a BN crucible to 1750°C gradually for 3 h in flowing N_2 . The as-synthesized AlON powder was mixed homogeneously with 0.10 wt% MgO, 0.08 wt% Y_2O_3 , and 0.025 wt% La_2O_3 . The resulting powder was made into pellets at low pressure and then cold isostatically pressed at 200 MPa. The green bodies were pressurelessly sintered in a graphite furnace at 1950°C for 12 h in nitrogen atmosphere. Figure 2.29 shows a photograph of the AlON transparent ceramics sintered at 1950°C for 12 h.

Similar to other transparent ceramics, AlON ceramics have also been processed by using various sintering techniques, such as pressureless sintering [286], microwave sintering [27, 287], HP [288], HIP [286, 289, 290], and SPS [291]. For example, a simple one-step pressureless sintering was proposed, using α - Al_2O_3 and aluminum powder as starting material [286]. The starting material was first nitrified into high activity AlN, from which $\text{Al}_{23}\text{O}_{27}\text{N}_5$ was then synthesized in situ by reacting with α - Al_2O_3 . The optimal one-step pressureless sintering process was observed to occur at 1750°C for 2 h, which resulted in samples with flexural strength of as high as 321 MPa.

A reactive SPS method has been developed to prepare AlON transparent ceramics [291]. Al_2O_3 and AlN powder mixtures were used as precursors. Reactive SPS was conducted at temperatures between 1400°C and 1650°C for 15–45 min at 40 MPa

Fig. 2.29 Photograph of the AlON transparent ceramics sintered at 1950 °C for 12 h. Reproduced with permission from [285]. Copyright © 2015, Elsevier



under N_2 gas flow. AlON phase formation was initiated in the samples sintered above 1430 °C, according to the XRD analysis. The complete transformation from the precursor phases (Al_2O_3 and AlN) to AlON was observed at 1650 °C for 30 min at 40 MPa. High temperature and low heating rate were favorable to the formation of AlON. The highest value of hardness was recorded to be 16.7 GPa. The sample with highest content of AlON possessed a fracture toughness of $3.95 \text{ MPa m}^{1/2}$.

A two-step method to prepare AlON ceramics was developed, with nanosized Al_2O_3 and AlN as precursors [292]. Single-phase AlON powder was obtained at 1750 °C for 4 h in flowing nitrogen atmosphere through direct reaction of the nanosized Al_2O_3 and AlN. After ball milling, the powder had an average size of several microns and showed quite high sintering activity. The high reactive AlON powder was used to fabricate transparent ceramics at 1880 °C.

By using MgO and Y_2O_3 as sintering aids, transparent AlON ceramics were successfully prepared by solid-state reactive sintering [293]. The effects of sintering aids and holding time on densification of AlON ceramics were investigated. Co-doping of MgO and Y_2O_3 was found to be more effective in enhancing the densification of AlON than the doping of either MgO or Y_2O_3 . It was observed that, at a given doping level of Y_2O_3 , e.g., 0.08 wt%, transmission coefficient of the ceramics increased with increasing concentration of MgO. A 1 mm thick sample, co-doped with 0.08 wt% Y_2O_3 and 1 wt% MgO, sintered at 1950 °C for 12 h in N_2 atmosphere, had an in-line transmittance of 60 % at 600 nm.

The single-phase AlON powder used in this experiment was obtained at relatively low temperature by the solid-state reaction method with nanosized AlN powder and nanosized alumina powder [292]. The obtained powder was ground by ball milling and doped with Y_2O_3 . Then, it was shaped into pellets. Transparent ceramics sintering was carried out at 2153 K (1880 °C) for 5, 10, and 20 h. Obtained

samples for three sintering times were all transparent, while the light transmittance of samples increased with increasing holding time at the sintering temperature. The transmittance of the sample sintered for 20 h is 55 pct at near 5 μm . X-ray diffraction (XRD) measurement indicated that all samples were single-phase AlN. The fracture surfaces of samples from SEM analysis showed that, with increasing the holding time, the grain size grew slightly, while the pore size and porosity decreased rapidly, so that the transmittance increased. The pore size and the porosity were the main factors affecting the light transmitting properties of samples.

2.7.2 Aluminum Nitride (AlN)

An effective processing method was studied to fabricate the translucent AlN ceramics [294]. AlN ceramics with 80 mm diameter have been prepared, which exhibited promising optical performances, e.g., transparent over wavelengths of 0.2–2.2 μm .

Transient liquid phase (TLP) sintering of CaF_2 additive on the densification behaviors and microstructural development of AlN ceramics are investigated [295]. It is found that 1 wt% CaF_2 can effectively promote densification process. Increasing content of CaF_2 results in finer grain size and slower densification during intermediate sintering stage. XRD results show that grain boundary phase of CaAl_4O_7 is formed at 1150 $^\circ\text{C}$ from reactions of $\text{AlN}-\text{CaF}_2-\text{Al}_2\text{O}_3$. With further temperature increasing, the grain boundary phases of CA2 and $\text{CaAl}_{12}\text{O}_{18}$, which were formed from the reaction between CaF_2 and oxide layers, experienced transformations first into CaAl_4O_7 above 1600 $^\circ\text{C}$ and into CaAl_2O_4 at higher temperatures. SEM and TEM results show that formed grain boundary phases can evaporate from sintering bodies during further soaking, leaving clean grain boundaries. The efficiency of TLP sintering mechanism is further manifested by the preparation of transparent AlN ceramics with good combination properties.

Optical spectroscopy of Er^{3+} doped into bulk AlN ceramics has been reported [296]. The material was prepared by using hot press sintering of AlN with Er_2O_3 and $(\text{NH}_4)(\text{ErF}_4)$, which yielded fully dense, translucent, hexagonal AlN. The Er^{3+} concentration was a small fraction of a percent, and resided in multiple sites, with one type of center dominant. A number of the energy levels of Er^{3+} were identified for this center. The temperature dependent fluorescence lifetime was probably radiative, with which the stimulated emission and absorption cross section spectra were derived for the $^4\text{I}_{13/2} \rightarrow ^4\text{I}_{15/2}$ transitions.

2.7.3 Sialon

SiAlONs are ceramics based on the elements of silicon (Si), aluminum (Al), oxygen (O), and nitrogen (N). They are solid solutions based on silicon nitride (Si_3N_4), with

three basic forms. Each form is isostructural with one of the two common forms of silicon nitride, i.e., β and α , and silicon oxynitride. Sialon ceramics are a special class of high-temperature refractory materials, with high strength at both room temperature and high temperatures, good thermal shock resistance, and exceptional resistance to wetting or corrosion by molten nonferrous metals, compared to other refractory materials such as, for example, alumina. Recently, with the advancement in sintering techniques, translucent or transparent Sialon ceramics have emerged as a new group of engineering ceramics with special optical properties.

A report is available on microstructure and properties of translucent Mg-sialon ceramics prepared by SPS [297]. The translucent Mg-sialon ceramics were prepared using SPS α - Si_3N_4 powders with 9 wt% AlN and 3 wt% MgO as sintering additives. Microstructural observations indicate that the optical and mechanical properties of Mg-sialon ceramics are affected by the density and α' : β' -phase ratio in sintered bodies, which are tailored by controlling the content of formed liquid phase and optimizing the parameters of SPS in present study. The material is toughened by the existence of a small amount of β' -sialon. The reason that the two-phase composite does not greatly compromise optical property could be attributed to the fine equiaxed microstructures and low content of β' -phase. Translucent Mg-sialon ceramics achieving 66.4 % of maximum transmittance, 21.4 ± 0.3 GPa hardness, and 6.1 ± 0.1 MPa $\text{m}^{1/2}$ fracture toughness were prepared by SPS at 1850 °C for 5 min. Figure 2.30 shows photographs of representative samples of the Mg-sialon ceramics.

Another example is (Mg, Y)- α/β -Sialon translucent ceramics processed by using hot pressing [298–302]. Although MgO is a suitable sintering aid for the development of translucent Mg- α/β -Sialon ceramics by using HP sintering, it is difficult to achieve complete densification, because MgO has high viscosity and high melting point. It has been acknowledged that Y_2O_3 is one of the promising sintering aids to facilitate complete densification and provide good mechanical properties of ceramics based on silicon nitride. Therefore, a combination of Y_2O_3 and MgO was proposed to prepare Mg- α/β -Sialon ceramics [298]. It was found that the amount of α -Sialon phase was increased with increasing content of Y_2O_3 up to 1 wt%. Too high content, e.g., 2 wt% Y_2O_3 , β -Sialon phase was observed. Thermal

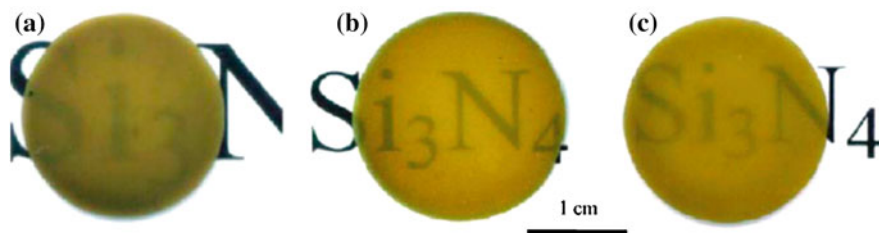


Fig. 2.30 Photographs of the translucent Mg-sialon ceramic slices of 0.5 mm in thickness sintered at different temperatures: **a** 1800 °C, **b** 1850 °C and, **c** 1870 °C. Reproduced with permission from [285]. Copyright © 2015, Elsevier

conductivity and CTE values were increased with increasing amount of Y_2O_3 . However, the presence of Y_2O_3 had a negative effect on transparency of the final ceramics.

Very few works have been report on the processing and characterization of Si_3N_4 transparent ceramics, because in principle they cannot be transparent. More recently, a study indicated that Si_3N_4 translucent ceramics could be obtained by using SPS [303]. Sintering aids, including Y_2O_3 , MgO and Al_2O_3 , were used to promote the densification of Si_3N_4 . The density, crystal phase, microstructure, transmittance, hardness, and fracture toughness of sintered Si_3N_4 were investigated. Highly densified sintered bodies were obtained in single Y_2O_3 and MgO systems, but not in single Al_2O_3 system. The XRD results indicated that sintered bodies were composed of $\beta\text{-Si}_3\text{N}_4$. The SEM images showed that all the sintered bodies had a fine-grained microstructure with an average diameter of 0.29–0.37 μm . The thickness of grain boundary was changed with additive content. The transmittance (T) and the wavelength (λ) followed the relationship of $T \propto \exp(-\lambda^{-2.3})$ due to the light scattering. The transmittance was mainly influenced by the refractive index of additives and the thickness of grain boundary phase. The hardness and fracture toughness of sintered ceramics were 12.6–15.5 GPa and 6.2–7.2 $\text{MPa m}^{1/2}$, respectively.

2.8 Summary

Various transparent ceramics have been developed by using various sintering technologies. Cubic crystal structure is one of the requirements for ceramics to be transparent, which should be modified, because noncubic crystalline transparent ceramics have been available. Furthermore, with the advancement of new sintering technologies, especially SPS, some ceramics that cannot be made to be transparent by using the conventional sintering methods, have emerged more recently. Although transparent ceramics for solid-state laser applications still form the main stream of these special materials, the number of transparent ceramics for other applications is rapidly increasing. It is highly suggested to pay attention to the new development of transparent ceramics, such as transparent ceramics derived from glasses and multicomponent transparent ceramics, which are different from the traditional transparent ceramics.

References

1. Chaim R, Shen ZJ, Nygren M (2004) Transparent nanocrystalline MgO by rapid and low-temperature spark plasma sintering. *J Mater Res* 19:2527–2531
2. Chaim R, Shen ZJ, Nygren M (2005) Transparent nanocrystalline MgO by low temperature spark plasma sintering. In: Lu S, Hu MZ, Gogotsi Y (eds) *Ceramic nanomaterials and nanotechnology III*. American Ceramic Society, Westerville, pp 21–30

3. Chen DY, Jordan EH, Gell M (2008) Pressureless sintering of translucent MgO ceramics. *Scripta Mater* 59:757–759
4. Fang Y, Agrawal D, Skandan G, Jain M (2004) Fabrication of translucent MgO ceramics using nanopowders. *Mater Lett* 58:551–554
5. Ikegami T, Matsuda SI, Suzuki H (1974) Effect of halide dopants on fabrication of transparent polycrystalline MgO. *J Am Ceram Soc* 57:507
6. Sanamyan T, Cooper C, Gilde G, Sutorik AC, Dubinskii M (2014) Fabrication and spectroscopic properties of transparent Nd³⁺:MgO and Er³⁺:MgO ceramics. *Laser Phys Lett* 11:065801
7. Miles GD, Sambell RAJ, Rutherford J, Stephens Gw (1967) Fabrication of fully dense transparent polycrystalline magnesia. *Trans Br Ceram Soc* 66:319
8. Misawa T, Moriyoshi Y, Yajima Y, Takenouchi S, Ikegami T (1999) Effect of silica and boron oxide on transparency of magnesia ceramics. *J Ceram Soc Jpn* 107:343–348
9. Suzuki M, Ikegami T, Yokoyama M, Komatsu T, Fukahori A (2005) Effects of chloride ion on densification transparency magnesia ceramics. *J Ceram Soc Jpn* 113:149–153
10. An LQ, Ito A, Zhang J, Tang DY, Goto T (2014) Highly transparent Nd³⁺:Lu₂O₃ produced by spark plasma sintering and its laser oscillation. *Opt Mater Express* 4:1420–1426
11. Antipov OL, Golovkin SY, Gorshkov ON, Zakharov NG, Zinovov AP, Kasatkin AP et al (2011) Structural, optical, and spectroscopic properties and efficient two-micron lasing of new Tm³⁺:Lu₂O₃ ceramics. *Quant Electron* 41:863–868
12. Chen QW, Shi Y, An LQ, Chen JY, Shi JL (2006) Fabrication and photoluminescence characteristics of Eu³⁺-Doped Lu₂O₃ transparent ceramics. *J Am Ceram Soc* 89:2038–2042
13. Kim W, Baker C, Bowman S, Florea C, Villalobos G, Shaw B, et al (2013) Laser oscillation from Ho³⁺ doped Lu₂O₃ ceramics. *Opt Mater Express* 3:176WL
14. Lu J, Takaichi K, Uematsu T, Shirakawa A, Musha M, Ueda K et al (2002) Promising ceramic laser material: highly transparent Nd³⁺:Lu₂O₃ ceramic. *Appl Phys Lett* 81:4324–4326
15. Seeley ZM, Kuntz JD, Cherepy NJ, Payne SA (2011) Transparent Lu₂O₃: Eu ceramics by sinter and HIP optimization. *Opt Mater* 33:1721–1726
16. Shi Y, Chen QW, Shi JL (2009) Processing and scintillation properties of Eu³⁺ doped Lu₂O₃ transparent ceramics. *Opt Mater* 31:729–733
17. Gheorghe C, Lupei A, Lupei V, Ikesue A, Enculescu M (2011) Intensity parameters of Tm³⁺ doped Sc₂O₃ transparent ceramic laser material. *Opt Mater* 33:501–505
18. Gheorghe C, Lupei A, Voicu F, Enculescu M (2012) Sm³⁺-doped Sc₂O₃ polycrystalline ceramics: spectroscopic investigation. *J Alloy Compd* 535:78–82
19. Lupei V, Lupei A, Ikesue A (2005) Transparent Nd and (Nd, Yb)-doped Sc₂O₃ ceramics as potential new laser materials. *Appl Phys Lett* 86
20. Alderighi D, Pirri A, Toci G, Vannini M, Esposito L, Costa AL et al (2010) Characterization of Yb:YAG ceramics as laser media. *Opt Mater* 33:205–210
21. Ba XW, Li J, Pan YB, Zeng YP, Kou HM, Liu WB et al (2013) Comparison of aqueous- and non-aqueous-based tape casting for preparing YAG transparent ceramics. *J Alloy Compd* 577:228–231
22. Bagayev SN, Osipov VV, Solomonov VI, Shitov VA, Maksimov RN, Lukyashin KE et al (2012) Fabrication of Nd³⁺:YAG laser ceramics with various approaches. *Opt Mater* 34:1482–1487
23. Chaim R, Kalina M, Shen JZ (2007) Transparent yttrium aluminum garnet (YAG) ceramics by spark plasma sintering. *J Eur Ceram Soc* 27:3331–3337
24. Chen ZH, Li JT, Hu ZG, Xu JJ (2008) Fabrication of YAG transparent ceramics by two step sintering process. *J Inorg Mater* 23:130–134
25. Frage N, Kalabukhov S, Sverdlov N, Ezersky V, Dariel MP (2010) Densification of transparent yttrium aluminum garnet (YAG) by SPS processing. *J Eur Ceram Soc* 30:3331–3337

26. Guo W, Lu TC, Tong SH (2007) Effect of phase of YAG powder synthesized by co-precipitation on transparent ceramic sintering. In: Pan W, Gong JH (eds) High-performance ceramics IV, Pts 1-3. Trans Tech Publications Ltd, Stafa-Zurich, pp 2054–2057
27. Agrawal D, Cheng JP, Roy R (2002) Microwave reactive sintering to fully transparent aluminum oxynitride (AlON) ceramics. In: McCauley JW, Crowson A, Gooch WA, Rajendran AM, Bless SJ, Logan KV et al (eds) Ceramic armor materials by design. American Ceramic Society, Westerville, pp 587–593
28. Hartnett TM, Bernstein SD, Maguire EA, Tustison RW (1998) Optical properties of AlON (aluminum oxynitride). *Infrared Phys Technol* 39:203–211
29. Jiang HW, Du HB, Tian TY, Wu H (2010) Influence of Y_2O_3 additive on transparent of AlON ceramics. In: Pan W, Gong JH (eds) Chinese ceramics communications, pp 580–581
30. Wang J, Zhang F, Chen F, Zhang J, Zhang HL, Tian R et al (2015) Effect of Y_2O_3 and La_2O_3 on the sinterability of gamma-AlON transparent ceramics. *J Eur Ceram Soc* 35:23–28
31. Choi JJ, Ryu J, Kim HE (2001) Microstructural evolution of transparent PLZT ceramics sintered in air and oxygen atmospheres. *J Am Ceram Soc* 84:1465–1469
32. Hertling GH (1971) Improved hot-pressed electrooptic ceramics in (Pb, La)(Zr, Ti) O_3 system. *J Am Ceram Soc* 54:303–309
33. Haertling GH (1999) Ferroelectric ceramics: history and technology. *J Am Ceram Soc* 82:797–818
34. Fang Y, Roy R, Agrawal DK, Roy DM (1996) Transparent mullite ceramics from diphasic aerogels by microwave and conventional processings. *Mater Lett* 28:11–15
35. Zhang GM, Wang YC, Fu ZY, Wang H, Wang WM, Zhang JY et al (2009) Transparent mullite ceramic from single-phase gel by spark plasma sintering. *J Eur Ceram Soc* 29:2705–2711
36. Dang KQ, Takei S, Kawahara M, Nanko M (2011) Pulsed electric current sintering of transparent Cr-doped Al_2O_3 . *Ceram Int* 37:957–963
37. Jiang D, Hulbert DM, Anselmi-Tamburini U, Ng T, Land D, Mukherjee AK (2008) Optically transparent polycrystalline Al_2O_3 produced by spark plasma sintering. *J Am Ceram Soc* 91:151–154
38. Krell A, Klimke J, Hutzler T (2009) Advanced spinel and sub- μm Al_2O_3 for transparent armour applications. *J Eur Ceram Soc* 29:275–281
39. Lu SZ, Yang QH (2009) Fluorescence characteristics of Al_2O_3 transparent ceramics. *Chin J Inorg Chem* 25:1642–1645
40. Nanko M, Dang KQ (2014) Two-step pulsed electric current sintering of transparent Al_2O_3 ceramics. *Adv Appl Ceram* 113:80–84
41. Penilla EH, Koderia Y, Garay JE (2013) Blue-green emission in terbium-doped alumina (Tb: Al_2O_3) transparent ceramics. *Adv Funct Mater* 23:6036–6043
42. Roussel N, Lallemand L, Chane-Ching JY, Guillemet-Fristch S, Durand B, Garnier V et al (2013) Highly dense transparent- Al_2O_3 ceramics from ultrafine nanoparticles via a standard SPS sintering. *J Am Ceram Soc* 96:1039–1042
43. Yang QH, Zeng ZJ, Xu J, Ding J, Su LB (2006) Spectroscopic characteristics of Cr^{4+} in transparent polycrystalline Al_2O_3 . *Acta Phys Sin* 55:4166–4169
44. Zhang XJ, Qiao GJ, Zhang X (2011) Effect of Mg doping on the microstructure and properties of α - Al_2O_3 transparent ceramics. In: Tan HH (ed) Mechanical, materials and manufacturing engineering, Pts 1–3. Trans Tech Publications Ltd, Stafa-Zurich, pp 1264–1269
45. Kim BN, Hiraga K, Morita K, Yoshida H (2007) Spark plasma sintering of transparent alumina. *Scripta Mater* 57:607–610
46. Kim BN, Hiraga K, Morita K, Yoshida H, Miyazaki T, Kagawa Y (2009) Microstructure and optical properties of transparent alumina. *Acta Mater* 57:1319–1326
47. Krell A, Blank P, Ma HW, Hutzler T, van Bruggen MPB, Apetz R (2003) Transparent sintered corundum with high hardness and strength. *J Am Ceram Soc* 86:12–18
48. Kim BN, Hiraga K, Morita K, Yoshida H (2009) Effects of heating rate on microstructure and transparency of spark-plasma-sintered alumina. *J Eur Ceram Soc* 29:323–327

49. Mizuta H, Oda K, Shibasaki Y, Maeda M, Machida M, Ohshima K (1992) Preparation of high strength and translucent alumina by hot isostatic pressing. *J Am Ceram Soc* 75:469–473
50. Apetz R, van Bruggen MPB (2003) Transparent alumina: a light-scattering model. *J Am Ceram Soc* 86:480–486
51. Krell A, Klimke J (2006) Effects of the homogeneity of particle coordination on solid-state sintering of transparent alumina. *J Am Ceram Soc* 89:1985–1992
52. Pauling L, Hendricks SB (1925) The crystal structures of hematite and corundum. *J Am Chem Soc* 47:781–790
53. Jin XH, Gao L, Sun J (2010) Highly transparent alumina spark plasma sintered from common-grade commercial powder: the effect of powder treatment. *J Am Ceram Soc* 93:1232–1236
54. Wei GC, Rhodes WH (2000) Sintering of translucent alumina in a nitrogen-hydrogen gas atmosphere. *J Am Ceram Soc* 83:1641–1648
55. Mao XJ, Wang SW, Shimai S, Guo JK (2008) Transparent polycrystalline alumina ceramics with orientated optical axes. *J Am Ceram Soc* 91:3431–3433
56. Li JG, Ye YP (2006) Densification and grain growth of Al_2O_3 nanoceramics during pressureless sintering. *J Am Ceram Soc* 89:139–143
57. Godlinski D, Kuntz M, Grathwohl G (2002) Transparent alumina with submicrometer grains by float packing and sintering. *J Am Ceram Soc* 85:2449–2456
58. Liu W, Bo TZ, Xie ZP, Wu Y, Yang XF (2011) Fabrication of injection moulded translucent alumina ceramics via pressureless sintering. *Adv Appl Ceram* 110:251–254
59. Roh JY, Kwon J, Lee CS, Choi JS (2011) Novel fabrication of pressure-less sintering of translucent powder injection molded (PIM) alumina blocks. *Ceram Int* 37:321–326
60. Liu W, Xie ZP, Bo TZ, Yang XF (2011) Injection molding of surface modified powders with high solid loadings: a case for fabrication of translucent alumina ceramics. *J Eur Ceram Soc* 31:1611–1617
61. Kim DS, Lee JH, Sung RJ, Kim SW, Kim HS, Park JS (2007) Improvement of translucency in Al_2O_3 ceramics by two-step sintering technique. *J Eur Ceram Soc* 27:3629–3632
62. Liu W, Xie ZP, Liu GW, Yang XF (2011) Novel preparation of translucent alumina ceramics induced by doping additives via chemical precipitation method. *J Am Ceram Soc* 94:3211–3215
63. Liu GW, Xie ZP, Liu W, Chen LX, Wu Y (2012) Fabrication of translucent alumina ceramics from pre-sintered bodies infiltrated with sintering additive precursor solutions. *J Eur Ceram Soc* 32:711–715
64. Hotta Y, Tsugoshi T, Nagaoka T, Yasuoka M, Nakamura K, Watari K (2003) Effect of oligosaccharide alcohol addition to alumina slurry and translucent alumina produced by slip casting. *J Am Ceram Soc* 86:755–760
65. Petit J, Dethare P, Sergeant A, Marino R, Ritti MH, Landais S et al (2011) Sintering of alpha-alumina for highly transparent ceramic applications. *J Eur Ceram Soc* 31:1957–1963
66. Suarez M, Fernandez A, Menendez JL, Torrecillas R (2009) Grain growth control and transparency in spark plasma sintered self-doped alumina materials. *Scripta Mater* 61:931–934
67. Alvarez-Clemares I, Mata-Osoro G, Fernandez A, Lopez-Esteban S, Pecharroman C, Palomares J et al (2010) Transparent alumina/ceria nanocomposites by spark plasma sintering. *Adv Eng Mater* 12:1154–1160
68. Roussel N, Lallemant L, Durand B, Guillemet S, Ching JYC, Fantozzi G et al (2011) Effects of the nature of the doping salt and of the thermal pre-treatment and sintering temperature on spark plasma sintering of transparent alumina. *Ceram Int* 37:3565–3573
69. Grasso S, Hu CF, Maizza G, Kim BN, Sakka Y (2011) Effects of pressure application method on transparency of spark plasma sintered alumina. *J Am Ceram Soc* 94:1405–1409
70. Stuer M, Zhao Z, Aschauer U, Bowen P (2010) Transparent polycrystalline alumina using spark plasma sintering: effect of Mg, Y and La doping. *J Eur Ceram Soc* 30:1335–1343
71. Brosnan KH, Messing GL, Agrawal DK (2003) Microwave sintering of alumina at 2.45 GHz. *J Am Ceram Soc* 86:1307–1312

72. Watzig K, Hutzler T, Krell A (2009) Transparent spinel by reactive sintering of different alumina modifications with MgO. *CFI-Ceram Forum Int* 86:E47–E49
73. Krell A, Baur G, Dahne C (2003) Transparent sintered sub- μm Al_2O_3 with IR transmissivity equal to sapphire. In: Tustison RW (ed) *Window and dome technologies VIII*. SPIE-Int Soc Optical Engineering, Bellingham, pp 199–207
74. Krell A (1998) The effects of load, grain size, and grain boundaries on the hardness of alumina. In: Bray D (ed) *22nd annual conference on composites, advanced ceramics, materials, and structures: B*, pp 159–68
75. Saha D, Mistry KK, Giri R, Guha A, Sensgupta K (2005) Dependence of moisture absorption property on sol-gel process of transparent nano-structured $\gamma\text{-Al}_2\text{O}_3$ ceramics. *Sens Actuators B-Chem* 109:363–366
76. Lei LW, Fu ZY, Wang H, Lee SW, Niihara K (2012) Transparent yttria stabilized zirconia from glycine-nitrate process by spark plasma sintering. *Ceram Int* 38:23–28
77. Zhang HB, Kim BN, Morita K, Yoshida H, Lim JH, Hiraga K (2010) Optimization of high-pressure sintering of transparent zirconia with nano-sized grains. *J Alloy Compd* 508:196–199
78. Anselmi-Tamburini U, Woolman JN, Munir ZA (2007) Transparent nanometric cubic and tetragonal zirconia obtained by high-pressure pulsed electric current sintering. *Adv Funct Mater* 17:3267–3273
79. Peuchert U, Okano Y, Menke Y, Reichel S, Ikesue A (2009) Transparent cubic- ZrO_2 ceramics for application as optical lenses. *J Eur Ceram Soc* 29:283–291
80. Vahldiek FW (1967) Translucent ZrO_2 prepared at high pressures. *J Less-Common Metals* 13:530–540
81. Mazdizyas KS, Lynch CT, Smith JS (1967) Cubic phase stabilization of translucent yttria-zirconia at very low temperatures. *J Am Ceram Soc* 50:532–537
82. Duran P, Recio P, Jurado JR, Pascual C, Moure C (1989) Preparation, sintering and properties of translucent Er_2O_3 -doped tetragonal zirconia. *J Am Ceram Soc* 72:2088–2093
83. Srdic VV, Winterer M, Hahn H (2000) Sintering behavior of nanocrystalline zirconia prepared by chemical vapor synthesis. *J Am Ceram Soc* 83:729–736
84. Srdic VV, Winterer M, Hahn H (2000) Sintering behavior of nanocrystalline zirconia doped with alumina prepared by chemical vapor synthesis. *J Am Ceram Soc* 83:1853–1860
85. Tsukuma K (1986) Transparent titania yttria zirconia ceramics. *J Mater Sci Lett* 5:1143–1144
86. Casolco SR, Xu J, Garay JE (2008) Transparent/Translucent polycrystalline nanostructured yttria stabilized zirconia with varying colors. *Scripta Mater* 58:516–519
87. Alaniz JE, Perez-Gutierrez FG, Aguilar G, Garay JE (2009) Optical properties of transparent nanocrystalline yttria stabilized zirconia. *Opt Mater* 32:62–68
88. Tsukuma K, Yamashita I, Kusunose T (2008) Transparent 8 mol% $\text{Y}_2\text{O}_3\text{-ZrO}_2$ (8Y) ceramics. *J Am Ceram Soc* 91:813–818
89. Zhang H, Kim B-N, Morita K, Hiraga HYK, Sakka Y (2011) Effect of sintering temperature on optical properties and microstructure of translucent zirconia prepared by high-pressure spark plasma sintering. *Sci Technol Adv Mater* 12:055003
90. Klimke J, Krell A (2005) Polycrystalline ZrO_2 -transparent ceramics with high refractive index. Fraunhofer Institute for Ceramic Technologies and Sintered Materials (IKTS), p 23
91. Trunec M, Chlup Z (2009) Higher fracture toughness of tetragonal zirconia ceramics through nanocrystalline structure. *Scripta Mater* 61:56–59
92. Klimke J, Trunec M, Krell A (2011) Transparent tetragonal yttria-stabilized zirconia ceramics: influence of scattering caused by birefringence. *J Am Ceram Soc* 94:1850–1858
93. Chaim R, Hefetz M (1998) Fabrication of dense nanocrystalline $\text{ZrO}_2\text{-3 wt.}\%$ Y_2O_3 by hot-isostatic pressing. *J Mater Res* 13:1875–1880
94. Nigara Y (1968) Measurement of optical constants of yttrium oxide. *Jpn J Appl Phys* 7:404–408
95. Fukabori A, Yanagida T, Pejchal J, Maeo S, Yokota Y, Yoshikawa A et al (2010) Optical and scintillation characteristics of Y_2O_3 transparent ceramic. *J Appl Phys* 107:073501

96. Hou XR, Zhou SM, Jia TT, Lin H, Teng H (2011) Investigation of up-conversion luminescence properties of RE/Yb co-doped Y_2O_3 transparent ceramic (RE = Er, Ho, Pr, and Tm). *Phys B-Condens Matter* 406:3931–3937
97. Micheli AL, Dungan DF, Mantese JV (1992) High-density yttria for practical ceramic applications. *J Am Ceram Soc* 75:709–711
98. Iwasawa J, Nishimizu R, Tokita M, Kiyohara M, Uematsu K (2007) Plasma-resistant dense yttrium oxide film prepared by aerosol deposition process. *J Am Ceram Soc* 90:2327–2332
99. Lefever RA, Matsko J (1967) Transparent yttrium oxide ceramics. *Mater Res Bull* 2:865–869
100. Huang YH, Jiang DL, Zhang JX, Lin QL (2009) Fabrication of transparent lanthanum-doped yttria ceramics by combination of two-step sintering and vacuum sintering. *J Am Ceram Soc* 92:2883–2887
101. Ikegami T, Li JG, Mori T, Moriyoshi Y (2002) Fabrication of transparent yttria ceramics by the low-temperature synthesis of yttrium hydroxide. *J Am Ceram Soc* 85:1725–1729
102. Ikegami T, Mori T, Yajima Y, Takenouchi S, Misawa T, Moriyoshi Y (1999) Fabrication of transparent yttria ceramics through the synthesis of yttrium hydroxide at low temperature and doping by sulfate ions. *J Ceram Soc Jpn* 107:297–299
103. Jin LL, Zhou GH, Shimai S, Zhang J, Wang SW (2010) ZrO_2 -doped Y_2O_3 transparent ceramics via slip casting and vacuum sintering. *J Eur Ceram Soc* 30:2139–2143
104. Zhang J, An LQ, Liu M, Shimai S, Wang SW (2009) Sintering of $Yb^{3+}:Y_2O_3$ transparent ceramics in hydrogen atmosphere. *J Eur Ceram Soc* 29:305–309
105. Greskovich C, Chernoch JP (1973) Polycrystalline ceramic lasers. *J Appl Phys* 44:4599–4606
106. Rhodes WH (1981) Controlled transient solid 2nd-phase sintering of yttria. *J Am Ceram Soc* 64:13–19
107. Saito N, Matsuda S, Ikegami T (1998) Fabrication of transparent yttria ceramics at low temperature using carbonate-derived powder. *J Am Ceram Soc* 81:2023–2028
108. Podowitz SR, Gaume R, Feigelson RS (2010) Effect of europium concentration on densification of transparent $Eu:Y_2O_3$ scintillator ceramics using hot pressing. *J Am Ceram Soc* 93:82–88
109. Hou X, Zhou S, Jia T, Lin H, Teng H (2011) Effect of Nd concentration on structural and optical properties of $Nd:Y_2O_3$ transparent ceramic. *J Lumin* 131:1953–1958
110. Mouzon J, Maitre A, Frisk L, Lehto N, Oden M (2009) Fabrication of transparent yttria by HIP and the glass-encapsulation method. *J Eur Ceram Soc* 29:311–316
111. Eilers H (2007) Fabrication, optical transmittance, and hardness of IR-transparent ceramics made from nanophase yttria. *J Eur Ceram Soc* 27:4711–4717
112. Bezdorozhev O, Borodianska H, Sakka Y, Vasylykiv O (2011) Tough yttria-stabilized zirconia ceramic by low-temperature spark plasma sintering of long-term stored nanopowders. *J Nanosci Nanotechnol* 11:7901–7909
113. Yoshida H, Morita K, Kim B-N, Hiraga K, Kodo M, Soga K et al (2008) Densification of nanocrystalline yttria by low temperature spark plasma sintering. *J Am Ceram Soc* 91:1707–1710
114. Yoshida H, Morita K, Kim B-N, Hiraga K, Yamanaka K, Soga K et al (2011) Low-temperature spark plasma sintering of yttria ceramics with ultrafine grain size. *J Am Ceram Soc* 94:3301–3307
115. Chaim R, Shlayer A, Estournes C (2009) Densification of nanocrystalline Y_2O_3 ceramic powder by spark plasma sintering. *J Eur Ceram Soc* 29:91–98
116. An L, Ito A, Goto T (2012) Transparent yttria produced by spark plasma sintering at moderate temperature and pressure profiles. *J Eur Ceram Soc* 32:1035–1040
117. Zhang HB, Kim BN, Morita K, Yoshida H, Hiraga K, Sakka Y (2011) Fabrication of transparent yttria by high-pressure spark plasma sintering. *J Am Ceram Soc* 94:3206–3210
118. Wen L, Sun XD, Lu Q, Xu GX, Hu XZ (2006) Synthesis of yttria nanopowders for transparent yttria ceramics. *Opt Mater* 29:239–245
119. Huang YH, Jiang DL, Zhang JX, Lin QL, Huang ZR (2011) Synthesis of mono-dispersed spherical $Nd:Y_2O_3$ powder for transparent ceramics. *Ceram Int* 37:3523–3529

120. Ikesue A, Kamata K, Yoshida K (1996) Synthesis of transparent Nd-doped $\text{HfO}_2\text{-Y}_2\text{O}_3$ ceramics using HIP. *J Am Ceram Soc* 79:359–364
121. Majima K, Niimi N, Watanabe M, Katsuyama S, Nagai H (1993) Effect of LiF addition on the preparation of transparent Y_2O_3 by vacuum hot-pressing method. *J Jpn Inst Met* 57:1221–1226
122. Hou XR, Zhou SM, Li YK, Li WJ (2010) Effect of ZrO_2 on the sinterability and spectral properties of $(\text{Yb}_{0.05}\text{Y}_{0.95})_2\text{O}_3$ transparent ceramic. *Opt Mater* 32:920–923
123. Yi Q, Zhou S, Teng H, Lin H, Hou X, Jia T (2012) Structural and optical properties of Tm: Y_2O_3 transparent ceramic with La_2O_3 , ZrO_2 as composite sintering aid. *J Eur Ceram Soc* 32:381–388
124. Huang YH, Jiang DL, Zhang JX, Lin QL, Huang ZG (2010) Sintering of transparent yttria ceramics in oxygen atmosphere. *J Am Ceram Soc* 93:2964–2967
125. Serivalsatit K, Kokuzo B, Yazgan-Kokuzo B, Kennedy M, Ballato J (2010) Synthesis, processing, and properties of submicrometer-grained highly transparent yttria ceramics. *J Am Ceram Soc* 93:1320–1325
126. Gheorghe C, Lupei A, Lupei V, Gheorghe L, Ikesue A (2009) Spectroscopic properties of Ho^{3+} doped Sc_2O_3 transparent ceramic for laser materials. *J Appl Phys* 105:123110
127. Li JG, Ikegami T, Mori T (2005) Fabrication of transparent, sintered Sc_2O_3 ceramics. *J Am Ceram Soc* 88:817–821
128. Li JG, Ikegami T, Mori T, Yajima Y (2004) Sc_2O_3 nanopowders via hydroxyl precipitation: effects of sulfate ions on powder properties. *J Am Ceram Soc* 87:1008–1013
129. Kuck S, Fornasiero L, Mix E, Huber G (2000) Spectroscopic properties of Cr-doped Sc_2O_3 . *J Lumin* 87–9:1122–1125
130. Fornasiero L, Mix E, Peters V, Petermann K, Huber G (1999) New oxide crystals for solid state lasers. *Cryst Res Technol* 34:255–260
131. Li JG, Ikegami T, Mori T (2003) Fabrication of transparent Sc_2O_3 ceramics with powders thermally pyrolyzed from sulfate. *J Mater Res* 18:1816–1822
132. Lupei A, Lupei V, Gheorghe C, Ikesue A (2008) Excited states dynamics of Er^{3+} in Sc_2O_3 ceramic. *J Lumin* 128:918–920
133. Longuet L, Bravo AC, Autissier D, Vissie P, Longuet JL, Lambert S (2009) Preparation of Yb-doped Sc_2O_3 transparent ceramics for laser applications. In: Dierolf V, Fujiwara Y, Hommerich U, Ruterana P, Zavada JM (eds) *Rare-earth doping of advanced materials for photonic applications*. Materials Research Society, Warrendale, pp 161–166
134. Li JG, Ikegami T, Mori T (2004) Solution-based processing of Sc_2O_3 nanopowders yielding transparent ceramics. *J Mater Res* 19:733–736
135. Wang Y, Lu B, Sun X, Sun T, Xu H (2011) Synthesis of nanocrystalline Sc_2O_3 powder and fabrication of transparent Sc_2O_3 ceramics. *Adv Appl Ceram* 110:95–98
136. Serivalsatit K, Ballato J (2010) Submicrometer grain-sized transparent erbium-doped scandia ceramics. *J Am Ceram Soc* 93:3657–3662
137. Trabelsi I, Maalej R, Dammak M, Lupei A, Kamoun M (2010) Crystal field analysis of Er^{3+} in Sc_2O_3 transparent ceramics. *J Lumin* 130:927–931
138. An LQ, Ito A, Goto T (2011) Two-step pressure sintering of transparent lutetium oxide by spark plasma sintering. *J Eur Ceram Soc* 31:1597–1602
139. Wang ZF, Zhang WP, Lin L, You BG, Fu YB, Yin M (2008) Preparation and spectroscopic characterization of $\text{Lu}_2\text{O}_3\text{:Eu}^{3+}$ nanopowders and ceramics. *Opt Mater* 30:1484–1488
140. An LQ, Ito A, Goto T (2011) Fabrication of transparent lutetium oxide by spark plasma sintering. *J Am Ceram Soc* 94:695–698
141. Kan A, Moriyama T, Takahashi S, Ogawa H (2011) Low-temperature sintering and microwave dielectric properties of MgO ceramic with LiF addition. *Jpn J Appl Phys* 50:09NF2
142. Rhodes WH, Sellers DJ (1967) Mechanism of pressure sintering MgO with LiF additions. *Am Ceram Soc Bull* 46:469
143. Hart PE, Pask JA (1971) Effect of LiF on creep of MgO. *J Am Ceram Soc* 54:315–316

144. Itatani K, Tsujimoto T, Kishimoto A (2006) Thermal and optical properties of transparent magnesium oxide ceramics fabricated by post hot-isostatic pressing. *J Eur Ceram Soc* 26:639–645
145. Xu GG, Zhang XD, He W, Liu H, Li H, Boughton RI (2006) Preparation of highly dispersed YAG nano-sized powder by co-precipitation method. *Mater Lett* 60:962–965
146. Ikesue A, Furusato I, Kamata K (1995) Fabrication of polycrystalline transparent YAG ceramics by a solid-state reaction method. *J Am Ceram Soc* 78:225–228
147. Ikesue A, Kinoshita T, Kamata K, Yoshida K (1995) Fabrication and optical properties of high performance polycrystalline Nd-YAG ceramics for solid-state lasers. *J Am Ceram Soc* 78:1033–1040
148. Zhang XD, Liu H, He W, Wang JY, Li X, Boughton RI (2005) Novel synthesis of YAG by solvothermal method. *J Cryst Growth* 275:E1913–E1917
149. Liu Q, Liu J, Li J, Ivanov M, Medvedev A, Zeng Y et al (2014) Solid-state reactive sintering of YAG transparent ceramics for optical applications. *J Alloy Compd* 616:81–88
150. Li JG, Ikegami T, Lee JH, Mori T (2000) Low-temperature fabrication of transparent yttrium aluminum garnet (YAG) ceramics without additives. *J Am Ceram Soc* 83:961–963
151. Zych E, Brecher C (2000) Temperature dependence of host-associated luminescence from YAG transparent ceramic material. *J Lumin* 90:89–99
152. Liu J, Liu K, Wang HS, Gao F, Liao R (2012) Preparation of silicon nitride porous ceramics. In: Pan W, Gong JH (eds) *High-performance ceramics III, Parts 1 and 2*. Trans Tech Publications Ltd, Stafa-Zurich, pp 824–827
153. Zhou J, Zhang WX, Wang LA, Shen YQ, Li J, Liu WB et al (2011) Fabrication, microstructure and optical properties of polycrystalline $\text{Er}^{3+}:\text{Y}_3\text{Al}_5\text{O}_{12}$ ceramics. *Ceram Int* 37:119–125
154. Li J, Chen Q, Feng GY, Wu WJ, Xiao DQ, Zhu JG (2012) Optical properties of the polycrystalline transparent Nd:YAG ceramics prepared by two-step sintering. *Ceram Int* 38: S649–S652
155. Dewith G, Vandijk HJA (1984) Transparent $\text{Y}_3\text{Al}_5\text{O}_{12}$ ceramics. *Mater Res Bull* 19:1669–1674
156. Liu W, Li J, Jiang B, Zhang D, Pan Y (2012) Effect of La_2O_3 on microstructures and laser properties of Nd:YAG ceramics. *J Alloy Compd* 512:1–4
157. Yang H, Qin X, Zhang J, Ma J, Tang D, Wang S et al (2012) The effect of MgO and SiO_2 codoping on the properties of Nd:YAG transparent ceramic. *Opt Mater* 34:940–943
158. Appagyeyi KA, Messing GL, Dumm JQ (2008) Aqueous slip casting of transparent yttrium aluminum garnet (YAG) ceramics. *Ceram Int* 34:1309–1313
159. Stevenson AJ, Li X, Martinez MA, Anderson JM, Suchy DL, Kupp ER et al (2011) Effect of SiO_2 on densification and microstructure development in Nd:YAG transparent ceramics. *J Am Ceram Soc* 94:1380–1387
160. Liu WB, Zhang WX, Li J, Kou HM, Zhang D, Pan YB (2011) Synthesis of Nd:YAG powders leading to transparent ceramics: the effect of MgO dopant. *J Eur Ceram Soc* 31:653–657
161. Chen C, Zhou SM, Lin H, Yi Q (2012) Selection of different sintering aids and heat-treatment of Y_2O_3 raw powders for $\text{Yb}^{3+}:\text{Y}_3\text{Al}_5\text{O}_{12}$ transparent ceramics. In: Shao J, Sugioka K, Stolz CJ (eds) *Pacific rim laser damage 2011: optical materials for high power lasers*, p 820620
162. Li YK, Zhou SM, Lin H, Hou XR, Li WJ, Teng H et al (2010) Fabrication of Nd:YAG transparent ceramics with TEOS, MgO and compound additives as sintering aids. *J Alloy Compd* 502:225–230
163. Chen PL, Chen IW (1996) Sintering of fine oxide powders: I, Microstructural evolution. *J Am Ceram Soc* 79:3129–3141
164. Liu WB, Zhang WX, Li J, Kou HM, Shen YH, Wang L et al (2010) Influence of pH values on (Nd + Y): Al molar ratio of Nd:YAG nanopowders and preparation of transparent ceramics. *J Alloy Compd* 503:525–528
165. Esposito L, Piancastelli A (2009) Role of powder properties and shaping techniques on the formation of pore-free YAG materials. *J Eur Ceram Soc* 29:317–322

166. Serantoni M, Piancastelli A, Costa AL, Esposito L (2012) Improvements in the production of Yb:YAG transparent ceramic materials: spray drying optimisation. *Opt Mater* 34:995–1001
167. Liu WB, Zhang WX, Li J, Zhang D, Pan YB (2012) Preparation of spray-dried powders leading to Nd:YAG ceramics: the effect of PVB adhesive. *Ceram Int* 38:259–264
168. Gong H, Zhang J, Tang DY, Xie GQ, Huang H, Ma J (2011) Fabrication and laser performance of highly transparent Nd:YAG ceramics from well-dispersed Nd:Y₂O₃ nanopowders by freeze-drying. *J Nanopart Res* 13:3853–3860
169. Rabinovitch Y, Bogicevic C, Karolak F, Tetard D, Dammak H (2008) Freeze-dried nanometric neodymium-doped YAG powders for transparent ceramics. *J Mater Process Technol* 199:314–320
170. Yagi H, Takaichi K, Ueda K, Yanagitani T, Karninskii AA (2006) Influence of annealing conditions on the optical properties of chromium-doped ceramic Y₃Al₅O₁₂. *Opt Mater* 29:392–396
171. Li J, Wu Y, Pan Y, Guo J (2006) Fabrication of Cr⁴⁺, Nd³⁺:YAG transparent ceramics for self-Q-switched laser. *J Non-Cryst Solids* 352:2404–2407
172. Nishiura S, Tanabe S, Fujioka K, Fujimoto Y (2011) Properties of transparent Ce:YAG ceramic phosphors for white LED. *Opt Mater* 33:688–691
173. Feng T, Shi JL, Jiang DY (2006) Preparation and optical properties of transparent Eu³⁺:Y₃Al_{5(1-x)}Sc_{5x}O₁₂ ceramics. *J Am Ceram Soc* 89:1590–1593
174. Fu Y, Li J, Liu Y, Liu L, Zhao H, Pan Y (2014) Effect of air annealing on the optical properties and laser performance of Nd:YAG transparent ceramics. *Opt Mater Express* 4:2108–2115
175. Zhang W, Lu T, Wei N, Ma B, Li F, Lu Z et al (2012) Effect of annealing on the optical properties of Nd:YAG transparent ceramics. *Opt Mater* 34:685–690
176. Yanagida T, Kamada K, Fujimoto Y, Yokota Y, Yoshikawa A, Yagi H et al (2011) Scintillation properties of transparent ceramic and single crystalline Nd:YAG scintillators. *Nucl Instr Meth Phys Res Sect A* 631:54–57
177. Jiang BX, Lu X, Zeng YP, Liu SP, Li J, Liu WB et al (2013) Synthesis and properties of Yb:LuAG transparent ceramics. *Phys Status Solidi C* 10(6):958–961
178. Li HL, Liu XJ, Huang LP (2005) Fabrication of transparent cerium-doped lutetium aluminum garnet (LuAG:Ce) ceramics by a solid-state reaction method. *J Am Ceram Soc* 88:3226–3228
179. Li HL, Liu XJ, Huang LP (2006) Fabrication of transparent Ce:LuAG ceramics by a solid-state reaction method. *J Inorg Mater* 21:1161–1166
180. Liao YK, Jiang DY, Feng T, Zhang N (2007) Preparation, spectroscopic properties and enhanced luminescence of Tb³⁺-doped LuAG phosphors and transparent ceramics by introduction of Sc³⁺. *J Mater Sci* 42:5406–5410
181. Luo D, Zhang J, Xu C, Lin H, Yang H, Zhu H et al (2013) Mode-locked Yb:LuAG ceramics laser. *Phys Status Solidi C* 10(6):967–968
182. Luo D, Zhang J, Xu C, Yang H, Lin H, Zhu H et al (2012) Yb:LuAG laser ceramics: a promising high power laser gain medium. *Opt Mater Express* 2:1425–1431
183. Pirri A, Vannini M, Babin V, Nikl M, Toci G (2013) CW and quasi-CW laser performance of 10 at.% Yb³⁺:LuAG ceramic. *Laser Phys* 23
184. Shen YQ, Feng XQ, Babin V, Nikl M, Vedda A, Moretti F et al (2013) Fabrication and scintillation properties of highly transparent Pr:LuAG ceramics using Sc, La-based isovalent sintering aids. *Ceram Int* 39:5985–5990
185. Wagner N, Herden B, Dierkes T, Plewa J, Justel T (2012) Towards the preparation of transparent LuAG:Nd³⁺ ceramics. *J Eur Ceram Soc* 32:3085–3089
186. Zhang WX, Li J, Liu WB, Pan YB, Guo JK (2009) Fabrication and properties of highly transparent Tm₃Al₅O₁₂ (TmAG) ceramics. *Ceram Int* 35:2927–2931
187. Goldstein A (2012) Correlation between MgAl₂O₄-spinel structure, processing factors and functional properties of transparent parts (progress review). *J Eur Ceram Soc* 32:2869–2886

188. du Merac MR, Kleebe HJ, Muller MM, Reimanis IE (2013) Fifty years of research and development coming to fruition; unraveling the complex interactions during processing of transparent magnesium aluminate (MgAl_2O_4) spinel. *J Am Ceram Soc* 96:3341–3365
189. Ganesh I (2013) A review on magnesium aluminate (MgAl_2O_4) spinel: synthesis, processing and applications. *Int Mater Rev* 58:63–112
190. Rothman A, Kalabukhov S, Sverdlov N, Dariel MP, Frage N (2014) The effect of grain size on the mechanical and optical properties of spark plasma sintering-processed magnesium aluminate spinel MgAl_2O_4 . *Int J Appl Ceram Technol* 11:146–153
191. Sepulveda JL, Loutfy RO, Chang SY, Ibrahim S (2011) High performance spinel ceramics for IR windows and domes. In: Tustison RW (ed) *Window and dome technologies and materials*, vol XII, p 801604
192. Bratton RJ (1974) Translucent sintered MgAl_2O_4 . *J Am Ceram Soc* 57:283–286
193. Dericioglu AF, Kagawa Y (2003) Effect of grain boundary microcracking on the light transmittance of sintered transparent MgAl_2O_4 . *J Eur Ceram Soc* 23:951–959
194. Li JG, Ikegami T, Lee JH, Mori T (2000) Fabrication of translucent magnesium aluminum spinel ceramics. *J Am Ceram Soc* 83:2866–2868
195. Dericioglu AF, Boccaccini AR, Dlouhy I, Kagawa Y (2005) Effect of chemical composition on the optical properties and fracture toughness of transparent magnesium aluminate spinel ceramics. *Mater Trans* 46:996–1003
196. Wang C, Zhao Z (2009) Transparent MgAl_2O_4 ceramic produced by spark plasma sintering. *Scripta Mater* 61:193–196
197. Morita K, Kim BN, Hiraga K, Yoshida H (2008) Fabrication of transparent MgAl_2O_4 spinel polycrystal by spark plasma sintering processing. *Scripta Mater* 58:1114–1117
198. Meir S, Kalabukhov S, Froumin N, Dariel MP, Frage N (2009) Synthesis and densification of transparent magnesium aluminate spinel by SPS processing. *J Am Ceram Soc* 92:358–364
199. Frage N, Cohen S, Meir S, Kalabukhov S, Dariel MP (2007) Spark plasma sintering (SPS) of transparent magnesium-aluminate spinel. *J Mater Sci* 42:3273–3275
200. Sokol M, Kalabukhov S, Dariel MP, Frage N (2014) High-pressure spark plasma sintering (SPS) of transparent polycrystalline magnesium aluminate spinel (PMAS). *J Eur Ceram Soc* 34:4305–4310
201. Kim BN, Morita K, Lim JH, Hiraga K, Yoshida H (2010) Effects of preheating of powder before spark plasma sintering of transparent MgAl_2O_4 spinel. *J Am Ceram Soc* 93:2158–2160
202. Morita K, Kim BN, Yoshida H, Hiraga K (2009) Spark-plasma-sintering condition optimization for producing transparent MgAl_2O_4 spinel polycrystal. *J Am Ceram Soc* 92:1208–1216
203. Tsukuma K (2006) Transparent MgAl_2O_4 spinel ceramics produced by HIP post-sintering. *J Ceram Soc Jpn* 114:802–806
204. Villalobos GR, Sanghera JS, Aggarwal ID (2005) Degradation of magnesium aluminum spinel by lithium fluoride sintering aid. *J Am Ceram Soc* 88:1321–1322
205. Krell A, Hutzler T, Klimke J, Potthoff A (2010) Fine-grained transparent spinel windows by the processing of different nanopowders. *J Am Ceram Soc* 93:2656–2666
206. DiGiovanni AA, Fehrenbacher L, Roy DW (2005) Hard transparent domes and windows from magnesium aluminate spinel. In: Tustison RW (ed) *Window and dome technologies and materials* IX, pp 56–63
207. Bernard-Granger G, Benameur N, Guizard C, Nygren M (2009) Influence of graphite contamination on the optical properties of transparent spinel obtained by spark plasma sintering. *Scripta Mater* 60:164–167
208. Kleebe HJ, Reimanis IE, Cook RL (2005) Processing and microstructure characterization of transparent spinel monoliths. In: DiAntonio CB (ed) *Characterization and modeling to control sintered ceramic microstructures and properties*, pp 61–68
209. Goldstein A, Goldenberg A, Yeshurun Y, Hefetz M (2008) Transparent MgAl_2O_4 spinel from a powder prepared by flame spray pyrolysis. *J Am Ceram Soc* 91:4141–4144

210. Sutorik AC, Gilde G, Swab JJ, Cooper C, Gamble R, Shanholtz E (2012) The production of transparent MgAl_2O_4 ceramic using calcined powder mixtures of $\text{Mg}(\text{OH})_2$ and $\gamma\text{-Al}_2\text{O}_3$ or AlOOH . *Int J Appl Ceram Technol* 9:575–587
211. Ping LR, Azad AM, Dung TW (2001) Magnesium aluminate (MgAl_2O_4) spinel produced via self-heat-sustained (SHS) technique. *Mater Res Bull* 36:1417–1430
212. du Merac MR, Reimanis IE, Smith C, Kleebe H-J, Mueller MM (2013) Effect of impurities and LiF additive in hot-pressed transparent magnesium aluminate spinel. *Int J Appl Ceram Technol* 10:E33–E48
213. Reimanis IE, Kleebe H-J (2007) Reactions in the sintering of MgAl_2O_4 spinel doped with LiF. *Int J Mater Res* 98:1273–1278
214. Reimanis IE, Rozenburg K, Kleebe HJ, Cook RL (2005) Fabrication of transparent spinel: the role of impurities. In: Tustison RW (ed) *Window and dome technologies and materials IX*, pp 48–55
215. Rozenburg K, Reimanis IE, Kleebe HJ, Cook RL (2007) Chemical interaction between LiF and MgAl_2O_4 spinel during sintering. *J Am Ceram Soc* 90:2038–2042
216. Rozenburg K, Reimanis IE, Kleebe HJ, Cook RL (2008) Sintering kinetics of a MgAl_2O_4 spinel doped with LiF. *J Am Ceram Soc* 91:444–450
217. Sutorik AC, Gilde G, Cooper C, Wright J, Hilton C (2012) The effect of varied amounts of LiF sintering aid on the transparency of alumina rich spinel ceramic with the composition $\text{MgO-1.5 Al}_2\text{O}_3$. *J Am Ceram Soc* 95:1807–1810
218. Sutorik AC, Gilde G, Swab JJ, Cooper C, Gamble R, Shanholtz E (2012) Transparent solid solution magnesium aluminate spinel polycrystalline ceramic with the alumina-rich composition $\text{MgO-1.2 Al}_2\text{O}_3$. *J Am Ceram Soc* 95:636–643
219. Krell A, Waetzig K, Klimke J (2011) Effects and elimination of nanoporosity in transparent sintered spinel (MgAl_2O_4). In: *Window and dome technologies and materials XII*, vol 8016, p 801602
220. Harris DC (2005) History of development of polycrystalline optical spinel in the U.S. In: Tustison RW (ed) *Window and dome technologies and materials IX*. *Spie-Int Soc Optical Engineering*, Bellingham, pp 1–22
221. Gledhill AD, Li DS, Mroz T, Goldman LM, Padture NP (2012) Strengthening of transparent spinel/ Si_3N_4 nanocomposites. *Acta Mater* 60:1570–1575
222. Wollmershauser JA, Feigelson BN, Gorzkowski EP, Ellis CT, Goswami R, Qadri SB et al (2014) An extended hardness limit in bulk nanoceramics. *Acta Mater* 69:9–16
223. Jiang H, Zou YK, Chen Q, Li KK, Zhang R, Wang Y et al (2005) Transparent electro-optic ceramics and devices. In: Ming H, Zhang XP, Chen MY (eds) *Optoelectronic devices and integration*, Pts 1 and 2. *Spie-Int Soc Optical Engineering*, Bellingham, pp 380–394
224. Sun P, Xu CN, Akiyama M, Watanabe T (1999) Controlled oxygen partial pressure sintering of $(\text{Pb}, \text{La})(\text{Zr}, \text{Ti})\text{O}_3$ ceramics. *J Am Ceram Soc* 82:1447–1450
225. Abe Y, Kakegawa K (2002) Fabrication of optically transparent lead lanthanum zirconate titanate ($(\text{Pb}, \text{La})(\text{Zr}, \text{Ti})\text{O}_3$) ceramics by a three-stage-atmosphere-sintering technique. *J Am Ceram Soc* 85:473–475
226. Kong LB, Ma J, Zhang TS, Zhang RF (2002) Transparent lead lanthanum zirconate titanate ceramics derived from oxide mixture via a repeated annealing process. *J Mater Res* 17:929–932
227. Wu YJ, Li J, Kimura R, Uekawa N, Kakegawa K (2005) Effects of preparation conditions on the structural and optical properties of spark plasma-sintered PLZT (8/65/35) ceramics. *J Am Ceram Soc* 88:3327–3331
228. Colla EV, Koroleva EY, Okuneva NM, Vakhrushev SB (1995) Long-time relaxation of the dielectric response in lead magnoniobate. *Phys Rev Lett* 74:1681–1684
229. Qiao L, Ye Q, Gan JL, Cai HW, Qu RH (2011) Optical characteristics of transparent PMNT ceramic and its application at high speed electro-optic switch. *Opt Commun* 284:3886–3890
230. Shvartsman VV, Kholkin AL, Orlova A, Kiselev D, Bogomolov AA, Sternberg A (2005) Polar nanodomains and local ferroelectric phenomena in relaxor lead lanthanum zirconate titanate ceramics. *Appl Phys Lett* 86:202937

231. Shvartsman VV, Kholkin AL, Verdier C, Lupascu DC (2005) Fatigue-induced evolution of domain structure in ferroelectric lead zirconate titanate ceramics investigated by piezoresponse force microscopy. *J Appl Phys* 98:094109
232. Park SE, Shrout TR (1997) Ultrahigh strain and piezoelectric behavior in relaxor based ferroelectric single crystals. *J Appl Phys* 82:1804–1811
233. Kamzina LS, Ruan W, Li GR, Zeng JT (2012) Transparent ferroelectric ceramics $\text{PbMg}_{1/3}\text{Nb}_{2/3}\text{O}_3\text{--}x\text{PbZr}_{0.53}\text{Ti}_{0.47}\text{O}_3$: dielectric and electro-optical properties. *Phys Solid State* 54:2024–2029
234. Kamzina LS, Wei R, Zeng JT, Li GR (2011) Effect of the La concentration on the dielectric and optical properties of the transparent ferroelectric ceramics $75\text{PbMg}_{1/3}\text{Nb}_{2/3}\text{O}_3\text{--}25\text{PbTiO}_3$. *Phys Solid State* 53:1608–1613
235. Tong XL, Lin K, Lv DJ, Yang MH, Liu ZX, Zhang DS (2009) Optical properties of PMN-PT thin films prepared using pulsed laser deposition. *Appl Surf Sci* 255:7995–7998
236. Ruan W, Li GR, Zeng JT, Bian JJ, Kamzina LS, Zeng HR et al (2010) Large electro-optic effect in La-doped $0.75\text{Pb}(\text{Mg}_{1/3}\text{Nb}_{2/3})\text{O}_3\text{--}0.25\text{PbTiO}_3$ transparent ceramic by two-stage sintering. *J Am Ceram Soc* 93:2128–2131
237. Wei ZH, Huang YL, Tsuboi T, Nakai Y, Zeng JT, Li GR (2012) Optical characteristics of Er^{3+} -doped PMN-PT transparent ceramics. *Ceram Int* 38:3397–3402
238. Ganesamoorthy S, Singh G, Bhaumik I, Karnal AK, Tiwari VS, Kitamura K et al (2005) Growth of relaxor ferroelectric single crystals $\text{PbZn}_{1/3}\text{Nb}_{2/3}\text{O}_3$ (PZN) by high temperature solution growth. *Ferroelectrics* 326:19–23
239. Wan S, Lynch CS (2001) Characterization of PZN single crystals. In: Streiffer SK, Gibbons BJ, Tsurumi T (eds) *Proceedings of the 2001 12th IEEE international symposium on applications of ferroelectrics*, vols I and II, pp 347–349
240. Kamzina LS, Krainik NN (1998) Electric-field-induced phase transition in single-crystal lead zinc niobate. *Phys Solid State* 40:485–488
241. Mulvihill ML, Cross LE, Cao WW, Uchino K (1997) Domain-related phase transitionlike behavior in lead zinc niobate relaxor ferroelectric single crystals. *J Am Ceram Soc* 80:1462–1468
242. Yin QR, Ding AL, Zheng XS, Qiu PS, Shen MR, Cao WW (2004) Preparation and characterization of transparent PZN-PLZT ceramics. *J Mater Res* 19:729–732
243. Zhou LJ, Zhao Z, Zimmermann A, Aldinger F, Nygren M (2004) Preparation and properties of lead zirconate stannate titanate sintered by spark plasma sintering. *J Am Ceram Soc* 87:606–611
244. Li K, Li FL, Wang Y, Kwok KW, Chan HLW (2011) Hot-pressed $\text{K}_{0.48}\text{Na}_{0.52}\text{Nb}_{1-x}\text{Bi}_x\text{O}_3$ ($x = 0.05\text{--}0.15$) lead-free ceramics for electro-optic applications. *Mater Chem Phys* 131:320–324
245. Li FL, Kwok KW (2013) Fabrication of transparent electro-optic $(\text{K}_{0.5}\text{Na}_{0.5})_{(1-x)}\text{Li}_x\text{Nb}_{1-x}\text{Bi}_x\text{O}_3$ lead-free ceramics. *J Eur Ceram Soc* 33:123–130
246. Shi YX, Shen J, Zhou J, Xu J, Chen W, Qi YY et al (2015) Structure and optical properties of Sn^{4+} doped $\text{Ba}(\text{Mg}_{1/3}\text{Nb}_{2/3})\text{O}_3$ transparent ceramics. *Ceram Int* 41:253–257
247. Huang YH, Jiang DL, Zhang JX, Lin QL (2010) Fabrication of Sn^{4+} doped $\text{Ba}(\text{Mg}_{1/3}\text{Ta}_{2/3})\text{O}_3$ transparent ceramics by a solid state reaction method. *Ceram Int* 36:1615–1619
248. Kintaka Y, Kuretake S, Tanaka N, Kageyama K, Takagi H (2010) Crystal structures and optical properties of transparent ceramics based on complex perovskite $\text{Ba}(\text{M}4+, \text{B}12+, \text{B}25+)\text{O}_3$ ($\text{M}4+=\text{Ti, Sn, Zr, Hf}$; $\text{B}12+=\text{Mg, Zn}$; $\text{B}25+=\text{Ta, Nb}$). *J Am Ceram Soc* 93:1114–1119
249. Schneider H, Schreuer J, Hildmann B (2008) Structure and properties of mullite—a review. *J Eur Ceram Soc* 28:329–344
250. Aramaki S, Roy R (1962) Revised phase diagram for the system $\text{Al}_2\text{O}_3\text{--SiO}_2$. *J Am Ceram Soc* 45:229–242
251. Aksay IA, Dabbs DM, Sarikaya M (1991) Mullite for structural, electronic and optical applications. *J Am Ceram Soc* 74:2343–2358
252. Ohashi M, Iida Y, Wada S (2000) Mullite-based substrates for polycrystalline silicon thin-film solar cells. *J Ceram Soc Jpn* 108:105–107

253. Bourdais S, Mazel F, Fantozzi G, Slaoui A (1999) Silicon deposition on mullite ceramic substrates for thin-film solar cells. *Prog Photovoltaics* 7:437–447
254. Slaoui A, Pihan E, Focsa A (2006) Thin-film silicon solar cells on mullite substrates. *Sol Energy Mater Sol Cells* 90:1542–1552
255. Focsa A, Gordon I, Auger JM, Slaoui A, Beaucarne G, Poortmans J et al (2008) Thin film polycrystalline silicon solar cells on mullite ceramics. *Renew Energy* 33:267–272
256. Mazdiyias KS, Brown LM (1972) Synthesis and mechanical properties of stoichiometric aluminum silicate (mullite). *J Am Ceram Soc* 55:548–552
257. Prochazka S, Klug FJ (1983) Infrared-transparent mullite ceramic. *J Am Ceram Soc* 66:874–880
258. Ohashi M, Tabata H, Abe O, Kanzaki S, Mitachi S, Kumazawa T (1987) Preparation of translucent mullite ceramics. *J Mater Sci Lett* 6:528–530
259. Schneider H, Schmucker M, Ikeda K, Kaysser WA (1993) Optically translucent mullite ceramics. *J Am Ceram Soc* 76:2912–2914
260. An L, Ito A, Goto T (2012) Effect of calcination temperature on the fabrication of transparent lutetium titanate by spark plasma sintering. *Ceram Int* 38:4973–4977
261. An L, Ito A, Goto T (2011) Highly transparent lutetium titanium oxide produced by spark plasma sintering. *J Eur Ceram Soc* 31:237–240
262. An LQ, Ito A, Goto T (2011) Effects of sintering and annealing temperature on fabrication of transparent $\text{Lu}_2\text{Ti}_2\text{O}_7$ by spark plasma sintering. *J Am Ceram Soc* 94:3851–3855
263. An LQ, Ito A, Goto T (2011) Fabrication of transparent $\text{La}_2\text{Zr}_2\text{O}_7$ by reactive spark plasma sintering. In: Goto T, Akatsu T (eds) *Advanced engineering ceramics and composites*. Trans Tech Publications Ltd, Stafa-Zurich, pp 135–138
264. An LQ, Ito A, Goto T (2013) Fabrication of transparent $\text{Lu}_2\text{Hf}_2\text{O}_7$ by reactive spark plasma sintering. *Opt Mater* 35:817–819
265. An LQ, Ito A, Goto T (2013) Transparent Lu_3NbO_7 bodies prepared by reactive spark plasma sintering and their optical and mechanical properties. *Ceram Int* 39:383–387
266. An L, Ito A, Goto T (2011) Fabrication of transparent Lu_3NbO_7 by spark plasma sintering. *Mater Lett* 65:3167–3169
267. Wang Z, Zhou G, Qin X, Yang Y, Zhang G, Menke Y et al (2013) Fabrication of $\text{LaGdZr}_2\text{O}_7$ transparent ceramic. *J Eur Ceram Soc* 33:643–646
268. Goldstein A, Yeshurun Y, Vulfson M, Kravits H (2012) Fabrication of transparent polycrystalline ZnAl_2O_4 -A new optical bulk ceramic. *J Am Ceram Soc* 95:879–882
269. Kim BN, Hiraga K, Jeong A, Hu C, Suzuki TS, Yun JD et al (2014) Transparent ZnAl_2O_4 ceramics fabricated by spark plasma sintering. *J Ceram Soc Jpn* 122:784–787
270. Xu Y, Fu P, Zhang BH, Gao J, Zhang L, Wang XH (2014) Optical properties of transparent ZnAl_2O_4 ceramics: a new transparent material prepared by spark plasma sintering. *Mater Lett* 123:142–144
271. Chesnaud A, Bogicevic C, Karolak F, Estournes C, Dezanneau G (2007) Preparation of transparent oxyapatite ceramics by combined use of freeze-drying and spark-plasma sintering. *Chem Commun* 1550–1552
272. Shen Y, Xu J, Tok A, Tang D, Khor KA, Dong Z (2010) Development of translucent oxyapatite ceramics by spark plasma sintering. *J Am Ceram Soc* 93:3060–3063
273. Allix M, Alahache S, Fayon F, Suchomel M, Porcher F, Cardinal T et al (2012) Highly transparent BaAl_4O_7 polycrystalline ceramic obtained by full crystallization from glass. *Adv Mater* 24:5570–5575
274. Alahache S, Al Saghir K, Chenu S, Veron E, Meneses DDS, Becerro AI et al (2013) Perfectly transparent $\text{Sr}_3\text{Al}_2\text{O}_6$ polycrystalline ceramic elaborated from glass crystallization. *Chem Mater* 25:4017–4024
275. Al Saghir K, Chenu S, Veron E, Fayon F, Suchomel M, Genevois C et al (2015) Transparency through structural disorder: a new concept for innovative transparent ceramics. *Chem Mater* 27:508–514

276. He LF, Fan GH, Lei MY, Lou ZL, Zheng SW, Su CY et al (2013) Preparation of $\text{MgAl}_2\text{O}_4/\text{Ce:YAG}$ transparent ceramics by hot-pressed sintering and its microstructure. *Rare Metal Mater Eng* 42:463–466
277. He LF, Fan GH, Lei MY, Lou ZL, Chen ZW, Xiao Y et al (2013) Preparation and optical properties of $\text{MgAl}_2\text{O}_4/\text{Ce:YAG}$ transparent ceramics. *Spectrosc Spectral Anal* 33:1175–1179
278. McCauley JW, Patel P, Chen MW, Gilde G, Strassburger E, Paliwal B et al (2009) AlON: a brief history of its emergence and evolution. *J Eur Ceram Soc* 29:223–236
279. McCauley JW, Corbin ND (1979) Phase-relations and reaction sintering of transparent cubic aluminium oxynitride spinel (AlON). *J Am Ceram Soc* 62:476–479
280. Kim YW, Park BH, Park HC, Lee YB, Oh KD, Riley FL (1998) Sintering, microstructure, and mechanical properties of AlON-AlN particulate composites. *Br Ceram Trans* 97:97–104
281. Zientara D, Bucko MM, Lis J (2007) Alon-based materials prepared by SHS technique. *J Eur Ceram Soc* 27:775–779
282. Rafaniello W, Cutler IB (1981) Preparation of sinterable cubic aluminum oxynitride by the carbothermal intridation of lauminum-oxide. *J Am Ceram Soc* 64:C128–C
283. Yuan XY, Liu XJ, Zhang F, Wang SW (2010) Synthesis of γ -AlON powders by a combinational method of carbothermal reduction and solid-state reaction. *J Am Ceram Soc* 93:22–24
284. Jin XH, Gao L, Sun J, Liu YQ, Gui LH (2012) Highly transparent AlON pressurelessly sintered from powder synthesized by a novel carbothermal nitridation method. *J Am Ceram Soc* 95:2801–2807
285. Su M, Zhou Y, Wang K, Yang Z, Cao Y, Hong M (2015) Highly transparent AlON sintered from powder synthesized by direct nitridation. *J Eur Ceram Soc* 35:1173–1178
286. Zhang N, Liang B, Wang XY, Kan HM, Zhu KW, Zhao XJ (2011) The pressureless sintering and mechanical properties of AlON ceramic. *Mater Sci Eng A-Struct Mater Prop Microstruct Process* 528:6259–6262
287. Cheng JP, Agrawal D, Zhang YJ, Roy R (2001) Microwave reactive sintering to fully transparent aluminum oxynitride (AlON) ceramics. *J Mater Sci Lett* 20:77–79
288. Zientara D, Bucko MM, Lis J (2007) Dielectric properties of aluminium nitride- γ -AlO materials. *J Eur Ceram Soc* 27:4051–4054
289. Kumar RS, Rajeswari K, Praveen B, Hareesh UNS, Johnson R (2010) Processing of aluminum oxynitride through aqueous colloidal forming techniques. *J Am Ceram Soc* 93:429–435
290. Clay D, Poslusny D, Flinders M, Jacobs SD, Cutler RA (2006) Effect of LiAl_5O_8 additions on the sintering and optical transparency of LiAlON. *J Eur Ceram Soc* 26:1351–1362
291. Sahin FC, Kanbur HE, Apak B (2012) Preparation of AlON ceramics via reactive spark plasma sintering. *J Eur Ceram Soc* 32:925–929
292. Qi JQ, Wang YZ, Lu TC, Yu Y, Pan L, Wei NA et al (2011) Preparation and light transmission properties of AlON ceramics by the two-step method with nanosized Al_2O_3 and AlN. *Metall Mater Trans A* 42A:4075–4079
293. Yuan XY, Zhang F, Liu XJ, Zhang Z, Wang SW (2011) Fabrication of transparent AlON ceramics by solid-state reaction sintering. *J Inorgan Mater* 26:499–502
294. Zhou YP, Wang DF, Zhuang HR, Wen SL, Guo JK (1998) Study of translucent AlN ceramics. *J Inorgan Mater* 13:256
295. Xiong Y, Wang H, Fu Z (2013) Transient liquid-phase sintering of AlN ceramics with CaF_2 additive. *J Eur Ceram Soc* 33:2199–2205
296. Merkle LD, Sutorik AC, Sanamyan T, Hussey LK, Gilde G, Cooper C et al (2012) Fluorescence of Er^{3+} :AlN polycrystalline ceramic. *Opt Mater Express* 2:78–91
297. Xiong Y, Fu ZY, Wang H, Wang YC, Zhang JY, Zhang QJ (2008) Microstructure and properties of translucent Mg-sialon ceramics prepared by spark plasma sintering. *Mater Sci Eng A* 488:475–481

298. Joshi B, Gyawali G, Wang H, Sekino T, Lee SW (2013) Thermal and mechanical properties of hot pressed translucent Y_2O_3 doped Mg- α/β -Sialon ceramics. *J Alloy Compd* 557:112–119
299. Joshi B, Lee HH, Kim YH, Fu Z, Niihara K, Lee SW (2012) Hot pressed translucent (Mg, Y)- α/β -Sialon ceramics. *Mater Lett* 80:178–180
300. Shan Y, Wang G, Liu G, Sun X, Xu J, Li J (2014) Hot-pressing of translucent Y- α -Sialon ceramics using ultrafine mixed powders prepared by planetary ball mill. *Ceram Int* 40:11743–11749
301. Su XL, Wang PL, Chen WW, Zhu B, Cheng YB, Yan DS (2004) Translucent α -Sialon ceramics by hot pressing. *J Am Ceram Soc* 87:730–732
302. Joshi B, Li B, Kshetri YK, Wang H, Lee SW (2014) IR transparent hot pressed Mg- α/β -Sialon:Ba²⁺ ceramics. *Ceram Int* 40:13041–13047
303. Yang W, Hojo J, Enomoto N, Tanaka Y, Inada M (2013) Influence of sintering aid on the translucency of spark plasma-sintered silicon nitride ceramics. *J Am Ceram Soc* 96:2556–2561

Transparent Ceramics

Kong, L.B.; Huang, Y.Z.; Que, W.; Zhang, T.S.; Li, S.;

Zhang, J.; Dong, Z.L.; Tang, D.Y.

2015, XII, 734 p. 408 illus., 127 illus. in color.,

Hardcover

ISBN: 978-3-319-18955-0